MECHANISTIC STUDY OF SORBENT INJECTION FOR VANADIUM EMISSION CONTROL IN COMBUSTION SYSTEMS

By

SANG-RIN LEE

A DISSERTATION PRESENTED TO THE GRADUATE SCHOOL
OF THE UNIVERSITY OF FLORIDA IN PARTIAL FULFILLMENT
OF THE REQUIREMENTS FOR THE DEGREE OF
DOCTOR OF PHILOSOPHY

UNIVERSITY OF FLORIDA

2005

This achievement is dedicated to my parents, Jung-Sik Lee and Ho-Suk Bae. My father died in 1995, but his dedication and love remain in my heart. Without my mother's encouragement and support, I could not have this achievement.

ACKNOWLEDGMENTS

My sincere gratitude is given to Dr. Chang-Yu Wu for his support and guidance in this academic endeavor. It was the cornerstone of my life as an aerosol researcher when he admitted me as his first Ph.D. student. His advice, encouragement and patience have been invaluable during my graduate career. Special thanks go to Dr. Jean M Andino who taught me the meaning of atmospheric chemistry and gave me continuous comments and advice on my research. I sincerely thank Dr. David W. Hahn for allowing me to use his Raman spectroscopy and for giving me advice on product identification and high-temperature reactor design. I appreciate Dr. Wolfgang Sigmund's advice and research comments. I give special thanks to Dr. Dale Lundgrun for allowing me to use his low-pressure impactor. His abundant experience with and knowledge of aerosols are my example of expertise.

I also thank the staff in Engineering Research Center and Major Analytic Instrument Center. They teach and allow me to use many instruments such as ICP, SEM/EDX, and BET. I would like to thank our past and present group members. Special thanks go to Nawarat, David, Scott, and Shanna. I also thank the other air group graduate and undergraduate students.

I appreciate the Korean students in the Environmental Engineering and Sciences department. They helped to get me settled here in Gainesville. My special thanks go to Dr. Jae-Hyun Cho and his family who treated me like family. I also appreciate my tennis friends. They helped me to blow off stress and energize myself to work.

Finally I would like to give my sincere gratitude to my mother, Ho-Sok Bae. Even though she lost her husband in 1995, she kept encouraging her only son, me, to study abroad. Without her endless care and support, I could not have achieved this goal. I also appreciate the support and patience of my four older sisters and their families.

TABLE OF CONTENTS

LIST OF TABLES

LIST OF FIGURES

Figure Page

KEY TO SYMBOLS OR ABBREVIATIONS

0	subscript *0* represents initial condition
b_0	constant, f(σ) b_0=0.633+0.092 σ^2-0.022 σ^3
co	continuum regime
d_p	particle size (μm)
d_{pg}	geometric mean size (μm)
f, c	subscript *f* represents fine mode, *c* represents coarse mode
fm	free molecule regime
K_0	initial inter-coagulation rate
k_B	Boltzman's constant (dyne cm/K)
n	aerosol number concentration distribution function (#/cm^3cm)
N	total number concentration (#/cm^3)
n_s	monomer number concentration at saturation (molecules/cm^3)
m_1	mass of monomer (g)
M_{3f}	total volume concentration of free molecule regime (cm^3/cm^3)
M_{3c}	total volume concentration of continuum regime (cm^3/cm^3)
M_k	k^{th} moment of aerosol size distribution
S	saturation ratio
t	time (s)
T	temperature (K)

$t_{1/2}$ particle half life time (s)

t_r particle removal time (s)

v_1 Volume of monomer (cm^3)

β collision frequency function

λ mean free path of air (cm)

μ gas viscosity (g/cm s)

σ_g geometric standard deviation

ρ_p particle density (g/cm^3)

τ_s fine mode particle scavenge characteristic time (second)

Abstract of Dissertation Presented to the Graduate School
of the University of Florida in Partial Fulfillment of the
Requirements for the Degree of Doctor of Philosophy

MECHANISTIC STUDY OF SORBENT INJECTION FOR VANADIUM EMISSION CONTROL IN COMBUSTION SYSTEMS

By

Sang-Rin Lee

May, 2005

Chair: Chang-Yu Wu
Major Department: Environmental Engineering Sciences

Mechanistic study of sorbent injection for vanadium emission control in combustion systems was conducted experimentally and theoretically. Potential sorbent material for chemisorption was determined by thermodynamic equilibrium analysis. The computer code, STANJAN, was used to implement the calculations. Ca-, Na- and Mg-based sorbents were evaluated for a wide range of combustion temperatures. The strong affinity between vanadium and these sorbents was identified which implies the great potential of these sorbents to chemically adsorb vanadium. Sulfur was found to strongly impair the performance of these sorbents at lower temperatures (<1000K) due to the formation of sorbent sulfates that depleted the available sorbents in the system.

Bimodal lognormal model was applied to investigate the impact of inter-coagulation rate on the size distributions of fine-mode aerosols. Fine mode particle removal time was found to strongly depend on the number concentration of coarse mode particles but independent on the number concentration of fine mode particles. A 60%

increase of geometric standard deviation of fine mode particles significantly increased the dimensionless removal time. Fine mode particles ultimately approached monodisperse when the dominant mechanism was inter-coagulation. Meanwhile, coarse mode particles approached the asymptotic shape because intra-coagulation was the dominant mechanism. On a constant mass, monodisperse and 1 μm mean diameter are the optimal condition for coarse particles to effectively remove fine particles through inter-coagulation.

Aerosol reactor was applied for a mechanistic study of sorbent injection. Condensation was found to be the preferred mechanism for sorbent injection based on experimental results. $CaCO_3$ sorbent which has strong chemical affinity with vanadium and silica sorbent which has no chemical affinity but high surface area successfully reduced vanadium submicron particle formation. Vanadium was highly concentrated where surface area was high. Surface hydrolysis enhanced physical adsorption while gas phase hydrolysis reduced the efficiency of sorbent technique by forming nano particles.

Bimodal lognormal modeling based on the experimental condition showed that condensation was a very effective means to scavenge vanadium oxide vapor. A high number concentration of fine particles by instant nucleation reduced inter-coagulation rate and quickly scavenged vanadium oxide vapor. Therefore, enhancing condensation while suppressing nucleation was shown to be critical to successful removal of vanadium compound.

CHAPTER 1
GENERAL INTRODUCTION

Heavy metal emissions from combustion sources such as utility boilers and incinerators are of great concern because of their adverse effects on human health and the environment. Because of the increased concern, research is being conducted to assess the actual exposure of human beings to toxic metals (Hogu, 2000), and vanadium is one of these metals. Vanadium is an abundant metal constituent in coal, heavy oil, and petroleum coke (Bryers, 1995; Linak and Miller, 2000; Swain, 1991; Yee and Rosenquist, 1996). The Energy Information Administrator (EIA, 1996) estimated North America emitted about 497 tons/year of Vanadium into the atmosphere in 2000, and 92% of it was emitted by coal and oil combustion sources. Thus, power and heat-producing plants using fossil fuel cause the most widespread discharge of vanadium into the environment. In ambient fine particle characterization studies, vanadium is often an excellent marker for oil combustion aerosol (Campen et al., 2001; Divita et al., 1996; Tolocka et al., 2004).

Once emitted, vanadium can be transported long distances in the atmosphere, resulting in adverse environmental and health effects (Bylinska, 1996). Vanadium is known to be more toxic when inhaled and relatively less toxic when ingested (Boyd and Kustin, 1984). It may also cause cardiovascular diseases, bronchitis, and lung cancer (Yee and Rosenquist, 1996). There are also several reports of ecological disasters caused by poorly controlled industrial emissions containing high concentrations of toxic metals including vanadium (Lin and Chiu, 1995; Pirrone et al., 1999).

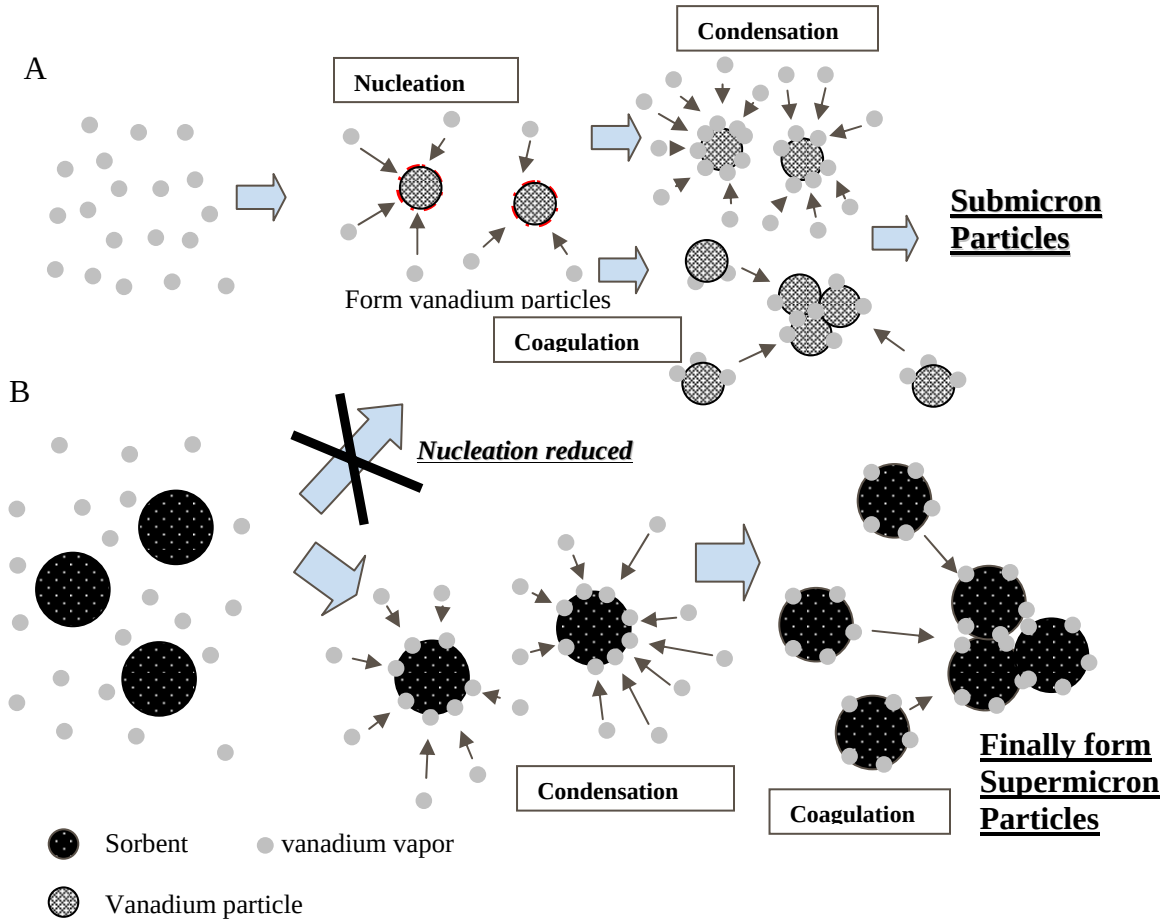

Figure 1-1. Aerosol dynamic processes of vanadium in a combustion system A) Vanadium only. B) Sorbent injection.

Vanadium, like many other metals in the fuel matrix, may enter the gas stream in combustion systems by vaporization of volatile organic vanadium compounds, or by entrainment of particles containing vanadium compounds. At high temperatures, it undergoes various chemical reactions to speciate into different compounds such as oxides, chlorides or sulfates, depending on the combustion environment and the composition of the system. As the temperature decreases once the gas stream exits the combustion zone, various aerosol dynamics such as (nucleation, coagulation and condensation) proceed, resulting in the transformation of vanadium into the particulate phase. Many studies have shown that metals undergoing this pathway generally form

aerosols in the submicron regime. Figure 1-1 provides a mechanistic description of such a process. The resultant particle size distribution depends on the temperature history and the existing particles in the system (Helble and Sarofim, 1989; Lighty et al., 2000; Wu and Biswas, 2000). In a study on characterizing the particulate emissions from a large oil fuel fired power plant, 88 wt% of vanadium was reported to be in the size range of 0.01 to 1.0 μm (Bacci et al., 1983). Linak and Wendt (1994) summarized that vanadium as a trace metal was enriched in submicron fly ash, in many coal combustion investigations. Unfortunately, traditional particulate control devices have their minimum control efficiencies in this size regime (Biswas and Wu, 1998; Flagan and Seinfeld, 1988; Linak et al., 1993). The consequence is further illustrated by ambient particulate matter measurement that showed vanadium enrichment in the submicron regime (Tolocka et al., 2004). Thus, it is important to develop new techniques to effectively control vanadium emissions.

Sorbent technique is one promising measure to control submicron particles. In recent years, various studies have been conducted using mineral sorbents to capture heavy metals. In most studies, sorbent particles are injected into combustion systems to chemically adsorb heavy metals on the injected particle surface. As these sorbent particles are typically in the supermicron range, the metal-sorbent particles can be collected easily using traditional particulate control devices. Figure 1-1b illustrates the mechanism of the sorbent injection technique. Shadman and co-workers (Scotto et al., 1994; Uberoi and Shadman, 1991) used silica, alumina and various naturally available materials (bauxite, kaolinite, and lime) to capture lead and cadmium. Linak et al. (1995) used them to capture nickel, lead, and cadmium. Mahuli et al. (1997) tested hydrated

lime, alumina, and silica for arsenic control. Venkatesh et al. (1996) evaluated various mineral sorbents constituting a spectrum of alumino-silicate compounds and a pulgite clay for immobilization of several trace metallic species. Biswas and co-workers (McMillin et al., 1996; Owens and Biswas, 1996; Wu et al., 1998) generated sorbent particles with very high surface area *in-situ* to capture lead and mercury. However, no study using mineral sorbent materials to capture vanadium has been conducted. Chlorine and sulfur (common constituents of coal and oil) may react with the metal or with the sorbent, thus reducing the effectiveness of the sorbent technique to remove the metal (Linak et al., 1995; Linak and Wendt, 1993; Owens et al., 1995; Wu and Biswas, 1993). Therefore, the impact of chlorine and sulfur on the sorbent process must also be evaluated.

Figure 1-1 shows the aerosol dynamic processes in a combustion system (including chemical reaction, nucleation, condensation, and coagulation) resulting in the evolution of the particle size distribution that ultimately affects the fate of the metals. Consequently the development of a dynamic aerosol size distribution model considering all these mechanisms is instrumental to provide insights into the processes and to determine the key mechanisms of a sorbent injection technique in such a complex system.

There are several aerosol models available to describe aerosol dynamic processes: moment (Frenklach and Harris, 1987; Whitby, 1979), continuous (Tsang and Brock, 1982), and sectional model (Gelbard and Seinfeld, 1980; Landgrebe and Pratsinis, 1990; Wu and Biswas, 1998). These models were categorized by their mathematical size distribution function. Whitby et al. (1991) and Williams and Loyalka (1991) reviewed these models in more details. Among them, aerosol moment model is one of the most

commonly applied, because of its flexible model structure and low computational cost. Assuming a uni-modal log-normal aerosol size distribution, Lin and Biswas (1994) developed a model to study metallic particle formation and growth dynamic during incineration. Wu and Biswas (2000) also used a uni-modal lognormal size distribution model to evaluate the effects of chlorine on the evolution of lead aerosol size distribution. However, such models may not be appropriate for a metal-sorbent system, because of the extreme differences between their particle sizes. Metals alone in a combustion system eventually form submicron particles through nucleation, condensation, and coagulation. The presence of supermicron sorbent particles may suppress the formation of submicron metal particles through inter-coagulation, and condensation which are the key parameters for the effectiveness of the sorbent technique (Biswas and Wu, 1998). Consequently, a bimodal lognormal model will more pertinently represent a metal-sorbent system.

The sorbent processes can be divided into two steps: mass transfer (vanadium transfer to the surface of sorbent), and followed by surface interaction. The mass transfer step is condensation, and/or coagulation while the surface interaction is chemical, and/or physical adsorption. In previous studies (Carey et al., 2000; Linak et al., 1995; Linak et al.1998; Uberoi and Shadman, 1991), the system was generally condensation favored condition because the temperature was very high where the metals were in the vapor state. However, Friedlander et al. (1991) demonstrated that scavenging fine particles by coarse mode particles through coagulation can be the dominant mechanism. Surface interaction can be either physical adsorption or chemical adsorption. Previous sorbent studies (Mahuli et al., 1997; Punjak et al., 1989; Uberoi and Shadman, 1991) demonstrated that the dominant mechanism of surface interaction was chemical

adsorption, according to their XRD measurement data. Though its amount was much less than chemical adsorption, physical adsorption was also identified in some sorbent-metal systems (Chen et al., 2001; Punjak et al., 1989).

Nucleation of vaporized metal compound results in nano-size particles in the fine mode. Eventually they can grow to the submicron regime by coagulation, and condensation. However, their typical concentration, and short residence time in a combustion system do not allow these fine particles to grow to the supermicron regime (Biswas and Wu, 1998; Friedlander et al., 1991). Thus, coagulation with larger particles is the only mechanism to remove submicron fine mode particles once they are formed. Figure 1-2 conceptually depicts the two types of coagulation mechanisms (inter-coagulation, and intra-coagulation) in a system consisting of bimodally distributed particles. Intra-coagulation is self growth within the same mode. Meanwhile inter-coagulation is the process to transfer the fine mode to the coarse mode which plays the key role in the sorbent technique.

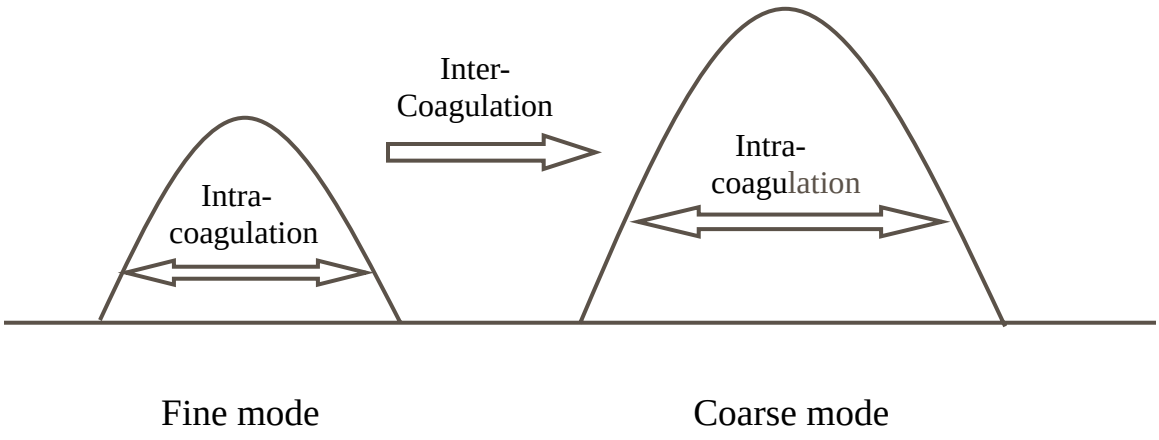

Figure 1-2. Various types of coagulation for bimodally distributed particles

In summary, the sorbent technique is a promising measure to control vanadium emission. Mechanisms of the sorbent injection technique were investigated theoretically, and experimentally. Modal Aerosol Dynamic (MAD) model was used for theoretical study. An aerosol reactor system was applied for experimental study. In Chapter 2, the potential materials for sorbent injection technique were determined by thermodynamic equilibrium analysis. The impact of chlorine, and sulfur on the effectiveness of the process was also assessed. In Chapter 3, the evolution of fine mode particles due to coagulation with coarse mode particles (sorbent) was investigated using a bimodal lognormal model. Effects of size distribution parameters (such as number concentration, standard deviation, and mean diameter on inter-coagulation) were evaluated. In Chapter 4, a feasibility study was conducted to verify the result of Chapter 2. Mechanistic experiments using an aerosol reactor were then performed. The preferable mechanism (condensation or coagulation) for the mass transfer process, and the surface interaction was determined. Finally, the bimodal lognormal model developed in Chapter 3 was applied to investigate the role of condensation, and nucleation in the sorbent technique. In Chapter 5, conclusion of this work and recommendations were provided.

CHAPTER 2
VANADIUM EMISSION CONTROL IN COMBUSTION SYSTEMS BY THERMODYNAMIC EQUILIBRIUM ANALYSES

Introduction

Toxic metal emissions from combustion sources (such as utility boilers and incinerators) are of great concerns. Because of the increased concerns, research is being conducted to assess the actual exposure of human beings to toxic metals (Hogu, 2000), and vanadium is one of these metals. Vanadium is one of the highly concentrated metals in certain types of coal (DeIuliis, 1993). In addition to coal, heavy oil and petroleum coke also have been reported to have high concentrations of vanadium (Bryers, 1995; Linak and Miller, 2000; Swain, 1991; Yee and Rosenquist, 1996). It is also found enriched in combustion ash and interest has even been developed to recover vanadium from ash (Alemany et al., 1998; Fang et al., 1998; Tsuboi et al., 1991) due to its high market values. Once emitted, it can be transported to distance, resulting in adverse environmental and health effects (Bylinska, 1996). It is known that vanadium may cause cardiovascular disease, bronchitis, and lung cancer (Yee and Rosenquist, 1996). There are several reports of ecological disasters caused by poorly controlled industrial emissions containing high concentrations of toxic metals including vanadium (Lin and Chiu, 1995; Pirrone et al., 1999). Even in the Arctic, the annual flux of vanadium is estimated to be 474 tonnes (Akeredolu et al., 1994).

Vanadium, like many other metals in the fuel matrix, may enter the gas stream in combustion systems by vaporization of volatile organic vanadium compounds or by

entrainment of particles containing vanadium compounds. At high temperatures, it undergoes various chemical reactions to speciate into different compounds (such as oxides, chlorides or sulfates) depending on the combustion environment and the composition in the system. As the temperature decreases once the gas stream exits the combustion zone, various aerosol dynamics proceed resulting in the transformation of vanadium into particulate phase. The particle size distribution depends on the temperature history and the existing particles in the system (Wu and Biswas, 2000; Helble and Sarofim, 1989; Lighty et al., 2000). Many research studies have shown that metals undergoing this pathway generally form aerosols in the submicrometer regime. In a study on characterizing the particulate emissions from a large oil fuel fired power plant, 88 wt% of vanadium is in the size range of 0.01 to 1.0 μm (Bacci et al., 1983). Unfortunately, traditional control devices have their minimum control efficiencies in this size regime (Flagan and Seinfeld, 1988). Thus, it is important to develop new techniques to effectively control vanadium emissions.

In recent years, various studied have been conducted to use mineral sorbents to capture heavy metals. Sorbent particles are injected into combustion systems and heavy metals can be chemically adsorbed on the injected particle surface. As these sorbent particles are typically in the supermicron range, the metal-sorbent particles can be easily collected using traditional particulate control devices. Shadman and co-workers (Scotto et al., 1994; Uberoi and Shadman, 1991) used silica, alumina, and various naturally available materials (bauxite, kaolinite, and lime) to capture lead and cadmium. Mahuli et al. (1997) tested hydrated lime, alumina and silica for arsenic control. Venkatesh et al. (1996) evaluated various mineral sorbents constituting a spectrum of alumino-silicate

compounds and a pulgite clay for immobilization of several heavy metals. Biswas and co-workers (McMillin et al., 1996; Owens and Biswas, 1996; Wu et al., 1998) generated sorbents particles with very high surface area *in-situ* to capture lead and mercury. However, no study using mineral sorbent materials to capture vanadium has been conducted.

At high temperature environments, reactions are fast and equilibrium conditions can very possibly be achieved. Hence thermodynamic equilibrium methods can be applied to determine the potential sorbent materials (Lee, 1988) that have chemical affinity with the metal. Equilibrium calculations have been applied to study the behavior of metals like lead, arsenic and cadmium in combustion systems. Good agreement between experimental data and theoretical predictions under certain conditions has been reported, indicating equilibrium calculation to be a good tool for estimating the behavior of metals in combustion systems (Biswas and Wu, 1998; Owens et al., 1995). The objective of this study was to use thermodynamic equilibrium calculations to determine effective materials that can chemically adsorb vanadium. Optimal conditions to achieve high collection efficiencies were determined. The impact of various common constituents in combustion systems on the performance was assessed. The most effective material for controlling vanadium was determined.

Methodology

The computer code STANJAN (Reynolds, 1995) was used to implement the equilibrium calculations. The principle of STANJAN is to minimize the Gibbs free energy of the system by using the method of elemental potentials combined with atom constraints. Thermodynamic data for all relevant species were obtained from the literature (Barin, 1995; Chase et al., 1986). Table 2-1 lists the potential sorbent materials

(using their element as the representative) and their corresponding vanadium-sorbent compounds. Table 2-2 lists the other species that were included in the calculations.

Table 2-1. Potential sorbents and corresponding vanadium-sorbent compounds.

Sorbent	Potential Vanadium-Sorbent Compounds
Ca-	Ca(VO3)2, Ca2V2O7, Ca3(VO4)2
Mg-	Mg(VO3)2, Mg2V2O7
Na-	NaVO3, Na3VO4, Na4V2O7

Table 2-2. Species used in the equilibrium calculations

Reactant	Phase	
V	Gas	V, VCl_2, VCl_4, VO, $VOCl_3$, VO_2
	Condensed	V, VCl_2, VCl_3, VCl_4, VO, VO_2, $VOCl_3$, VCl_4, V_2O_3, V_2O_4, V_2O_5
Ca	Gas	Ca, $CaCl_2$, CaS
	Condensed	Ca, $CaCl_2$, CaO, CaO_2, $CaSO_3$, $CaSO_4$, CaS, $Ca(OH)_2$, $CaCO_3$
Mg	Gas	Mg, $MgCl_2$, MgOH
	Condensed	Mg, $Mg(OH)_2$, $MgCO_3$, $MgCl_2$, MgO, $MgSO_4$
Na	Gas	Na, NaCl, NaOH, $Na_2O_2H_2$, Na_2SO_4
	Condensed	Na, NaCl, NaOH, $NaClO_4$, $NaHCO_3$, $Na_2O_2H_2$, Na_2CO_3, Na_2O, Na_2O_2, Na_2SO_3, Na_2SO_4
Common compound	Gas	CO, CO_2, O_2, HCl, HOCl, H_2S, NOCl, ClO, N, NO, NO_2, N_2, N_2O, S, SO_2, SO_3, H_2SO_4, HNO_3, H_2O
	Condensed	H_2O, S, Coal

Calculations were conducted for four scenarios. Simulation conditions are listed in Table 2-3. The concentrations of the various compounds correspond to the levels found in a typical coal combustion system burning Eastern bituminous coal (DeIuliis, 1993) with 20% excess air at 1 atmosphere. In order to establish the baseline, calculations were first conducted in Set I to determine the behavior of vanadium in a typical combustion system with no sorbent in the system. In Set II, the performance of each potential sorbent was individually investigated for a wide range of temperatures. As chlorine and sulfur in coal may very well react with vanadium or the sorbents, in Set III, parametric analyses were conducted to evaluate the impact of these constituents on the performance of the

chemisorptions process. In Set IV, all the sorbents were included in the calculations. Competition for vanadium among the sorbents was placed by varying their amounts to determine the best sorbent. All calculations were performed for temperatures ranging from 400 to 1700K.

Table 2-3. Simulation conditions for evaluating the performance of various sorbents in capturing vanadium.

Set.	V	Coal	O_2	N_2	SO_2	HCl	$CaCO_3$	Na_2O	MgO
I-1	9.64 $x10^{-5}$	1	29.7	111.7	0	0	0	0	0
I-2					0	$8.25\ x10^{-3}$	0	0	0
II-1					0	0	$2.52x10^{-2}$	0	0
II-2					0	0	0	$3.01x10^{-3}$	0
II-3					0	0	0	0	$7.28x10^{-3}$
III-1					0.285	0	$2.52x10^{-2}$	0	0
III-2					0.285	0	0	$3.01x10^{-3}$	0
III-3					0.285	0	0	0	$7.28x10^{-3}$
III-4					0	$8.25\ x10^{-3}$	$2.52x10^{-2}$	0	0
III-5					0	$8.25\ x10^{-3}$	0	$3.01x10^{-3}$	0
III-6					0	$8.25\ x10^{-3}$	0	0	$7.28x10^{-3}$
IV-1[a]					0.285	$8.25\ x10^{-3}$	$9.49x10^{-2}$	$9.49x10^{-2}$	$9.49x10^{-2}$
IV-1[b]							0.114	0.114	0.114
IV-1[c]							0.190	0.190	0.190
IV-1[d]							0.313	0.313	0.313

a : each sorbent is 33.3% of the stoichiometric amount of sulfur.
b : each sorbent is 40% of the stoichiometric amount of sulfur.
c : each sorbent is 66.7% of the stoichiometric amount of sulfur.
d : each sorbent is 110% of the stoichiometric amount of sulfur.

Results and Discussions

Set I: Baseline Behavior of Vanadium in a Typical Coal Combustion System without Sorbents

In the first set of calculations, the behavior of vanadium in a typical coal combustion system was studied, and it served as the baseline for evaluating the performance of the sorbents under various conditions. The partition of major vanadium species in such a system is shown Figure 2-1.

As shown, divanadium pentaoxide (V_2O_5) is the dominant species in the entire temperature range studied while V_2O_4 becomes increasingly important at high temperatures. As discussed earlier, metal oxides formed in combustion systems generally

form submicrometer aerosols and hence are not desired (Biswas and Wu, 1998). Chlorine is well known to have strong affinity for many metals (Owens et al., 1995; Wu and Biswas, 1993). Therefore, its effect on vanadium speciation was also studied. The results are shown in Figure 2-2. The result is very similar to that without chlorine (Figure 2-1). It indicates relatively weak affinity between chlorine and vanadium, compared with earlier studies on other heavy metals (Owens et al., 1995; Wu and Biswas, 1993). Hence, it is probable that the presence of chlorine in typical coal combustion systems will not significantly affect vanadium's speciation. Our finding agrees with the study of metals from combustion of waste oil conducted by Nerin et al. (1999). Although the chlorine content in the oil burn was very high, vanadium showed very low affinity with chlorine.

Sulfur has been also reported to possess strong affinity with certain metals (Biswas and Wu, 1998). However, it was not included in the baseline calculations because there were no thermodynamic data available for vanadium-sulfur compounds; hence, it was expected to have no effect on the baseline calculations.

Set II: Performance of Individual Sorbent

In Set II the performance of individual sorbent was studied. The partition of vanadium is shown in Figure 2-3A to 3C for Ca-, Na-, and Mg- based sorbent systems, respectively. Since the goal of the sorbent technique is to chemically react vanadium on sorbent particle surface, the total mole fraction of vanadium-sorbent compounds can also be interpreted as the capture efficiency of the proposed sorbent process.

The results are very encouraging. As shown, the predominant products are vanadium-sorbent species in all three systems (although they may be present in different forms). Undesirable vanadium oxide is present only at extremely high temperatures.

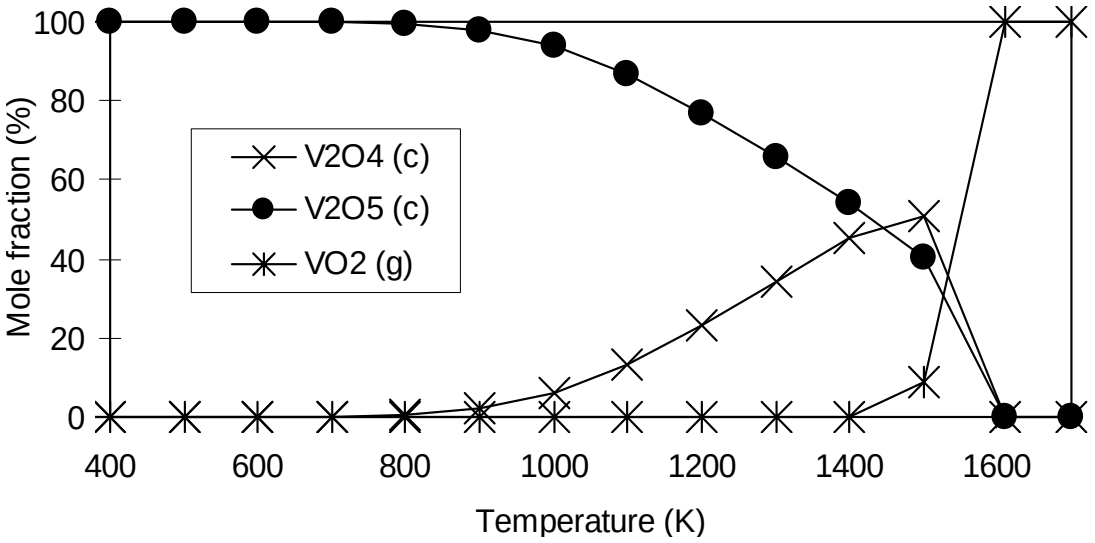

Figure 2-1. Partition of vanadium speciation in a typical coal combustion system. (c: condensed phase, g: gas phase)

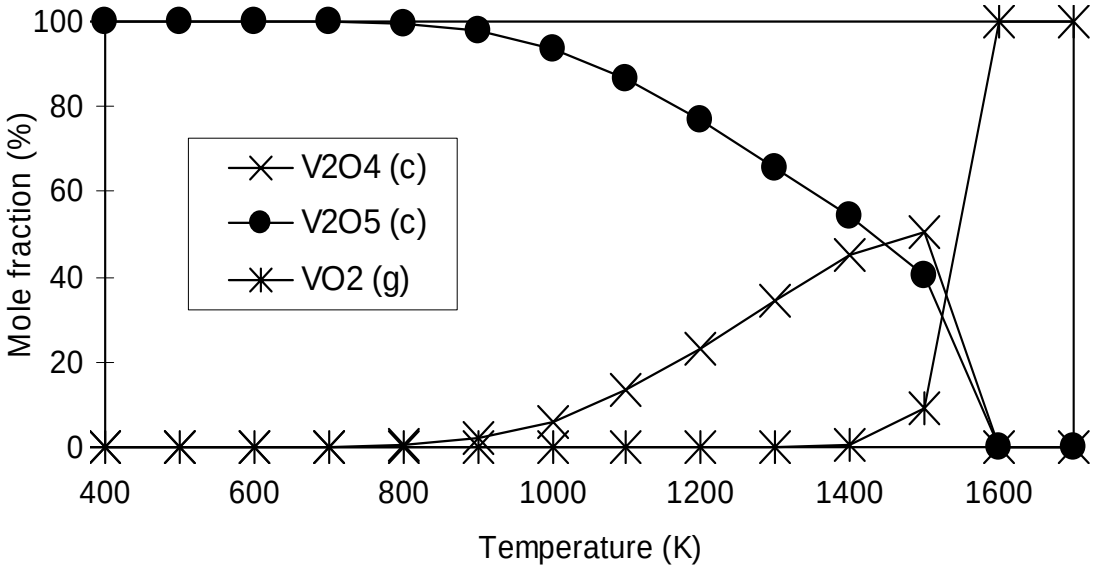

Figure 2-2 Partition of vanadium species in a typical coal combustion system with chlorine and sulfur (c: condensed phase, g: gas phase)

The strong affinity between vanadium and the sorbents demonstrates the excellent potential of the use of these sorbent materials to effectively capture vanadium in combustion systems. However it should be noted that there are some factors, such as chlorine and sulfur in the system, that may prohibit the success of this process. Their impact will be discussed more in the next section.

Set III: Effects of Chlorine and Sulfur on the Performance of Individual Sorbent

Chlorine and sulfur are very common in coal and other fuels. As discussed earlier, they have been reported to affect the speciation of metals and sorbent materials in the system. They may react with vanadium to form vanadium chloride or sulfate. In a pilot study of combustion of residual fuel oil with a high sulfur content, Huffman et al. (2000) identified vanadyl sulfate to be the major product in the fine particulate matter produced in the combustion process. Chlorine and sulfur can also react with the sorbent materials forming, for example, calcium sulfate (gypsum), thus reducing the available amount of sorbents to react with vanadium. Hence, it is important to investigate their impact. Calculations were performed for systems with sulfate and with chlorine. The results are shown in Figures 2-4 and 2-5 for sulfur cases and in Figure 2-6 for chlorine cases.

Effects of sulfur on the performance of individual sorbent

As shown in Figure 2-4A, Ca-based sorbent becomes ineffective to react with vanadium at lower temperatures (<900K) and V_2O_5 becomes the dominant species. The ineffectiveness is due to the strong affinity between sulfur and calcium, which depletes the available calcium in the system. This is evidenced by the predominant $CaSO_4$ shown in Figure 2-5A (the partition of Ca compounds). Ca-based sorbent is effective only at higher temperatures when $CaSO_4$ becomes less stable, releasing Ca for reacting with vanadium.

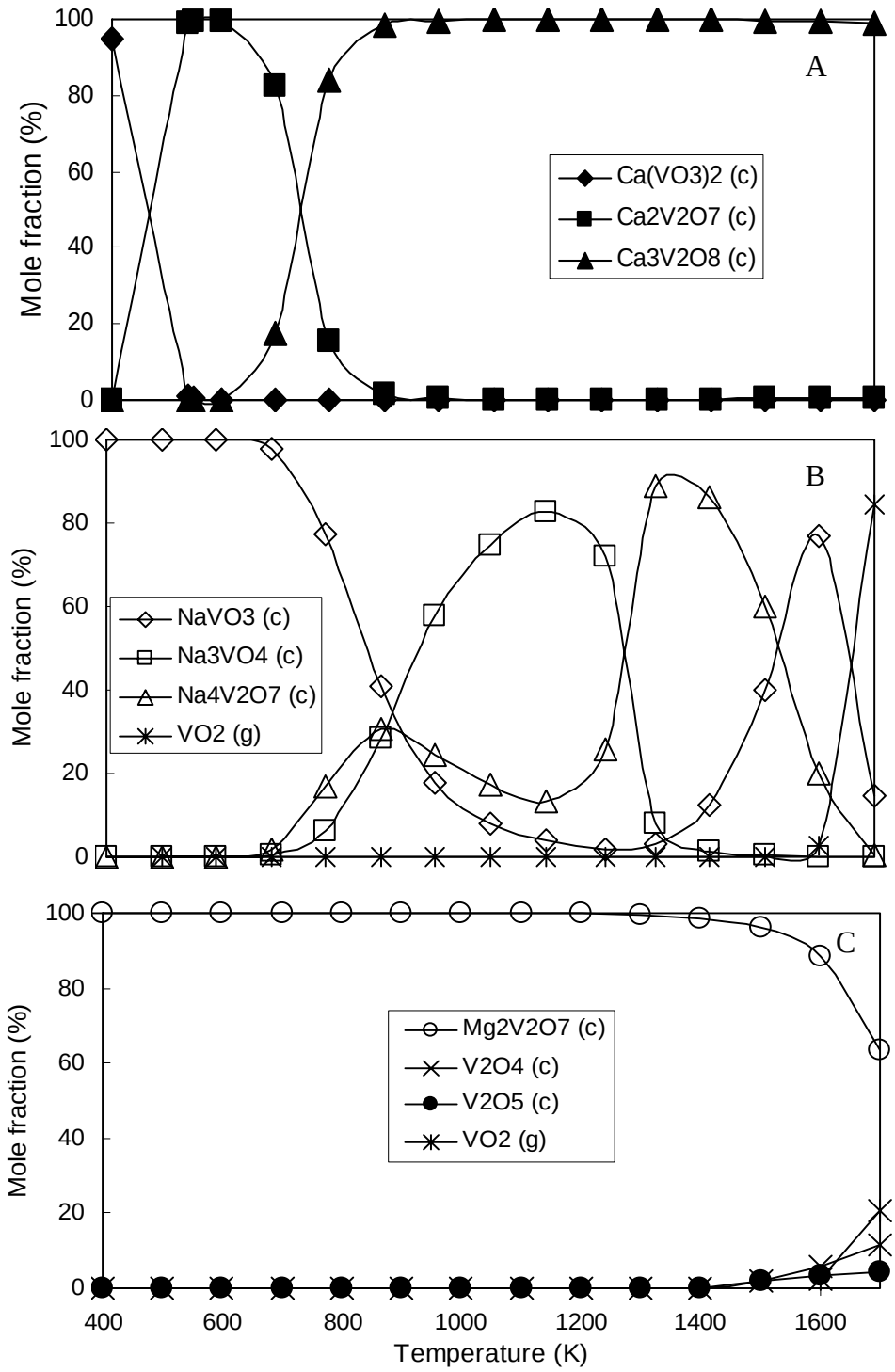

Figure 2-3. Partition of vanadium species in (c: condensed phase, g: gas phase) A) a coal-air-V-$CaCO_3$ system B) a coal-air-V-Na_2O system C) a coal-air-V-MgO system

Similar to Ca-based sorbent, Na-based sorbent becomes ineffective at lower temperatures (<800K) when sulfur is present in the system (Figure 2-4B). The strong affinity between sulfur and sodium (forming Na_2SO_4) depletes the available sodium sorbent in the system for capturing vanadium. The sorption process revives only at higher temperatures when Na_2SO_4 becomes less stable (Figure 2-5B).

Compared to the other two sorbents, Mg-based sorbent is the most severely affected by the presence of sulfur in the system. As shown in Figure 4C, it becomes ineffective in the entire temperature range studied. This is due to the high affinity between magnesium and sulfur forming $MgSO_4$ (Figure 2-5C). The depletion of Mg-based sorbent by sulfur in the system results in the absence of magnesium vanadate.

The results discussed above clearly evidenced that the presence of sulfur in the system significantly affects the performance of the sorption process.

Effects of chlorine on the performance of individual sorbent

When chlorine is present in the system, all sorbents still posses excellent capture efficiency as shown in Figure 2-6. The results for Ca- (Figure 2-6A) and Mg- (Figure 2-6C) based sorbents are similar to those with no chlorine. The results imply that neither magnesium nor calcium has strong affinity to react with chlorine.

However, the products for the Na- case (Figure 2-6B) are different from the no chlorine case (Figure 2-3B). Na_3VO_4 and $Na_4V_2O_7$ are the dominant species at high temperatures (above 800K) in the no chlorine case while $NaVO_3$ is the dominant in the same temperature range (except $Na_4V_2O_7$ at approx. 1100K) in the chlorine case. The shift of the Na/V ratio from 3 (Na_3VO_4) in the no chlorine case to 1 ($NaVO_3$) in the chlorine case indicates that there is competition between chlorine and vanadium for sodium.

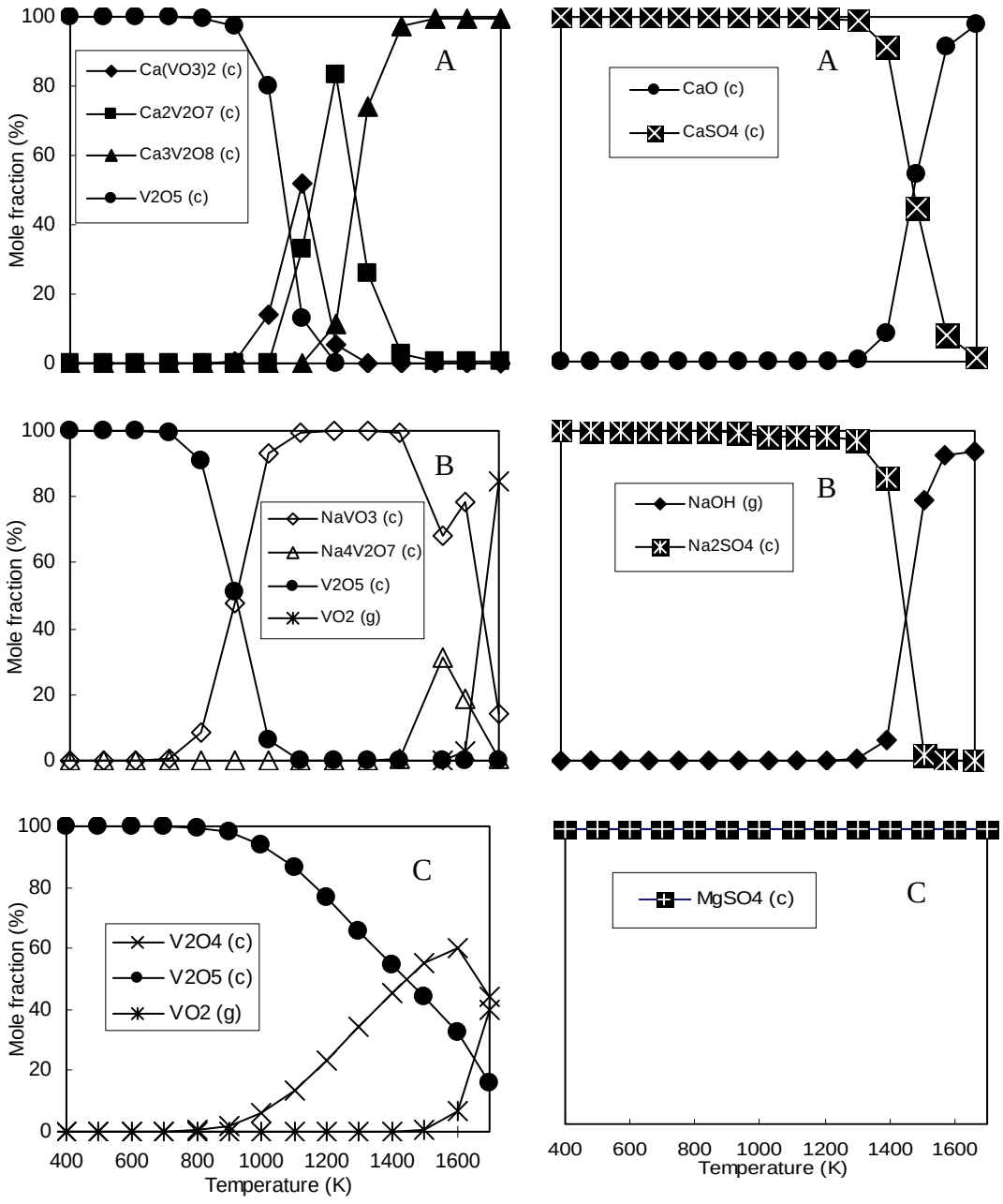

Figure 2-4. Partition of major vanadium species (c: condensed phase g: gas phase)
A) a coal-air-V-SO_2-$CaCO_3$ system
B) a coal-air-V-SO_2-Na_2O system
C) a coal-air-V-SO_2-MgO system

Figure 2-5. Partition of major sorbent species(c: condensed phase g: gas phase)
A) a coal-air-V-SO_2-$CaCO_3$ system
B) a coal-air-V-SO_2-Na_2O system
C) a coal-air-V-SO_2-MgO system

Earlier studies have also shown the adverse effects of chlorine on alkaline metal (Na, K)-based sorbents (Wu and Barton, 1999). Hence a higher level of Na- based sorbent in the system is necessary to ensure the adsorption of both vanadium and chlorine.

Set IV: Competition among Three Sorbents

As discussed, Ca-, Na- and Mg- based sorbents all have demonstrated excellent potential to capture vanadium in combustion systems. The natural question that comes next is which of the three is the most effective sorbent. Four conditions were simulated to determine the most effective sorbent by varying the amount of the sorbents in the system. In the first case (IV-1), the total amount of all sorbents was the exact amount required to stoichiometrically react with sulfur. The amount of sorbent was then increased and in the last case (IV-4) each sorbent itself was enough to completely deplete sulfur in the system. The results are shown in Figures 2-7A to 7D for the mole fraction of major vanadium species and Figure 2-7E – 7H for the partition of sulfur in the system.

Case IV-1: each sorbent is 33% of the stoichiometric amount of sulfur in the system

Because of the strong affinity of sulfur with all sorbents as discussed earlier, all sorbents are consumed by sulfur in this case (Figure 2-7E) and no sorbent is available to capture vanadium (i.e. forming vanadium-sorbent product) at temperatures below 600K (Figure 2-7A). Thus, V_2O_5 appears at low temperatures. When sulfur's affinity with each sorbent fades, some sorbents are released and start to react with vanadium. $NaVO_3$ is the dominant in the intermediate temperature range and $Ca_3(VO_4)_2$ is the major compound in the high temperature range. This can be explained by the relative affinity of these sorbents with sulfur shown in Figure 2-7E. Na_2SO_4 starts to gradually decrease from 600 K (though the change is indistinctive in Figure 7E at temperatures below 1200K).

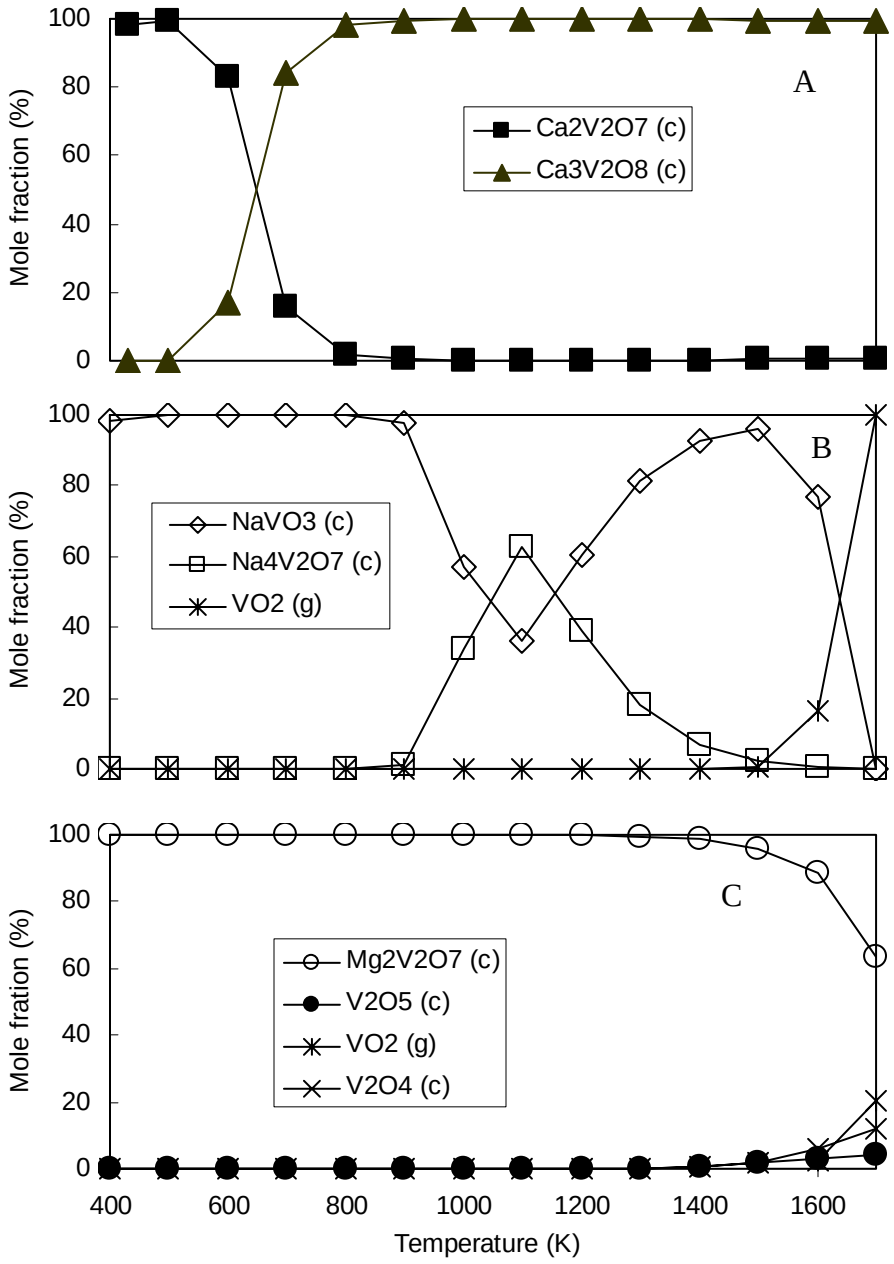

Figure 2-6. Partition of major vanadium species in (c: condensed phase g: gas phase) A) a coal-air-V-HCl-$CaCO_3$ system B) a coal-air-V-HCl-Na_2O system C) a coal-air-V-HCl-MgO system

As the concentration of vanadium is only a tiny fraction of that of sulfur (less than 0.05%), a slight release of Na-based sorbent would result in a high yield of vanadium-sorbent product. Thus $NaVO_3$ is the dominant species above 600K. $CaSO_4$ starts to decrease rapidly from 1100 K and disappears at 1300 K. Consequently, a lot more Ca-

based sorbent than Na-based sorbent is available at high temperatures, resulting in the dominance of calcium vanadate at higher temperatures. On the other hand, $MgSO_4$ is very stable in the entire temperature range studied. Thus, no magnesium-vanadium compound is formed.

Case IV-2: each sorbent is 40% of the stoichiometric amount of sulfur in the system

In this case, totally 20% more sorbent was provided. As discussed earlier, the stronger the affinity with sulfur, the less available the sorbent is. Mg-sorbent apparently has the strongest affinity with sulfur as it is completely converted into $MgSO_4$ (Figure 2-7F, mole fraction is 40% at all temperatures). Meanwhile, Ca-based sorbent is shown to have the weakest affinity with sulfur among the three sorbents. Only half of Ca-based sorbent (20% out of 40%) forms $CaSO_4$. Consequently, Ca-based sorbent is the most effective one in most of the temperature range due to its abundance (Figure 2-7B). However, Na-based sorbent is the most effective one at lower temperatures even though the amount of Na-based sorbent is much less than that of Ca-based sorbent. Thus, Na-based sorbent may have a stronger affinity with vanadium than Ca-based sorbent does. The reslts imply that the ultimate fate of vanadium depends on the relateive affinity and quantity of these two sorbents with vanadium and sulfur. This will be further manifested in the following sections.

Case IV-3 and IV-4: each sorbent is 66.7% and 110% of the stoichiometric amount of sulfur in the system

In case IV-3, while Mg-based sorbent is still completely consumed by sulfur (Figure 2-7G), more Na- and Ca-based sorbents are released, and the ratio of available Na-based sorbent/Ca-based sorbent not consumed by sulfur increases. As shown in Figure 2-7C, the dominant range of Na-based sorbent expands. The result suggests that

Na-based sorbent, if not impeded by sulfur, has a stronger affinity with vanadium in the entire temperature range then Ca-based sorbent does. This is further evidenced in Case IV-4 (Figure 2-7D), where the ratio of available Na-/Ca-based sorbent is approaching 1 and Na-V compounds are the dominant in the entire temperature range. The more available the Na- based sorbent is, the less the calcium-vanadium product is. A field measurement from an oil fuel fired power plant has also identified vanadium to be present in the form of $NaVO_3$ (Bacci et al., 1983).

From the above analyses, it can be concluded that Na-based sorbent has the strongest affinity to bind with vanadium. However, Na-based sorbent is also more vulnerable to the sulfur in the system than Ca-based sorbent is. The affinity of the three sorbents with vanadium and sulfur can be summarized as the following sequence.

Affinity with V: Na > Ca > Mg
Affinity with S: Mg > Na > Ca

It should be emphasized again that the competition of vanadium and sulfur for the available sorbents in the system ultimately determines the fate of vanadium. Nevertheless, it should be addressed that sorbent use is dependent upon mixing with the stream, porosity, surface area and others. Scrubbing of smaller metal particles by larger sorbent particles in the combustor is also a potential mechanism (e.g. fluidized bed combustion; Fan et al., 1999). Very often, these factors are dynamically interwined. For examples, porosity and surface area change as sulfur is scavenged and temperature goes up. The system studied is an ideal one where these factors are not considered.

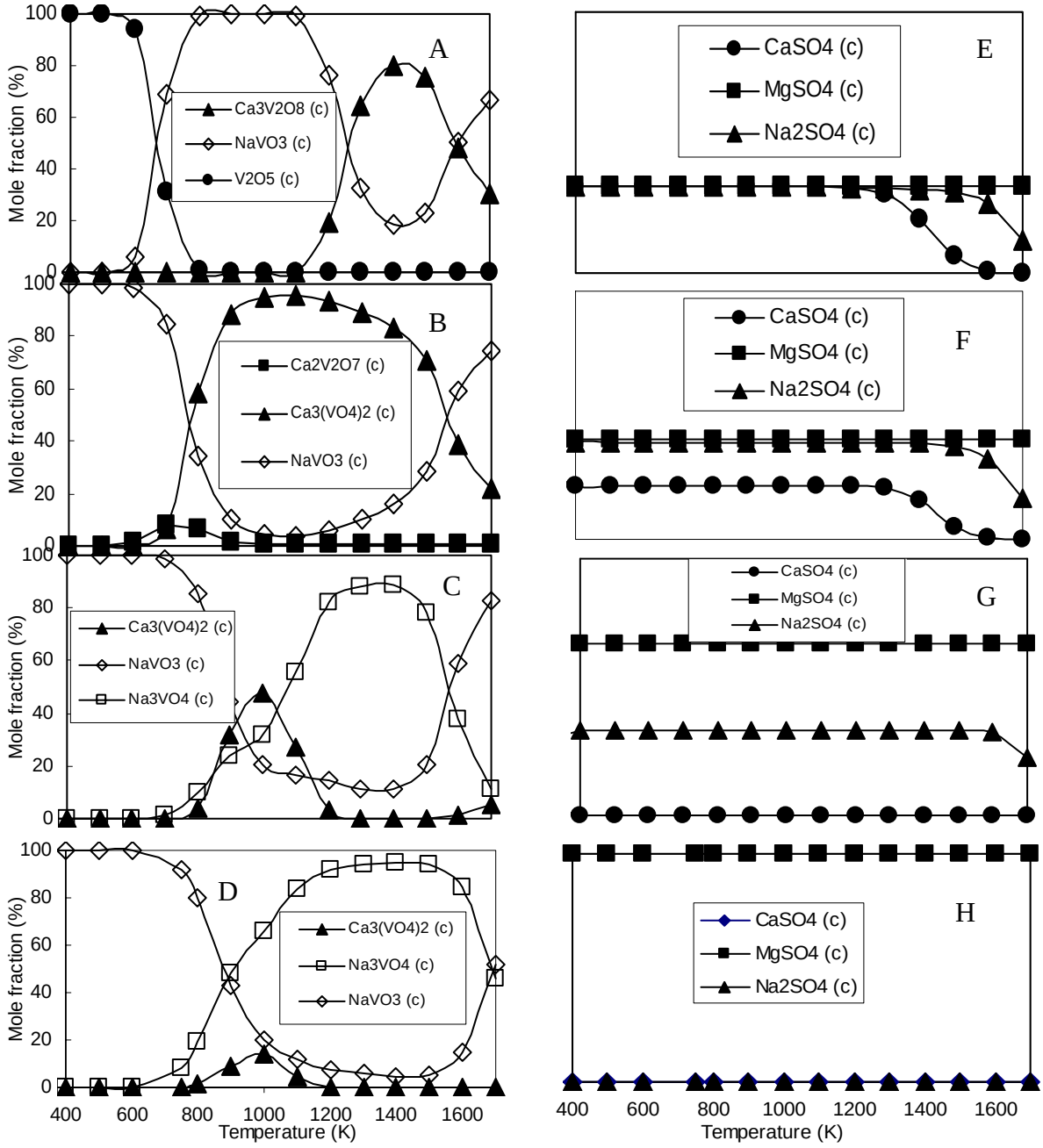

Figure 2-7. Mole fraction of major vanadium species (c: condensed phase, g: gas phase) in the coal combustion system where each sorbent is A) 33.3% B) 40% C) 66.7% D) 110% of the stoichiometric amount of sulfur; Partition of sulfur in the coal combustion system where each sorbent is E) 33.3% F) 40% G) 66.7% H) 110% of the stoichiometric amount of sulfur

Another important point to be addressed is the leachability of metal from the generated metal-sorbent product, a major consideration in the selection of a sorbent material. If the collected ash is to be landfilled, the vanadium-sorbent compound should have a low leachability. However, if vanadium is to be recovered from ash containing a high concentration of vanadium (Alemany et al., 1998; Fang et al., 1998; Tsuboi et al., 1991) soluble products are desired.

Conclusions

Vanadium is concentrated in various fuels and the emission of vanadium from combustion systems is of concern. Mineral sorbents have been demonstrated to be effective to control various toxic metals in combustion systems. In this study, equilibrium calculations were conducted to identify potential sorbent materials to chemically adsorb vanadium. Na-, Ca-, and Mg- based sorbents were found to be effective in a wide range of temperatures. However, the presence of sulfur in the system significantly affected the performance of these sorbents. Sulfur and sorbents were shown to have high affinity (forming sulfates) at temperatures lower than 1000K. The strong affinity resulted in the depletion of available sorbents in the system. Sufficient sorbent in excess of sulfur should be provided in this temperature range to effectively capture vanadium compounds. At high temperatures (> 1000K), the effectiveness of Na- and Ca-based sorbents to capture vanadium revived as sorbent sulfates became less stable, releasing available sorbents to react with vanadium. Meanwhile, Mg- based sorbent still showed very strong affinity with sulfur in the entire range of temperatures, resulting in the worst performance among the three sorbents. When sufficient sorbent is available, Na- based sorbent was found to be the most effective one.

This study provides the insight of the reactions between vanadium and sorbents as well as the impact of various operating conditions. The information obtained is important for developing a better strategy for managing vanadium emission problems.

CHAPTER 3
SIZE DISTRIBUTION EVOLUTION OF FINE AEROSOLS DUE TO INTER-COAGULATION WITH COARSE AEROSOLS

Introduction

Heavy metal emission from combustion sources is of great concern because of its toxicity to human health and the environment. It is well known that metal particles from combustion are enriched in submicron regime (Linak et al, 1993; Biswas and Wu, 1998). Unfortunately, submicron particles show poor capture efficiency in traditional particulate control devices (Flagan and Seinfeld, 1988). Sorbent technique is one promising technique to control these fine metal emissions. In recent years, various studies have been conducted that use mineral sorbents to capture heavy metals (Linak et al., 1995; Venkatesh et al., 1996; Mahuli et al., 1997).

Sorbent particles injected into combustion systems are expected to chemically adsorb heavy metals on the surface. As these sorbent particles are typically in the supermicron range, the metal-sorbent product can be easily collected using traditional particulate control devices. In addition to chemical adsorption, other mechanisms such as nucleation and coagulation are also present in the system. At combustion source, removal of metal vapor by condensation so that fine mode particle formation by vapor nucleation can be suppressed is the preferred mechanism. Rodriguez and Hall (2003) developed an aerosol dynamic model based on a hybrid sectional model to study condensational removal of heavy metals from exhaust gases onto sorbent particles. Comparison of their model results with experimental data (Rodriguez and Hall, 2001) showed good

agreement. Alternatively, after gas stream exits the combustion zone, coagulation with coarse mode sorbent particles can be a possible mechanism to scavenge fine mode particles (Fan et al., 1999). Friedlander et al. (1991) studied the scavenge of a coagulating fine aerosol by a coarse particle mode. They derived a simple analytical criterion for competing processes such as coagulation (intra-coagulation) and diffusion (inter-coagulation). Based on the assumption of monodisperse nucleated fine particles and entrained ash as the coarse particles, the criterion provides a convenient tool for estimating the importance of these competing processes. In real system, however, polydisperse fine particles are present and supermicron sorbent particles are injected. While important, there has been no modeling study about the role of coagulation in sorbent injection technique. The understanding of the evolution of fine mode particle size distribution in such a system is of fundamental importance, though it is seldom studied. Thus, a model to simulate the aerosol dynamics in the system can help understand the dynamic interactions between metals and sorbents as well as implement sorbent injection technique to real system.

There are several aerosol models available to describe aerosol dynamic processes such as moment (Whitby, 1979; Frenklach and Harris, 1987), continuous (Tsang and Brock, 1982), and sectional model (Gelbard and Seinfeld, 1980; Landgrebe and Pratsinis, 1990; Wu and Biswas, 1998). These models were categorized by their mathematical size distribution function. Whitby et al. (1991) and Williams and Loyalka (1991) reviewed these models in more details. Among them, aerosol moment model is one of the most commonly applied ones because of its flexible model structure and low computational cost. Assuming a uni-modal log-normal aerosol size distribution, Lin and Biswas (1994)

developed a model to study metallic particle formation and growth dynamic during incineration. Wu and Biswas (2000) also used a uni-modal lognormal size distribution model to evaluate the effects of chlorine on the evolution of lead aerosol size distribution. However, such models may not be appropriate for a metal-sorbent system because of the extreme differences between their particle sizes. Metals alone in a combustion system eventually form submicron particles through nucleation, condensation and coagulation. The presence of supermicron sorbent particles may suppress the formation of submicron metal particles through inter-coagulation and condensation which are the key parameters for the effectiveness of the sorbent technique (Biswas and Wu, 1998). Consequently, a bimodal lognormal model will more pertinently represent a metal-sorbent system.

Figure 3-1 conceptually depicts the two types of coagulation mechanisms, i.e. inter-coagulation and intra-coagulation, in a system consisting of bimodally distributed particles. Nucleation of vaporized metal compound result in nano-size particles in the fine mode. Eventually they can grow to the submicron regime by coagulation and condensation.

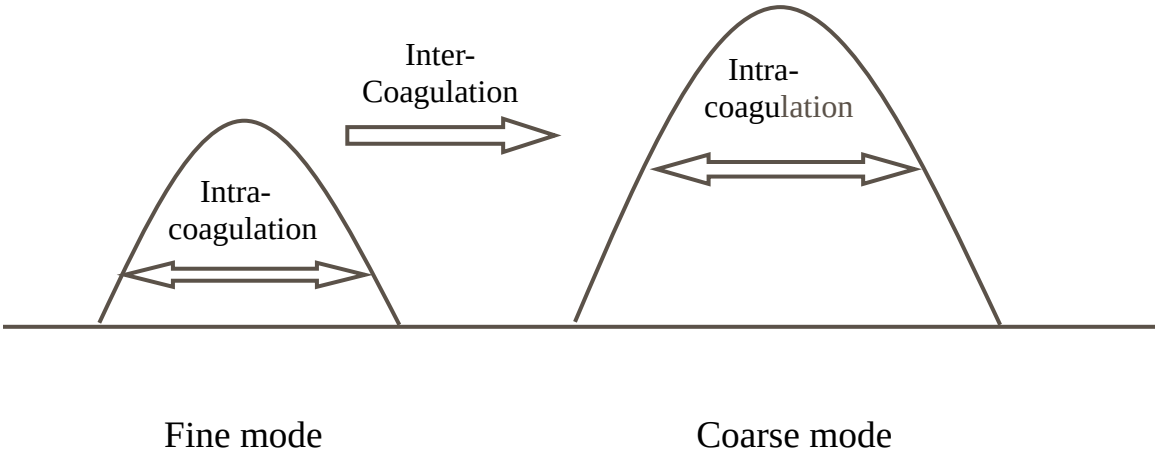

Figure 3-1. Various types of coagulation for bimodally distributed particles

However, their typical concentration and short residence time in combustion system do not allow these fine particles to grow to the supermicron regime by intra-coagulation alone (Biswas and Wu, 1998; Friedlander et al., 1991). Many measurements of metal compounds emission have confirmed that metals are enriched in the submicron regime (Bacci et al, 1983; Osan et al, 2000; Lyyranen et al, 1999). When coarse sorbent particles are introduced into the system, fine mode particles coagulating with the sorbent particles are then transformed into the supermicron regime, which can easily be collected by conventional particulate control devices. As shown, inter-coagulation plays the key role in removing fine mode particles and therefore its effect was the focus of this work.

In this study, the Modal Aerosol Dynamic (MAD) model (Whitby and McMurry, 1997) based on a lognormal moment model that has multi modal structure and low computation cost was adopted. The evolution of fine mode particles due to coagulation with coarse mode particles (sorbent) was investigated. The effects of size distribution parameters such as number concentration, standard deviation and mean diameter on inter-coagulation were evaluated.

Methodology

Model Description

The development of the MAD model adopted in this study was provided in detail in Whitby and McMurry (1997), and hence is not repeated. Only inter-coagulation which was the main mechanism to be investigated is discussed as follows. The inter-coagulation rate for the fine mode is

$$\frac{\partial}{\partial t}(M_{kf}) = -\int_0^\infty \int_0^\infty dp_f^k \beta(dp_f, dp_c) n_f(dp_f) n_c(dp_c) ddp_f ddp_c \qquad (3\text{-}1)$$

and for the coarse mode is

$$\frac{\partial}{\partial t}(M_{kc}) = \int_0^\infty \int_0^\infty (dp_f^3 + dp_c^3)^{k/3} \beta(dp_f, dp_c) n_f(dp_f) n_c(dp_c) ddp_f ddp_c - \int_0^\infty \int_0^\infty dp_c^k \beta(dp_f, dp_c) n_f(dp_f) n_c(dp_c) ddp_f ddp_c \quad (3\text{-}2)$$

where subscripts *k* is order of moment (0, 3 or 6) and *f*, *c* stand for fine and coarse, respectively. The definition of parameter is provided in the Nomenclature section. Once these moments are determined, the key size distribution parameters can then be determined according to

$$M_k = N dp_g^k \exp(\frac{k^2}{2} \ln^2 \sigma_g) \quad (3\text{-}3)$$

$$dp_g = \overline{M}_{k_1}^{\hat{k}_1} \overline{M}_{k_2}^{\hat{k}_2} \quad (3\text{-}4)$$

$$\ln^2 \sigma_g = \frac{2}{k_1(k_1 - k_2)} \ln(\frac{\overline{M}_{k_1}}{\overline{M}_{k_2}^r}) \quad (3\text{-}5)$$

where

$$\overline{M}_k = \frac{M_k}{N}$$

$$r = \frac{k_1}{k_2}$$

$$\hat{k}_1 = \frac{1}{r(k_2 - k_1)}$$

$$\hat{k}_2 = \frac{r}{(k_1 - k_2)}$$

With these size distribution parameters, the evolution of fine mode particle size distribution due to inter-coagulate with coarse mode particles can be investigated. In this study, harmonic average method (Pratsinis, 1988) was used to calculate the collision frequency function in the transition regime.

Inter-coagulation to remove fine particles is the key mechanism in this study. Thus, the time needed to remove fine mode particles is of interest. The fine mode particle scavenge characteristic time is defined as follows,

$$\tau_s = N_{f0} / K_o \tag{3-6}$$

where N_{f0} is the initial total number concentration of fine mode particles and K_o is the initial inter-coagulation rate. Once K_0 is calculated, the fine mode particle scavenge characteristic time can be easily estimated with size distribution parameters. The analytical solution (Whitby and McMurry, 1991) for the inter- coagulation rate of 0th moment for the continuum regime can be expressed by

$$K_{o,co} = N_f N_c (2k_B T / 3\mu)[2 + 1.392(\frac{2\lambda}{dp_{gf}})^{0.0783} \frac{2\lambda}{dp_{gf}} \{\exp[(\frac{1}{2})\ln^2 \sigma_{gf}] + (\frac{dp_{gf}}{dp_{gc}}) \exp[2\ln^2 \sigma_{gf}] \exp[(\frac{1}{2})\ln^2 \sigma_{gc}]\} + 1.392(\frac{2\lambda}{dp_{gc}})^{0.0783} \frac{2\lambda}{dp_{gc}} \{\exp[(\frac{1}{2})\ln^2 \sigma_{gc}] + (\frac{dp_{gf}}{dp_{gc}}) \exp[2\ln^2 \sigma_{gc}] \exp[(\frac{1}{2})\ln^2 \sigma_{gf}]\} + \{\frac{dp_{gf}}{dp_{gc}} + \frac{dp_{gc}}{dp_{gf}}\} \{\exp[(\frac{1}{2})\ln^2 \sigma_{gf}] \exp[(\frac{1}{2})\ln^2 \sigma_{gc}]\}] \tag{3-7}$$

and for the free molecule regime by

$$K_{o,fm} = N_f N_c \sqrt{3k_B T / \rho_P} b_0 \sqrt{dp_{gf}} \{\exp[(\frac{1}{8})\ln^2 \sigma_{gf}] + \sqrt{\frac{dp_{gc}}{dp_{gf}}} \exp[(\frac{1}{8})\ln^2 \sigma_{gc}] + 2(\frac{dp_{gc}}{dp_{gf}}) \exp[(\frac{1}{8})\ln^2 \sigma_{gf}] \exp[(\frac{1}{2})\ln^2 \sigma_{gc}] + (\sqrt{\frac{dp_{gc}}{dp_{gf}}})^4 \exp[(\frac{9}{8})\ln^2 \sigma_{gf}] \exp[2\ln^2 \sigma_{gc}] + (\sqrt{\frac{dp_{gc}}{dp_{gf}}})^3 \exp[2\ln^2 \sigma_{gf}] \exp[(\frac{9}{8})\ln^2 \sigma_{gc}] + 2(\sqrt{\frac{dp_{gf}}{dp_{gc}}}) \exp[(\frac{1}{2})\ln^2 \sigma_{gf}] \exp[(\frac{1}{8})\ln^2 \sigma_{gc}]\} \tag{3-8}$$

With emission control in mind, in this work the fine mode particle removal time (t_r) is defined as time to remove 99.99 wt% of fine mode particles. The dimensionless removal time can then be defined as t_r/τ_s

Simulation Conditions

Inter-coagulation rate depends on the size distributions of both modes. Hence the effect of number concentration, geometric standard deviation and geometric mean size of each mode on inter-coagulation rate was investigated. Table 3-1 summarizes all simulation conditions. In the first set of simulation, the number concentration of each mode was varied, and the corresponding size distribution and removal time of the fine mode were determined. In the second set, the effects of the geometric standard deviations of coarse mode and fine mode were studied. In the third set, the impact of varying the geometric mean size of each mode on inter-coagulation rate was evaluated. The final set of simulation was carried out to determine the optimal sorbent particle size distribution that could enhance inter-coagulation rate, when the mass loading of sorbent particles was fixed.

Table 3-1. Simulation condition for investigation of the effects of inter-coagulation on fine mode particle removal.

	d_{gf} (μm)	d_{gc}	σ_{gf}	σ_{gc}	N_{f0} (#/cc)	N_{c0} (#/cc)
Set I	0.01	10	1.3	1.3	$10^4 – 10^{15}$	10^6 - 10^{12}
Set II	0.01	10	1.0–1.6	1.0-3.0	10^8	10^8
Set III	0.01-0.5	1-500	1.3	1.3	10^8	10^8
Set IV	0.01	1-100	1.3	1.0-3.0	10^6	10^4-10^{13}

* All simulations conducted for T = 740^{o}C

Results and Discussion

Number Concentration

Since coagulation rate strongly depends on number concentration, inter-coagulation is expected to play a key role in enhancing the fine particle removal when the number

concentration are high. Figure 3-2 shows the simulation results of set I. As shown, for the same initial fine mode number concentration, the removal time strongly depends on the coarse mode number concentration. It decreases as the coarse mode number concentration increases. However, for a fixed coarse mode number concentration, interestingly, the removal time is not affected by the change of the fine mode number concentration unless the fine mode number concentration is 10 times more than the coarse mode number concentration. Careful examination of the coagulation rates (intra and inter) shows that when the fine mode intra-coagulation rate is much faster than the inter-coagulation rate, the growth of fine mode particles decreases its number concentration which subsequently yields a low inter-coagulation rate and therefore a longer removal time. Thus, the graph can be divided into two regions as shown in Figure 3-2 by the dashed line: inter-coagulation dominant and intra-coagulation dominant. In short, the coarse mode number concentration clearly plays a major role in determining fine mode removal time when inter-coagulation is the dominant mechanism; on the other hand, the fine mode number concentration must be considered to estimate the fine mode removal time (t_r) when intra-coagulation is the dominant mechanism.

These results were further presented by dimensionless removal time (t_r/τ_s) as a function of normalized number concentration N_{f0}/N_{c0} in Figure 3-3A. As shown, all data merge into one line, thus yielding a useful tool for estimating the dimensionless removal time as

$$\frac{t_r}{\tau_s} = 33.7 \qquad N_{f0}/N_{c0} < 10 \qquad (3\text{-}9)$$

and

$$\frac{t_r}{\tau_s} = 33.7 \exp(0.0007 \frac{N_{f0}}{N_{c0}}) \qquad N_{f0}/N_{c0} \geq 10 \qquad (3\text{-}10)$$

for the geometric standard deviation of the fine mode and the coarse mode of 1.3 and d_{gf} = 0.01μm. Hence, as long as τ_s is determined for a given system (Eq 3-6), the corresponding removal time (t_r) can be estimated accordingly. Since the prior study (Friedlander et al., 1991) used half life time ($t_{1/2}$), also included in the plot are the results for $t_{1/2}/\tau_s$. The corresponding equations are

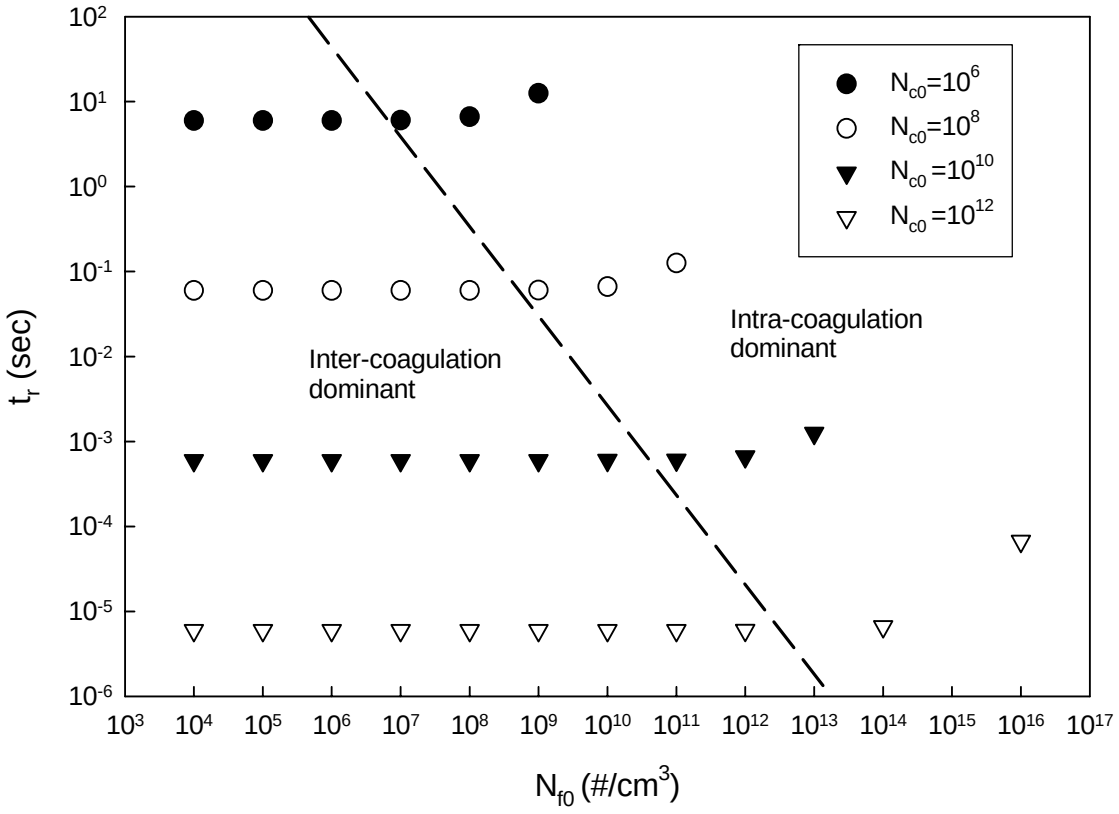

Figure 3-2. Fine mode removal time as a function of fine mode number concentration for various coarse mode number concentrations. The dashed line connects points where N_{f0}/N_{c0}=10.

$$\frac{t_{1/2}}{\tau_s} = 1.15 \qquad N_{f0}/N_{c0} < 10 \qquad (3\text{-}11)$$

and

$$\frac{t_{1/2}}{\tau_s} = 1.15\exp(0.0003\frac{N_{f0}}{N_{c0}}) \qquad N_{f0}/N_{c0} \geq 10 \qquad (3\text{-}12)$$

As shown, the same patterns are followed.

Since in practical applications, mass loading is of interest, Figure 3-3B shows dimensionless removal time as a function of normalized mass/volume. The same trend observed in Figure 3-3A exists. Dimensionless removal time is independent on normalized mass or volume until it exceeds 10^{-8}.

Geometric Standard Deviation:

It is well known that the geometric standard deviation of a log-normally distributed uni-modal aerosol approaches 1.35 and 1.32 for free molecule regime and continuum regime, respectively, when coagulation is the dominant mechanism (Pratsinis, 1988). Parallely, this applies to intra-coagulation for multi-modal aerosols. However, the effects of inter-coagulation on the geometric standard deviations of multi-mode aerosol have never been investigated before.

These effects were studied as set II and the results are presented in Figure 3-4 for the size distributions at various times. In this simulation condition (with sorbent application in mind), inter-coagulation was dominant for fine mode. As shown, fine mode became narrower with its mode size shifted toward the bigger size. It should be emphasized that the increase of the mode size was not due to intra-coagulation. Under intra-coagulation dominant case, there was no discernible change in the fine mode size distribution during the simulation time (0.1 s; also marked in Figure 3-4). Rather, it

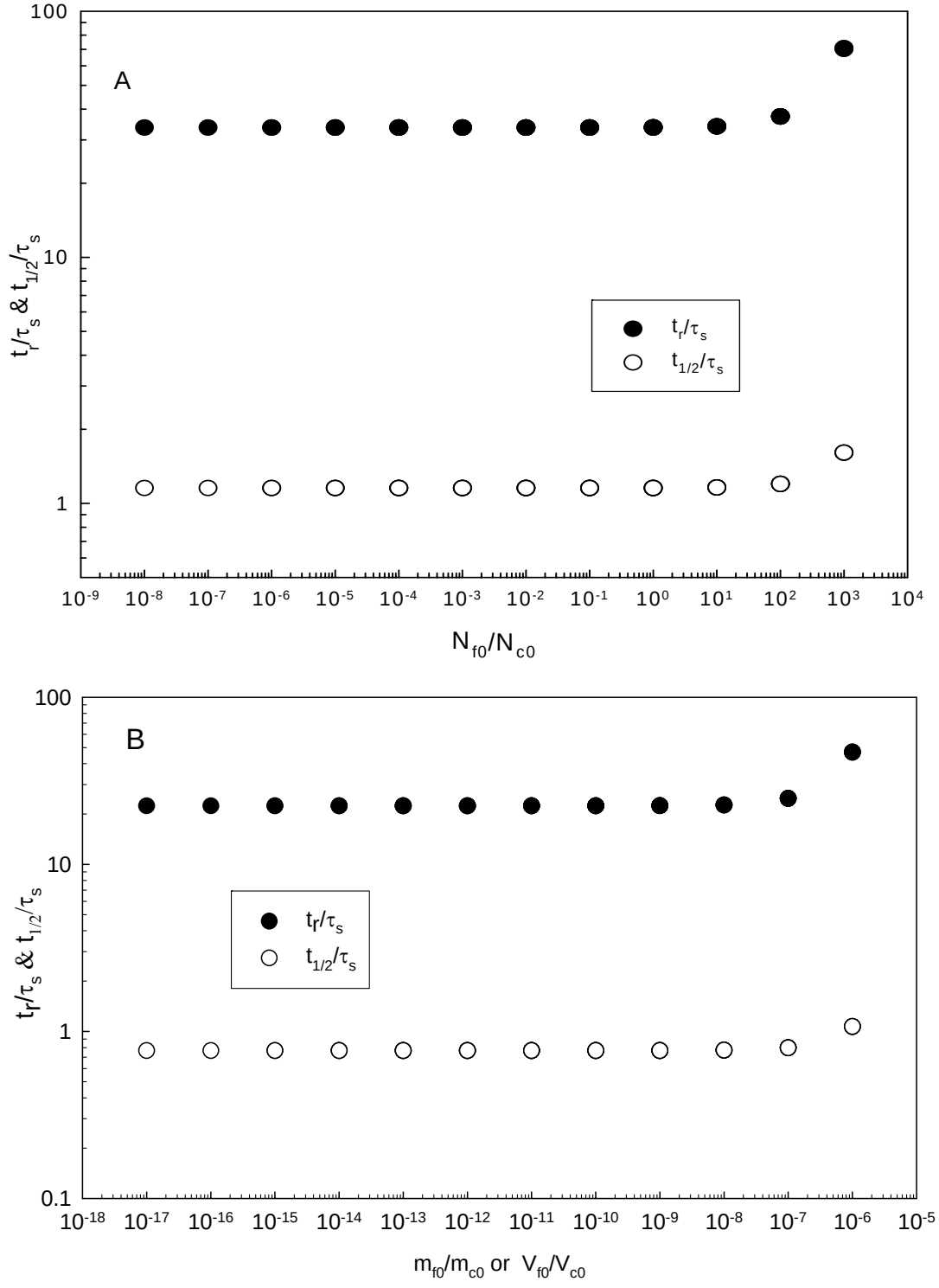

Figure 3-3. Dimensionless removal time as function of A) normalized number concentration B) normalized mass or volume concentration

resulted from the faster scavenge of the smaller sizes of the fine mode due to inter-coagulation. Inter-coagulation rate is dependent on collision frequency function, which strongly depends on particle size difference, and it increases as the size difference increases. Consequently, the smaller size of the fine mode aerosol is scavenged much faster then the larger size in the same mode. Therefore, when inter-coagulation is the dominant mechanism, σ_{gf} (fine mode geometric standard deviation) ultimately approaches monodisperse (i.e. $\sigma_{gf} = 1$). Meanwhile, intra-coagulation was dominant for the coarse mode since the addition of the fine mode moments to the coarse mode is rather insignificant. Although σ_{gc} (coarse mode geometric standard deviation) did not change in the short period (fine mode removal time) shown in the figure, it will finally approach the asymptotic value (1.32, not shown in Figure 3-4).

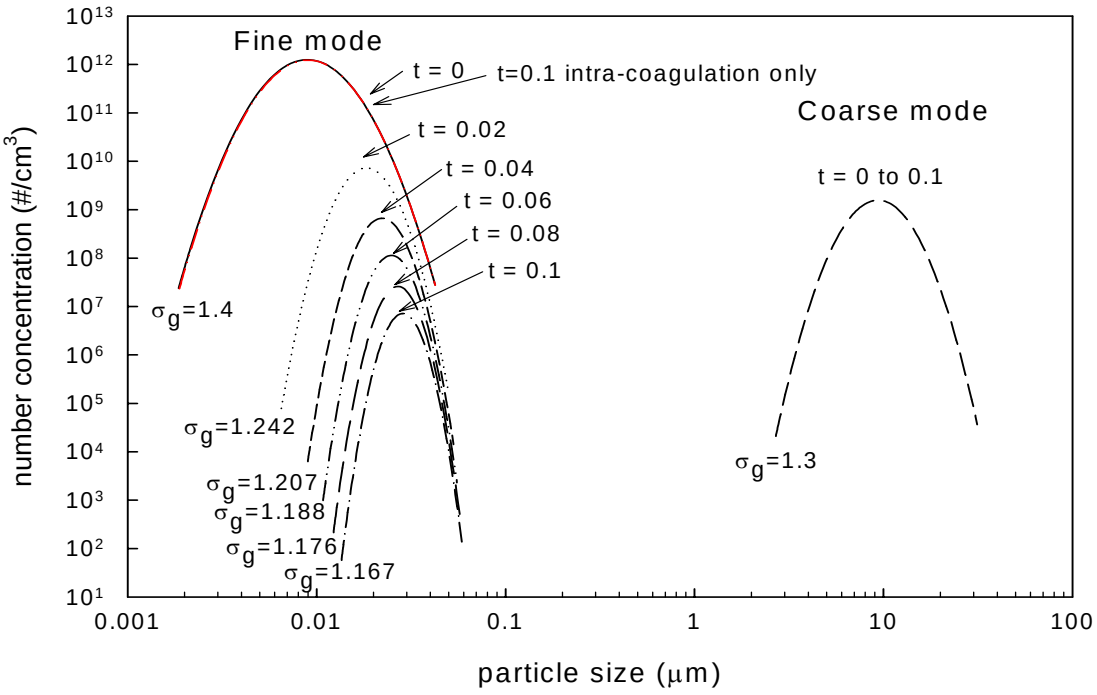

Figure 3-4. The evolution of fine mode (σ_{gf0}=1.4) and coarse mode (σ_{gc0}=1.3) particle size distribution by inter-coagulation to reach removal time (t_r=0.106 sec)

Figure 3-5A shows the dimensionless removal time and the half life time (note: two y-axes) as a function σ_{gf}, and Figure 3-5B shows the results for varying σ_{gc}. When σ_{gf} changed from 1 to 1.6, dimensionless removal time increased drastically from 9.3 to 250 demonstrating the sensitivity to the change of the fine mode distribution. A larger σ_{gf} implies more mass in the larger size part. The corresponding lower inter-coagulation rate for the larger size resulted in a longer removal time as discussed earlier. Similar to the previous set, an equation can be obtained as a useful tool for estimating the dimensionless time due to the change of σ_{gf} as

$$\frac{t_r}{\tau_s} = 0.0058897 \exp(6.658\sigma_{gf}) \tag{3-13}$$

$$\frac{t_{1/2}}{\tau_s} = 0.578 + 0.000276 \exp(5.88\sigma_{gf}) \tag{3-14}$$

In contrast, the dimensionless removal time changed within 3%, almost negligibly, when σ_{gc} was varied from 1 to 3. Clearly demonstrated above is that there is no point of using coarse mode particles with a wide size distribution to enhance inter-coagulation rate. The geometric standard deviation of the fine mode particles plays a more important role. Friedlander et al. (1991) assumed monodisperse nucleated particles (i.e. inter-coagulation rate was the fastest). In many practical systems, aerosols are present as polydisperse particles, including metal compounds from combustion system. As revealed by this study, polydispersity needs to be considered and the assumption of monodisperse particles underestimates the required time to scavenge polydisperse aerosol.

Mean Size Difference

If particle size difference is large, its collision frequency function is large which enhances coagulation. Figure 3-6A shows the effects of mean size difference.

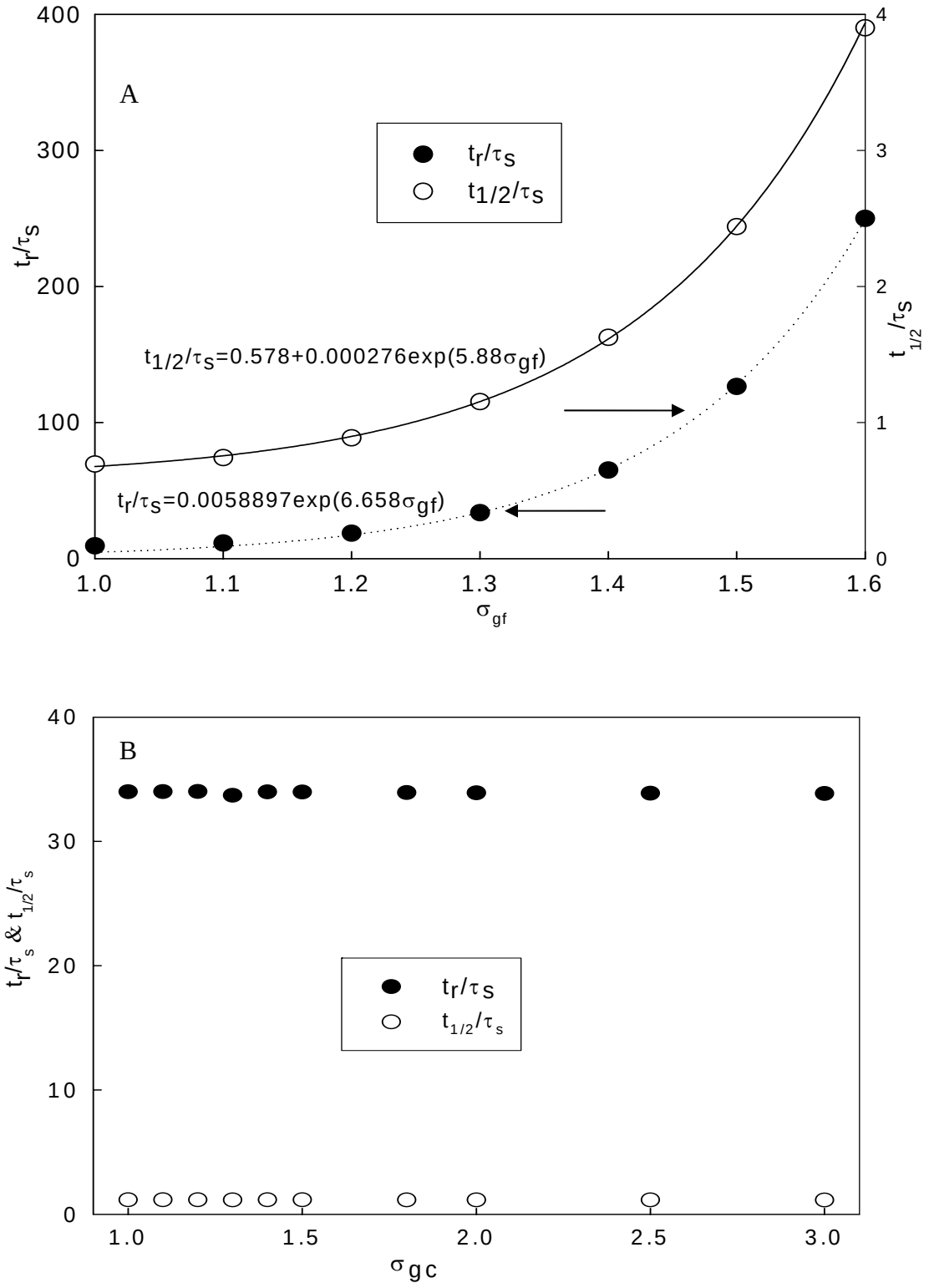

Figure 3-5. A dimensionless removal time as function of A) fine mode geometric standard deviation where σ_{gc0}=1.3. B) coarse mode geometric standard deviation where σ_{gf0}=1.3

As shown, when the mean size difference between the fine mode and the coarse mode increased, the removal time decreased accordingly. This clearly shows that large mean size sorbent (with same number concentration) will enhance inter-coagulation rate due to the large cross-section surface area for coagulation. When the results are presented in the dimensionless form as shown in Figure 3-6A, even though mean size difference increased, dimensionless removal time showed only 3-7% difference for two orders of magnitude of size ratio. The reason for the insignificant difference is due to the increase of fine mode scavenge characteristic time for increased mean size difference.

In addition to size difference, fine mode mean size also affects the dimensionless removal time. Their relationship is plotted in Figure 3-6B. A linear relationship in log graph is observed which can be expressed as

$$\frac{t_r}{\tau_s} = -9.493\log(d_{gf}) + 14.814 \tag{3-15}$$

$$\frac{t_{1/2}}{\tau_s} = -0.129\log(d_{gf}) + 0.891 \tag{3-16}$$

Considering the combined effects of number concentration, geometric standard deviation and mean size, the following final form can be used to estimate the removal time and half life time for $N_{f0}/N_{c0} < 10$,

$$\frac{t_r}{\tau_s} = 0.0058897\exp(6.658\sigma_{gf})\{-0.2852\log(d_{gf}) + 0.4296\} \tag{3-17}$$

$$\frac{t_{1/2}}{\tau_s} = \{0.578 + 0.000276\exp(5.88\sigma_{gf})\}\{-0.1126\log(d_{gf}) + 0.7748\} \tag{3-18}$$

and for $N_{f0}/N_{c0} \geq 10$

$$\frac{t_r}{\tau_s} = [0.0058897\exp(6.658\sigma_{gf})\{-0.2852\log(d_{gf}) + 0.4296\}]\exp(0.0007\frac{N_{f0}}{N_{c0}}) \qquad (3\text{-}19)$$

$$\frac{t_{1/2}}{\tau_s} = [\{0.578 + 0.000276\exp(5.88\sigma_{gf})\}\{-0.1126\log(d_{gf}) + 0.7748\}]\exp(0.0003\frac{N_{f0}}{N_{c0}}) \qquad (3\text{-}20)$$

Application to Sorbent Injection

For many practical applications such as sorbent injection for toxic metal removal, minimizing the mass loading while having good removal efficiency is desired as cost consideration is always important to the feasibility of the technology. With the same total mass concentration, there are several combinations of size distribution parameters (number concentration, geometric mean size, and geometric standard deviation). In other word, the optimal conditions based on mass concentration will be different from those obtained for number concentration. Figure 3-7A shows the removal time for various combinations of σ_{gc} and d_{gc}/d_{gf} based on the same number concentration. Figure 3-7B, on the other hand, shows the results based on the same mass concentration. As discussed earlier, a high number concentration of the coarse mode and a wide mean size difference allow for a short removal time (shown in Figure 3-7A). However, different patterns were observed for the results based on the same mass concentration (Figure 3-7B). As shown, a narrow size deviation and a small coarse mode mean size had the shortest removal time. Careful examination of the size distribution parameters reveals that under the same mass concentration, a smaller mean size and a narrower geometric standard deviation are translated into a higher number concentration, which is favorable for inter-coagulation. In summary, for practical application sorbent mean size close to 1 μm, monodisperse and a number concentration larger than 10^7 #/cm^3 are the most effective.

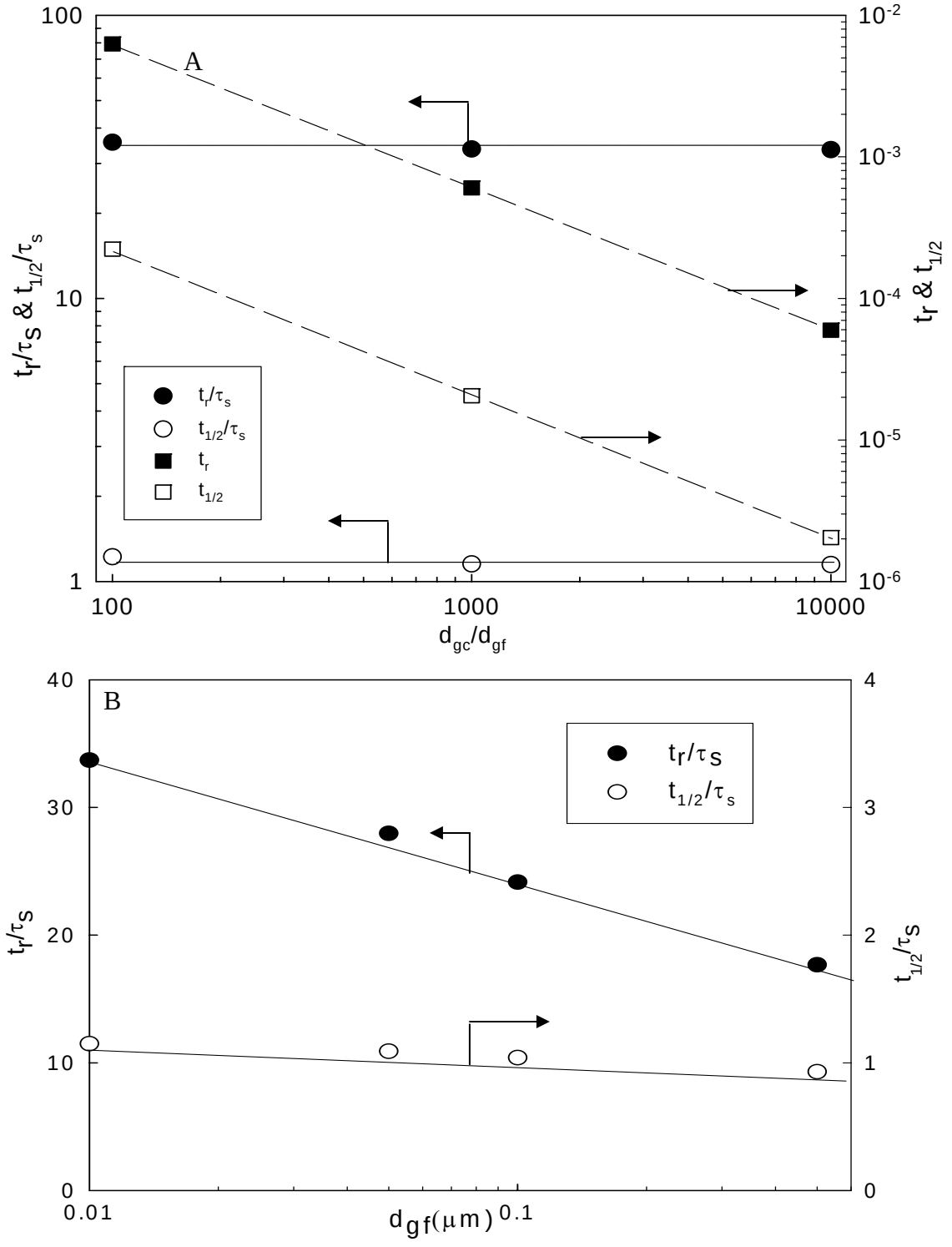

Figure 3-6. Dimensionless removal time and half removal time as function of A) d_{gc}/d_{gf} and B) fine mode mean size

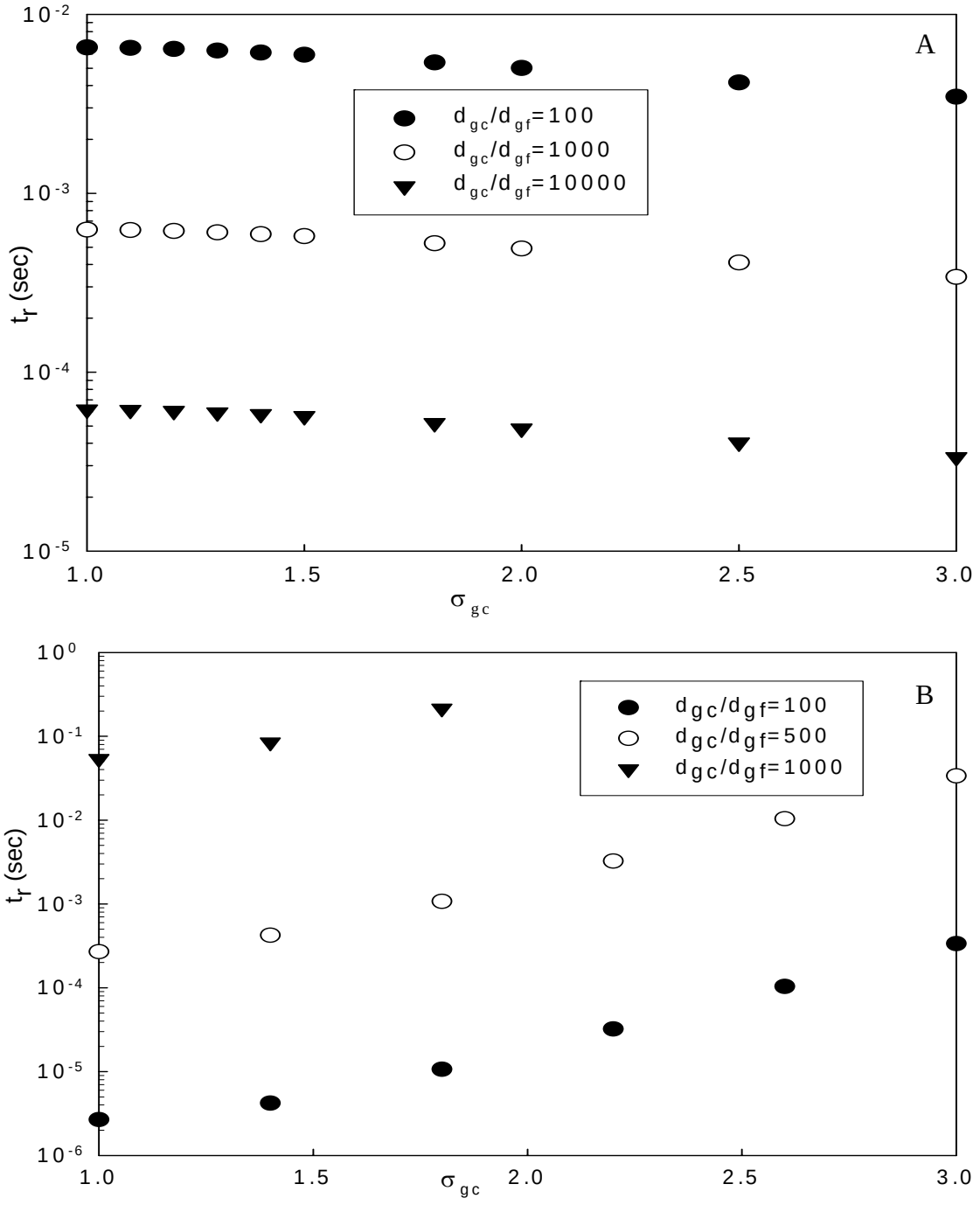

Figure 3-7. Removal time as function of coarse mode standard deviation and d_{gc}/d_{gf} A) with same number concentration ($10^{10}/cm^3$) and B) with same mass concentration ($10\mu g/cm^3$)

Our finding was also applied to an experimental study conducted by Linak et al. (2003). Kaolinite sorbent was used to reduce fine particle formation. A 35% reduction of metal compounds in the fine mode was observed. Condensation was reported to be the responsible mechanism while coagulation was said to have no effect on the reduction. The sorbent feed concentration was 680 mg/m^3 with a mean size of 1.4 μm, while the fine particle feed concentration rate was 83 mg/m^3, with a residence time of 4.1 s. Table 3-2 shows the size distribution parameters used in the calculation and the estimated removal times. Three cases based on the same mass concentration were studied. For case I, d_{gf} was assumed to be 0.01 μm and both geometric standard deviations were assumed to be 1 for the most effective condition. Equations 3-19 and 3-20 were used to calculate the dimensionless removal time and the half life time, and the fine mode particle scavenge characteristic time was calculated using Equation 3-7. The resultant removal time and half life time were 8.1×10^{85} and 8.6×10^{34} s, respectively, clearly showing that coagulation could not work for their system since these values were much greater than the residence time (4.1s). Case II was to simulate sorbent injection at a later stage where intra-coagulation had lowered the fine mode number concentration (using measured PSD of fine mode without sorbent that is reported in Linak et al., 2003). If the same amount of sorbent was injected at this stage, its corresponding removal and half life times were 2,094 and 263 s, both still much longer than the residence time. Other conditions (e.g. larger σ_g) will only result in a longer removal time. Hence, the operating condition in their system clearly was ineffective in removing the fine mode aerosol by inter-coagulation. However, if the sorbent feed was increased two orders higher (68,000 mg/m^3, Case III), the removal and the half life times were down to 2.65 and 0.12 s that

were shorter than the residence time. Using the formula developed in this work, the reason why coagulation was not important in their study was clearly seen and the criteria for effective removal by inter-coagulation can be clearly established.

Analysis was then carried out for an FGD (Flue Gas Desulfurization) system (Harris et al., 1993) that uses slurry droplet injection. For this case, particulate matters which are common components of flue gas also can potentially be removed by inter-coagulation. Table 3-3 summarizes the operating conditions (Harries et al., 1993) and the corresponding droplet size distribution. The particle size distribution of particulate matter (Bacci et al, 1983) is also listed in Table 3. Particulate matter and slurry mass ratio is about 1.07×10^{-6}. However, the large slurry droplet (bigger than 500 μm) with monodisperse assumption results in a very low number concentration ($2.3 \times 10^{2}/cm^{3}$) that requires an extremely long residence time to effectively remove particulate matter in the flue gas. If the droplet mean size is 10 μm instead and the geometric standard deviation is 1.3, its number concentration is 2.1×10^{7} #/cm^{3} and the corresponding particle removal time is only 0.5 sec. The analysis demonstrates that fine particulate matter can potentially be removed using a typical mass loading in an FGD system but the selection of particle size and number concentration is very critical to accomplishing the goal.

Table 3-2. Size distribution parameters and removal time for Linak et al. (2003).

	d_{gf} d_{gc} (μm)	σ_{gf} σ_{gc}	N_{f0} (#/cc)	N_{c0} (#/cc)	t_r (sec)	$t_{1/2}$ (sec)
Case I	0.01 1.4	1 1	4.72×10^{10}	1.80×10^{5}	8.1×10^{85}	8.6×10^{34}
Case II	0.07 1.4	1 1	1.38×10^{8}	1.80×10^{5}	2,094	263
Case III	0.01 1.4	1 1	4.72×10^{10}	1.80×10^{7}	2.65	0.12

Table 3-3. Operating parameters of a FGD system and particle size distribution from a power plant.

	FGD system (Harris, 1993)	Particulate matter (Bacci et al., 1983)
Operating Conditions	Diameter: 1.25 m L/G: 0.015 m^3/Nm^3 Gas flow: 2000 Nm^3/h Slurry flow: 30 m^3/h	N/A
Particle Size Distribution	Actual m_{c0}: 17.4×10^6 mg/m^3 Droplet size > 500 μm σ_{gc}: 1 (assumed) N_{c0}: $2.3x10^2$ $\#/cm^3$(calculated)	m_{f0} : 18.7 mg/m^3 MMD: 0.01 μm (assumed) σ_{gf} :1.3 (assumed) N_{f0} : $7.8x10^9$ $\#/cm^3$ (calculated)
	Desired Droplet size : 10 μm σ_{gc}: 1.3 (assumed) N_{c0}: $2.1x10^7$ $\#/cm^3$(calculated)	

Conclusions

Sorbent injection technique is one promising method to control the emission of submicron metal compounds from the combustion system. Under this bimodally distributed condition, inter-coagulation can be a key mechanism for sorbent injection technique.

In this work, the effects of inter-coagulation on removing fine mode aerosol were studied. High number concentration of coarse mode, large mean size difference, and narrow geometric standard deviation of fine mode were found to favor higher inter-coagulation rate. The removal time can also be expressed in the dimensionless form. Two key parameters that affect the dimensionless removal time are the geometric standard deviation of the fine mode (when the normalized fine mode concentration is less than 10)

and the geometric mean size of the fine mode. The developed formula can be used as a convenient tool to estimate the removal time once the particle scavenge characteristic time is determined.

When inter-coagulation is the dominant mechanism for removing fine mode particles, its geometric standard deviation approaches monodisperse. For coarse mode particles, the geometric standard deviation approaches the asymptotic value because intra-coagulation is still the dominant mechanism. With regard to sorbent application where minimal mass loading is desired, a narrow size deviation and a small mean size of the coarse mode yield the optimal effectiveness. The reason is due to the corresponding high number concentration that is the critical parameter to inter-coagulation. Using the formula developed in this work, the criteria for effective removal of fine mode aerosol can be clearly established.

CHAPTER 4
MECHANISTIC STUDY OF SORBENT INJECTION TO CONTROL VANADIUM EMISSION USING AEROSOL REACTOR

Introduction

Vanadium is one of the major trace components in coal and oil (Bryers, 1995; Linak and Miller, 2000; Swain, 1991; Yee and Rosenquist, 1996). In a study on characterizing the particulate emissions from a large oil fuel fired power plant, 88 wt% of vanadium was reported to be in the size range of 0.01 to 1.0 μm (Bacci et al., 1983). Ambient particulate matter sampling at urban area used vanadium as a primary marker for fuel oil combustion (Divita et. al., 1996) and showed it was highly concentrated in the submicron regime (Tolocka et. al, 2004). Vanadium is known to be more toxic when inhaled and relatively less so when ingested (Boyd and Kustin, 1984). It may also cause cardiovascular diseases, bronchitis and lung carcinoma (Yee and Rosenquist, 1996). Unfortunately, traditional control devices have their minimum collection efficiencies in the submicron size regime (Biswas and Wu, 1998; Flagan and Seinfeld, 1988; Linak et al, 1993). Thus, it is important to develop new techniques to effectively control vanadium emissions.

In recent years, various studies (Linak et al., 2003; Mahuli et al., 1997; Scotto et al, 1994; Uberoi and Shadman, 1991) have been conducted to use mineral sorbents to capture heavy metals. Figure 1-1 illustrates the mechanism of sorbent injection technique. As shown in Figure 1-1A, vanadium vapor will nucleate and then coagulate and/or condense to form submicron vanadium oxides particles. When sorbents are injected,

vanadium vapor can be adsorbed on the surface of sorbent and nucleation rate will be reduced (Figure 1-1B). As these sorbent particles are typically in the supermicron range, the metal-sorbent particles can be easily collected using traditional particulate control devices. Shadman and co-workers (Scotto et al, 1994; Uberoi and Shadman, 1991) used silica, alumina and various naturally available materials (i.e. bauxite, kaolinite and lime) to capture lead and cadmium. Linak et al. (1995) used them to capture nickel, lead and cadmium. Mahuli et al. (1997) tested hydrated lime, alumina and silica for arsenic control. Venkatesh et al. (1996) evaluated various mineral sorbents constituting a spectrum of alumino-silicate compounds and a pulgite clay for immobilization of several trace metallic species. Biswas and co-workers (McMillin et al., 1996; Owens and Biswas, 1996; Wu et al., 1998) generated sorbent particles with very high surface area *in-situ* to capture lead and mercury. However, there have been few studies that examine the use of mineral sorbent materials to capture vanadium.

The sorbent process can be divided into two steps: mass transfer (vanadium transfer to the surface of sorbent) followed by surface interaction. If the metal is in vapor phase, condensation is the mass transfer process. If sorbents are injected where the metal vapor has nucleated, coagulation is the mass transfer process. In the previous studies (Carey et al, 2000; Linak et al., 1995; Linak et al., 1998; Uberoi and Shadman, 1991), the system was generally condensation favored condition because temperature was very high where the metal was in the vapor phase. However, Friedlander et al. (1991) demonstrated that the scavenging of fine particles by coarse mode particles through coagulation can be the dominant mechanism. Surface interaction can be either physical adsorption or chemical adsorption. Previous sorbent studies (Mahuli et al., 1997; Punjak et al, 1989; Uberoi and

Shadman, 1991) demonstrated that the dominant mechanism of surface interaction was chemical adsorption according to their XRD measurement data. Though its amount was much less than chemical adsorption, physical adsorption was also identified in some sorbent-metal system (Chen et al, 2001; Punjak et al, 1989; Iida et al., 2004). In such a metal-sorbent system, there are fine mode particles formed by metal compound and coarse mode particles of injected sorbent. Thus, a bimodal aerosol model which incorporates various aerosol mechanisms can be a useful tool to investigate the dynamics of the system. Lee and Wu (2004) has developed a convenient equation to estimate the removal time (99.99 wt%) for sorbent injection technique using a bimodal lognormal model when coagulation is the dominant mechanism.

Most studies have focused on demonstrating the ability of various sorbent materials to remove metal vapors from the gas stream. In this study, a mechanistic study was conducted to determine the preferable mechanism for sorbent injection technique. First, sorbent material was selected by feasibility experiments based on their chemical affinity. Coagulation only and condensation only cases were then conducted and compared. Finally the effect of surface interaction was determined through the use of different sorbent materials. Bimodal lognormal modeling was also conducted to gain insights into the experimental results. With this study, the preferable process for mass transfer and limiting process for sorbent injection technique was determined.

Experiments

Pot Experiment: Feasibility Study

To verify the thermodynamic equilibrium results (Chapter 2), pot experiments were conducted. Two sorbent materials, $CaCO_3$ (Fisher, powder, 99%, reagent grade) and Na_2CO_3 (Fisher, powder, 99.5%, reagent grade) were tested. The furnace (Thermolyne, F-

A1730) was heated up to the designated temperature. A ceramic pot containing sorbent and/or vanadium (Fisher, vanadium powder 99.5%) in 2% nitric acid was then placed into the furnace. The sample was retrieved 10 minutes later. The products were identified by X Ray Diffraction (XRD) and compared with the result of thermodynamic analyses (Chapter 2). The experimental conditions are summarized in Table 4-1.

Table 4-1. Feasibility study experimental conditions

	Conditions	Molar ratio (sorbent : vanadium)	Temperature (^{o}C)
Set I	Vanadium only	0 : 1	400, 600
Set II	$CaCO_3$ + Vanadium	1.2 : 1	400, 600, 800
Set III	Na_2CO_3 + Vanadium	1.2 : 1	400,600

Aerosol Reactor Experiment

Coagulation dominant system

Figure 4-1 shows the schematic diagram of the experimental setup of the aerosol reactor system. Vanadium solution was prepared by dissolving elemental vanadium in 2% nitric acid which was introduced into the system by a Collison nebulizer (BGI, TN25). The atomized vanadium containing mist was passed through a diffusion dryer to remove the water content. The aerosol particle size can be controlled by varying the properties of the atomized droplets according to the following equation (Hinds, 1999) .

$$d_p=d_d(Fv)^{1/3} \quad (4\text{-}1)$$

where, d_p is diameter of final solid aerosol particle, d_d is droplet diameter, and Fv is volume fraction of solid material. Sorbent droplets were fed into the system using either a Collison nebulizer (BGI, TN25) or ultrasonic nebulizer (Sonaer, 24M) right before the inlet of the tubular aerosol reactor. The sorbent solution was also prepared by dissolving

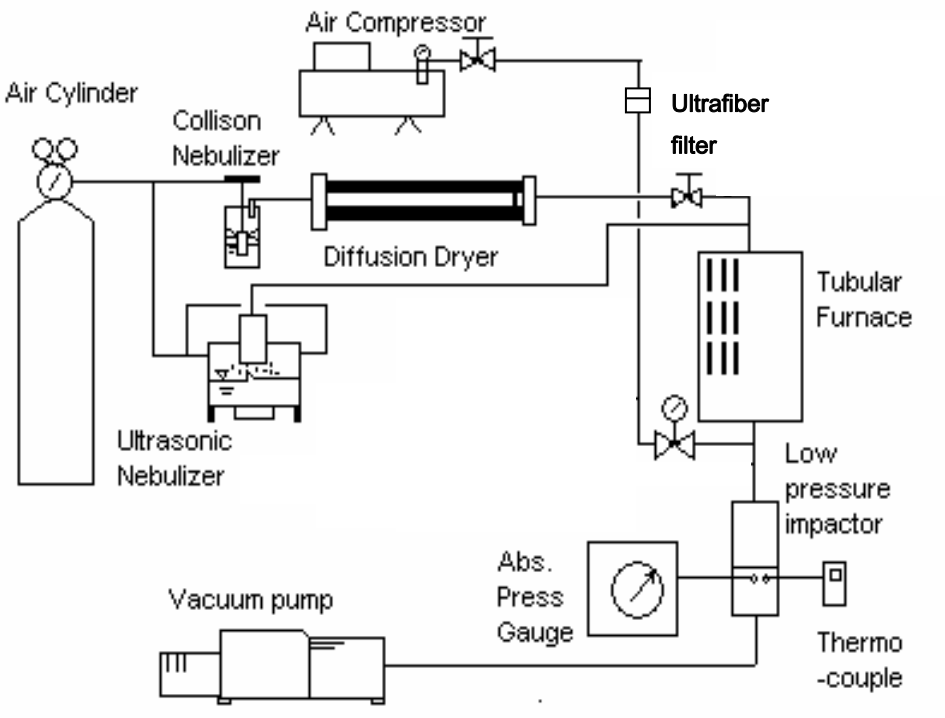

Figure 4-1. Experimental set-up of the aerosol reactor system

sorbent material in 2% nitric acid.An ultrasonic nebulizer can provide a higher number concentration of sorbent than a Collison nebulizer can and therefore was used to investigate the effect of number concentration change. The aerosol reactor (diameter: 1.651 cm, height: 45.72 cm, stainless steel) temperature was maintained by a tubular furnace (Thermolyne 73900). Reactor temperature profile at 740 ^{o}C is in Figure 4-2. Aerosol free dilution air through an ultra fiber filter (MSA, 76876) was introduced at the exit of the tubular reactor to quench the reaction and aerosol dynamics. A Lundgren low pressure impactor (LPI) was used downstream to collect and classify particles by their aerodynamic size. It has 6 stages for atmospheric pressure and 6 stages for low pressure (under 1 atm) which are designed to collect submicron particles. Glass fiber filter (Millipore, AP2004700) was placed at the last stage of impactor to collect particles less

than the cutoff size of the 5th stage. Its cutoff diameters are determined by orifice pressure and temperature (Lundgren and Vanderpool, 1988). When orifice temperature is 29.3^{o}C and pressure is 209.3 mmHg, its cutoff sizes are 11.05, 5.54, 2.91, 1.73, 0.96, 0.50, 0.44, 0.29, 0.18, 0.09 μm. Its upper limit (30 μm) and lowest limit (0.01 μm) of cutoff size were determined where the mass cumulated curve was 100%. Apiezon L grease (10% in benzene) was applied on stainless steel substrate to reduce bounce off effect. To eliminate condensed water vapor, substrates were dried in desiccators for at least one day before and after they were used. A highly sensitive micro balance (Sartorius, MC 210S, 10^{-5}g) was used to measure the sample mass.

Experimental condition

To investigate the effect of size distribution on the sorbent injection technique, the concentration of vanadium solution was varied and the sorbent was generated by two methods. Experiments were first conducted for vanadium alone to characterize its particle size distribution. Experiments were then carried out by adding $CaCO_3$ sorbents to examine its effect on the size distribution of vanadium particles. In set I, a Collison nebulizer (BGI, TN-25) was used and an ultrasonic nebulizer (Sonaer, 24M) was used in set II because the ultra sonic nebulizer generated 10 times more sorbent particles compared to the Collison nebulizer. Elemental calcium and vanadium mass concentration in reactor were 10 and 0.21 mg/m^3 for Set I, 12.7 and 0.07 mg/m^3 for Set II. The experimental conditions are summarized in Table 4-2.

Condensation dominant system

The experimental setup for the condensation dominant system is similar to that for the coagulation dominant system except the section of vanadium precursor generation.

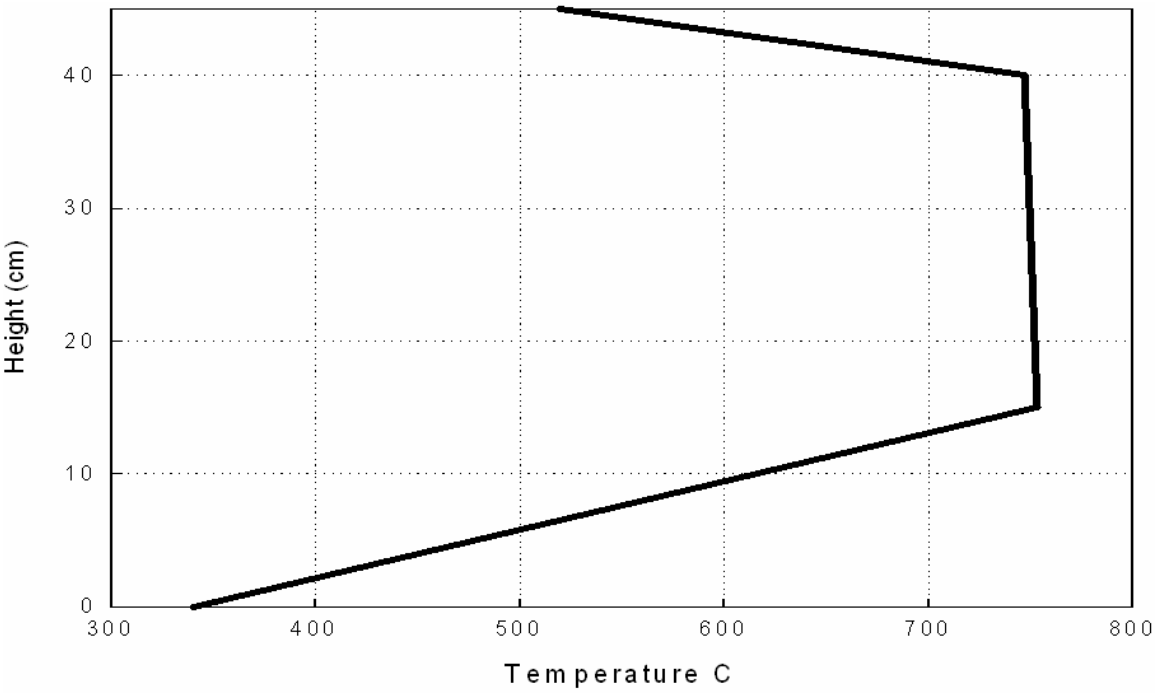

Figure 4-2. Measured reactor temperature profile from bottom to top at 740°C.

Table 4-2. Coagulation dominant system experimental conditions

	Solution concentration (ppm)		Time (hr)	Temperature (°C)	Residence time (sec)
	$CaCO_3$	Vanadium			
Set I-1	0	500	2	740	0.34
Set I-2	23,000	500	2	740	0.34
Set II-1	0	50	2	740	0.42
Set II-2	23,000	50	2	740	0.42

To provide vanadium in the vapor form, Vanadium Tri-I-Propoxy Oxide (VTIPO, Strem) which has a relatively high vapor pressure at room temperature was chosen. A bubbler was used to provide a constant vanadium precursor supply by saturating 2 L/min dry air with VTIPO vapor.

Experimental conditions

Experiments were first carried out for VTIPO. Since hydrolysis would be a key mechanism for generating vanadium oxide, the effect of temperature and humidity was investigated by using dry and humid air at room temperature and 740 ^{o}C. Finally, surface hydrolysis effect was tested by injecting water droplet instead of water vapor.

Experiments were then carried out for two types of sorbent. Based on the thermodynamic equilibrium study and feasibility study, $CaCO_3$ was chosen for chemical adsorption. Silica sorbent (specific surface area 170 m^2/g, amorphous fumed, Alfa Aesar) with high surface area but no chemical affinity with vanadium was selected for physical adsorption. $CaCO_3$ was dissolved in 2% nitric acid while silica was mixed and suspended in 2% nitric acid. The sorbent particles were generated by the same ultrasonic nebulizer. As baseline, the particle size distributions of $CaCO_3$ and silica sorbent were measured respectively. The sorbent was then introduced into the reactor together with VTIPO vapor. Elemental calcium, silica, vanadium mass concentration at reactor were 40, 80, and 9.25 mg/m^3, respectively. The experimental conditions are summarized in Table 4-3.

Product characterization

Element size distribution: To determine the elemental distribution by size, the collected particles at each impactor stage were dissolved in 2% nitric acid. The concentration of each element (V and Ca) was measured by Inductively Coupled Plasma emission spectroscopy (ICP, Perkin-Elmer Plasma 3200). The total amount at each stage was then determined by multiplying the concentration by the solution volume (50 mL).

Product morphology and elemental mapping: Scanning Electron Microscopy (SEM, JEOL 6330) / Energy Dispersive X-ray (EDX) was used for surface morphology and mapping elemental distribution on the surface of particles.

Table 4-3. Condensation dominant system experimental conditions

	Vanadium		Sorbent in 2% Nitric acid (10 g/L)		Temperature (^oC)	Residence time (sec)
	Material	Carrier air feedrate (L/min)	Material	Carrier air feedrate (L/min)		
Set I-1	VTIPO	2	dry air	5	room	0.3
Set I-2	VTIPO	2	humid air	5	room	0.3
Set I-3	VTIPO	2	dry air	5	740	0.3
Set I-4	VTIPO	2	humid air	5	740	0.3
Set I-5	VTIPO	2	Water	5	740	0.3
Set II-1	Air	2	$CaCO_3$	5	740	0.3
Set II-2	VTIPO	2	$CaCO_3$	5	740	0.3
Set III-1	Air	2	Silica	5	740	0.3
Set III-2	VTIPO	2	Silica	5	740	0.3

Product speciation: X-Ray Diffraction (XRD, Philips APD 3720**)** was used to identify crystalline species of collected particles. Raman spectroscopy (Confocal system, 632-nm excitation) was also used to identify species that were not in crystalline form.

Model Description

The Modal Aerosol Dynamic (MAD) model that was described in detail in Chapter 3 was used for this study to simulate and examine the aerosol dynamics in the system. In this study, coagulation and condensation were compared to determine the effective mechanism that was responsible for capturing vanadium.

The condensational volume growth for the fine mode (free molecule regime) is

$$\frac{\partial M_{3f}}{\partial t} = B_1(S-1)\int_0^\infty d_p^2 n(d_p) d(d_p) \qquad (4\text{-}2a)$$

and that for the coarse mode (continuum regime) is

$$\frac{dM_{3c}}{dt} = B_3(S-1)\int_0^{\infty} d_p^1 n(d_p)d(d_p) \tag{4-2b}$$

where, $B_1 = (36\pi)^{1/3} v_1 n_s \sqrt{\frac{k_B T}{2\pi m_1}}$ and $B_3 = \left(\frac{16}{9}\pi^2\right)^{1/3} \lambda v_1 n_s \sqrt{\frac{8k_B T}{\pi m_1}}$. Definition of the variables can be found in the Nomenclature section. Condensational volume growth is proportional to saturation ratio and its total surface area for the free molecule regime and total diameter for the continuum regime, respectively (Prastinis, 1988).

Volume change by inter-coagulation (Whitby and McMurry, 1997) for the fine mode and the coarse mode are given by

$$\frac{\partial}{\partial t}(M_{3f}) = -\int_0^{\infty}\int_0^{\infty} dp_f^3 \beta(dp_f, dp_c) n_f(dp_f) n_c(dp_c) ddp_f ddp_c \tag{4-3a}$$

$$\begin{aligned}\frac{\partial}{\partial t}(M_{3c}) = &\int_0^{\infty}\int_0^{\infty} (dp_f^3 + dp_c^3)\ \beta(dp_f, dp_c) n_f(dp_f) n_c(dp_c) ddp_f ddp_c \\ &-\int_0^{\infty}\int_0^{\infty} dp_c^3 \beta(dp_f, dp_c) n_f(dp_f) n_c(dp_c) ddp_f ddp_c\end{aligned} \tag{4-3b}$$

Nucleated particles are in the free molecule regime and sorbent particles are in the continuum regime. Volume of the fine mode particles is reduced while volume of the coarse mode is increased by inter-coagulation.

The initial conditions of the simulations were based on the experimental condition. Metal vapor was assumed as vanadium pentaoxide. Three cases were simulated. First, all vapor was assumed to have nucleated instantly. Simulations were conducted with sorbent particles and without sorbent particles. Mechanism for the case with sorbent particles was bimodal coagulation which includes intra-coagulation and inter-coagulation (case 1a). Mechanism for the case without sorbent particles is unimodal coagulation which is intra-coagulation (case 1b). Second, nucleation was suppressed and condensation was the only mechanism allowed (case 2). Finally, 50% of vanadium vapor assumed to have instantly

nucleated while the remaining 50% was in the vapor phase. Both condensation and coagulation were possible mechanisms in such a scenario (case 3). The simulation conditions are listed in Table 4-4.

Table 4-4. Summarized simulation conditions

	σ_{g1}	M_{10} (#/cm^3)	dp_1 (A)	σ_{g2}	M_{20} (#/cm^3)	dp_2 (μm)	Vapor pressure (mmHg)	Mechanism investigated
Case1a	1	6.210×10^{13}	6.285	2.087	3.89×10^{5}	1.07	N/A	Intra-, inter-coagulation
Case1b	1	6.210×10^{13}	6.285	N/A	N/A	N/A	N/A	Intra-coagulation
Case2	N/A	N/A	N/A	2.087	3.89×10^{5}	1.07	0.006572	Condensation
Case3	1	3.106×10^{13}	6.285	2.087	3.89×10^{5}	1.07	0.003496	Intra-, inter-coagulation Condensation

Results and Discussion

Pot Experiment

Figures 2-1 and 2-2 show the partition of vanadium species in a typical coal combustion system without and with chlorine and sulfur, according to equilibrium analysis. Vanadium pentaoxide was the dominant product until the temperature reached 1000 K. Figure 4-3 shows the XRD results for vanadium only case at 673 K and 873 K. These compounds were identified as vanadium pentaoxide which agreed with the prediction by the thermodynamic equilibrium analysis.

Figure 4-4 shows the crystalline species identified when $CaCO_3$ sorbent was added to the pot in addition to vanadium. It clearly showed that different compounds were formed at different temperatures. $Ca_2V_2O_7$ and $Ca_3(VO_4)_2$ were the major compounds. Other products such as CaO and $Ca(OH)_2$ were also detected since Ca-based sorbent was more than the stoichiometric amount of vanadium. Thermodynamic equilibrium

calculations showed that different dominating compounds at different temperatures (Figure 2-3A) and they well matched the results of the pot experiment.

Figure 4-5 shows the result when Na- based sorbent was added. It also well matched with the thermodynamic calculation (Figure 2-3B). This figure showed only the result at 673 K because the material produced at 873 K was extremely sensitive to ambient air moisture and formed damp material that could not be identified by XRD.

The feasibility study discussed above verified the results of thermodynamic equilibrium analysis and clearly demonstrated both sorbents' ability to chemically bond with vanadium. It should be noted that the residence time in a typical combustion system is much shorter than the residence time in the pot experiment. The ability of the sorbent to capture vanadium during the short flight time therefore needs to be evaluated in an aerosol reactor. Due to the difficulty to identify the speciation of Na- based sorbent system by XRD, Ca-based sorbent was selected for further study in the aerosol reactor.

Aerosol Reactor Experiment

Coagulation dominant

After vanadium vapor has nucleated, coagulation is the only mechanism to remove these submicron particles. Hence, coagulation dominant case was also investigated by introducing vanadium in particulate form. The element size distributions of vanadium only and vanadium with sorbents are shown in Figure 4-6. For both cases, the mass median diameter (MMD) of vanadium increased slightly (0.55 to 0.63 μm for Set I and 0.40 to 0.44 for Set II) when Ca sorbent (MMD was 0.74 and 0.97 μm for Set I and II) was fed into the system. As discussed in Chapter 3, the number concentrations of fine and coarse mode particle are the key parameters that determine whether inter-coagulation or

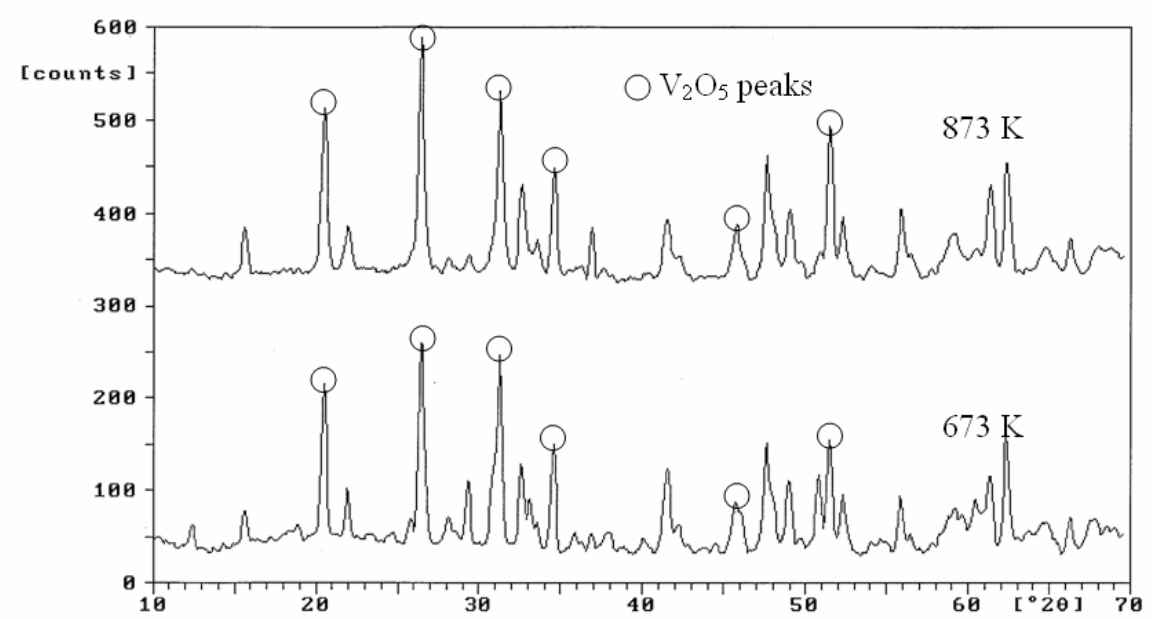

Figure 4-3. XRD result for vanadium only at 673 and 873K

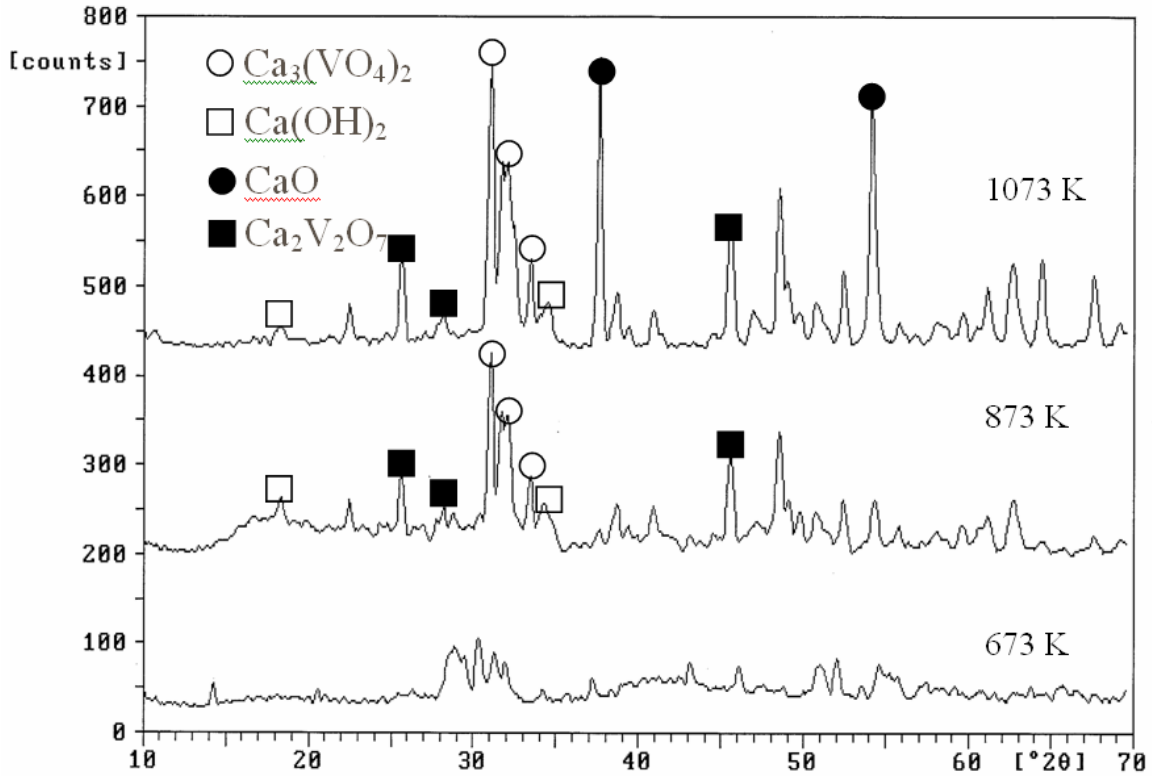

Figure 4-4. XRD result for $CaCO_3$ with vanadium at 673, 873, and 1073K

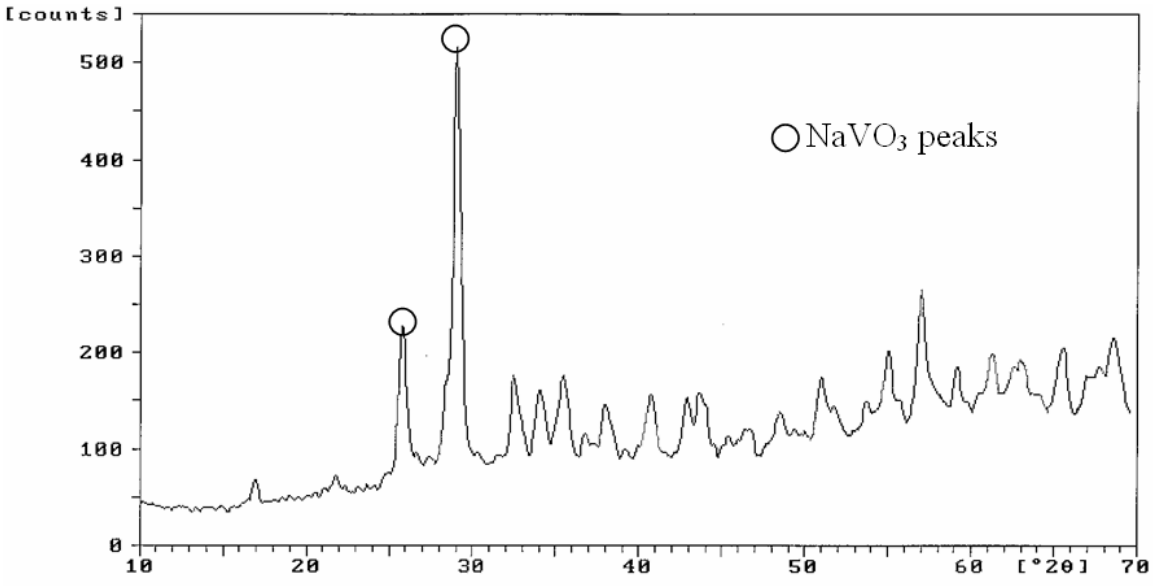

Figure 4-5. XRD results for Na_2CO_3 with vanadium at 673K

intra-coagulation is the dominant mechanism. The number concentration of vanadium particles was $2.27x10^6/cm^3$ and $2.37x10^6/cm^3$ for set I and II, respectively; and the number concentration of Ca-based sorbent was $5.43x10^3/cm^3$ and $6.45x10^4/cm^3$ for set I and II, respectively. Assuming the best condition (monodisperse aerosol for both fine mode and coarse mode) for inter-coagulation, its fine mode 99.99% removal time and half removal time following Eqs. 3.19 and 3.20 derived in Chapter 3 were more than 7.6 and 1.8 hours. Since the residence time of these sets of experiments was only 0.3 seconds, the theoretical analysis clearly showed that inter-coagulation could not work as the major mechanism to remove the fine mode vanadium particles under this experimental condition. Typically the flue gas residence time in a combustion system is less than 10 seconds. Thus, the proper number concentration of sorbent particles to reduce the removal time to less than 10 seconds should be more than $10^7/cm^3$. The result agrees with the observation reported by Linak et al. (2003) who applied kaolinite sorbent to reduce fine particle formation. Its number concentration of kaolinite sorbent was $1.80x10^5/cm^3$ while that of fine mode metal aerosol was $4.72x10^{10}$ #/cm^3. They reported

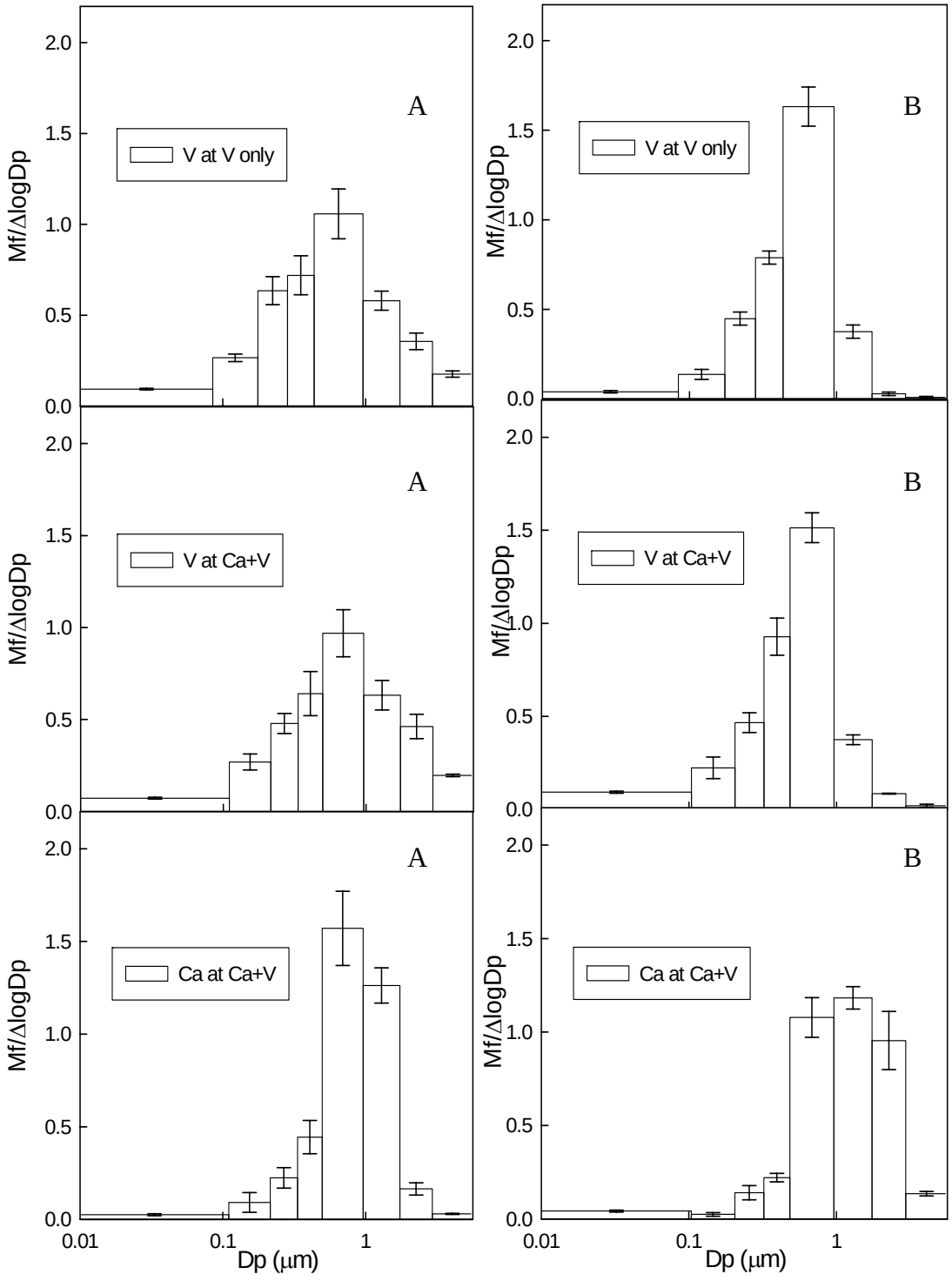

Figure 4-6. Element PSD of vanadium and calcium A) for Set I and B) for Set II at 740^{o}C

that 35% reduction of fine particles was due to condensation and there was no coagulation effect on fine particle reduction. To accomplish fine mode removal by coagulation, the sorbent feed needs to be increased at least 2 orders higher (See Table 3-2).

Condensation dominant

Vanadium precursor characterization. VTIPO forms vanadium oxide compound by hydrolysis and/or thermal decomposition. As baseline, VTIPO vapor was introduced into the reactor with dry air (no hydrolysis) at room temperature (no thermal decomposition). As expected, there were no particles collected by the LPI. To compare hydrolysis and thermal decomposition, VTIPO was introduced into the reactor with humid air and dry air at 740^{o}C respectively. With dry air, only thermal decomposition occurred, while both thermal decomposition and hydrolysis occurred with the presence of water vapor. Finally instead of water vapor, water droplets generated by ultra sonic nebulizer were introduced into the system. In this case, hydrolysis would occur on the surface of the water droplet.

Figure 4-7 shows the PSDs of vanadium element in dry air and humid air at 740^{o}C, respectively. These two cases showed very similar distributions. Vanadium mostly concentrated in the filter stage that is smaller than 0.178 μm. When vanadium precursor (VTIPO) undergoes hydrolysis or thermal decomposition, it forms vanadium oxides. These vanadium oxides quickly nucleate because their saturation vapor pressure is very low (1.12x10^{-8} mmHg and Saturation ratio: 5868) at 740^{o}C. Instantly, nucleation results in a burst of extremely high concentration of nanoparticles. These particles will grow following coagulation and/or condensation. However, the short residence time of the

aerosol reactor (only 0.3 seconds) would only allow the growth to very fine sizes. Figure 4-8 shows the morphology of vanadium oxide compound collected on the filter. When water vapor was present, vanadium oxide formed well shaped spherical particles indicating the strong effects of condensation (Figure 4-8A). On the other hand vanadium oxide formed by only thermal decomposition showed much smaller primary particles implying the importance of coagulation (Figure 4-8B).

VTIPO is one of metal alkoxides which undergo hydrolysis. The rate of hydrolysis of a metal alkoxide depends on the characteristics of the metal and those of the alkyl group. In general, silicon alkoxides are among the slowest to hydrolyze, and for a given metal alkoxide the hydrolysis rate increases as the length of the alkyl group decreases (Rahaman, 1995). There are limited studies about the hydrolysis of VTIPO. However, Titanium TetraIsoPropoxide (TTIP), which has the same alkyl group, is a common material to make TiO_2 nanoparticles and there are many studies on hydrolysis and thermal decomposition of TTIP. The reaction rate constant is $3.96x10^5 exp(-8479.7/T)$ for gas phase thermal decomposition (Okuyama et al., 1990) and $3x10^{15} exp(-1013.9/T)$ for gas phase hydrolysis (Seto et al., 1995). Hydrolysis clearly is much faster than thermal decomposition. Based on hydrolysis of TTIP, it is likely that hydrolysis of VTIPO is also faster than thermal decomposition of VTIPO. Supporting this analysis, the total amount of vanadium element collected in humid air was 5 times more than that in dry air in this study. Thermodynamic equilibrium analysis study in Chapter 2 showed that the stable compound for vanadium was vanadium pentaoxide. Assuming that hydrolysis of VTIPO generates vanadium pentaoxide, VTIPO hydrolysis can be given as follows.

$$2VO(OC_3H_7)_3 + 3H_2O \rightarrow V_2O_5 + 6C_3H_7OH$$

Figure 4-9 shows the collected particles on the filer for both cases. With humid air the particles collected were dark green, while with dry air yellow particles were observed. Its final product of vanadium oxide compound could be different based on the observation of the color of collected particles. These particles were characterized by XRD although no crystalline species were identified. Unfortunately Raman spectroscopy also could not identify the species.

The final set of experiment was injecting water droplets to the reactor instead of feeding water vapor. The mass mean diameter of water droplets generated by ultrasonic nebulizer was 1.7 μm (Sonaer, 24M). As shown in Figure 4-10, vanadium PSD with water droplets was shifted to much larger size. Gas phase hydrolysis generated nanoparticles. However, the surface of water droplets was also the active site for hydrolysis once VTIPO vapor diffused to the surface. The surface hydrolysis consequently captured vanadium and reduced the fine particle formation by gas phase hydrolysis.

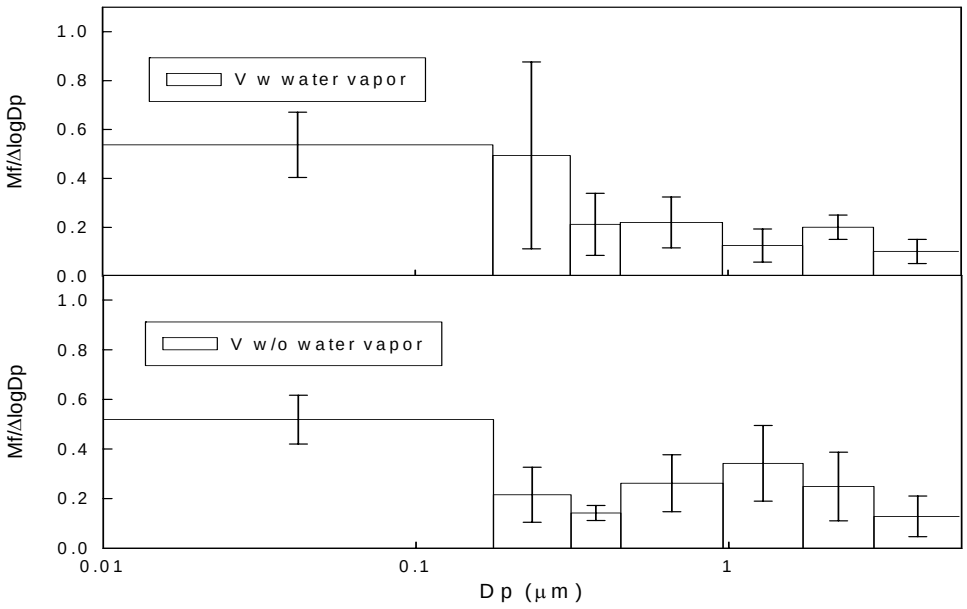

Figure 4-7. Element PSD of vanadium with and without water vapor at 740^{o}C

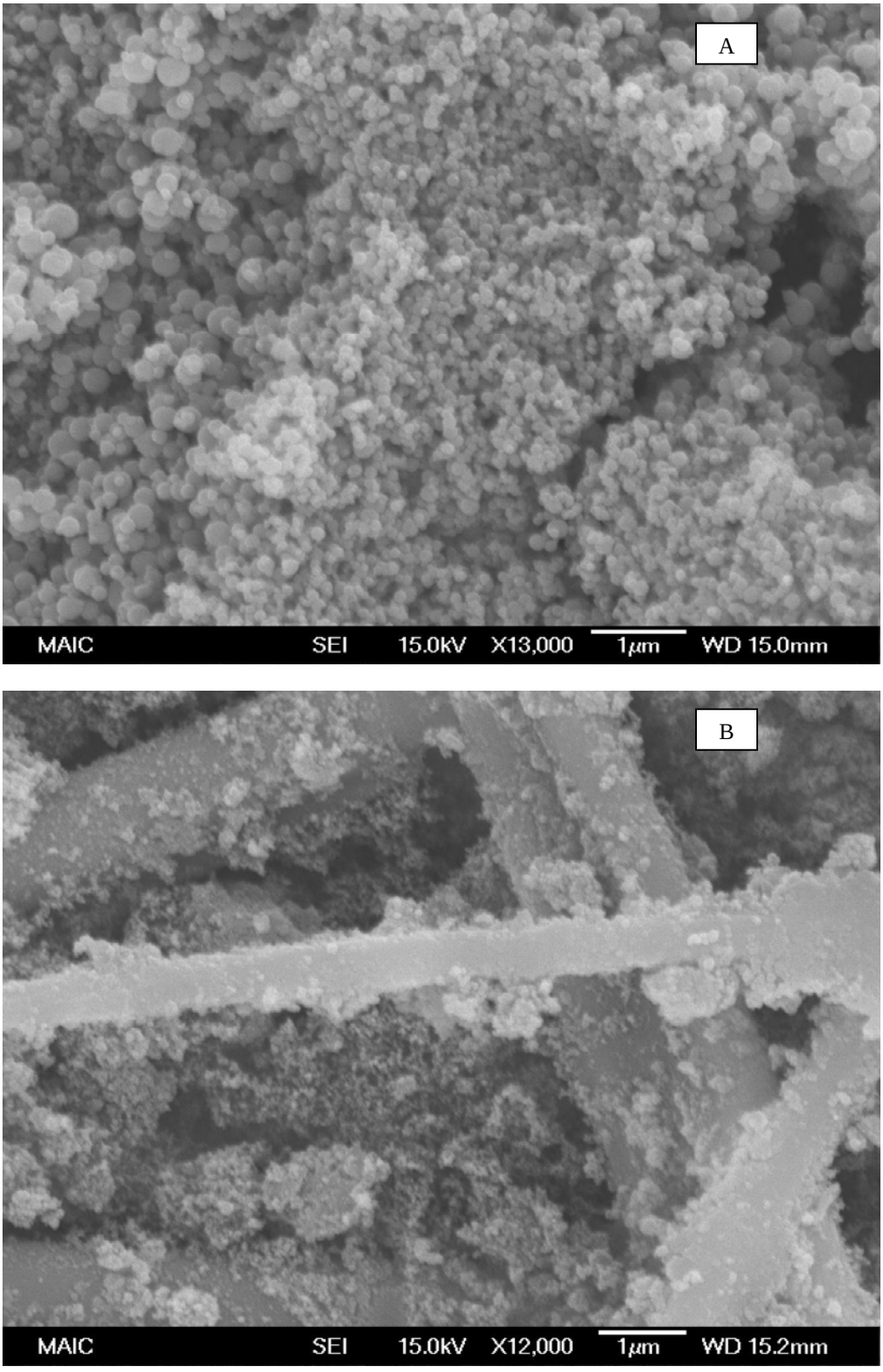

Figure 4-8. Morphology of vanadium oxide compound collected on fiber filter A) by hydrolysis and thermal decomposition and B) by thermal decomposition

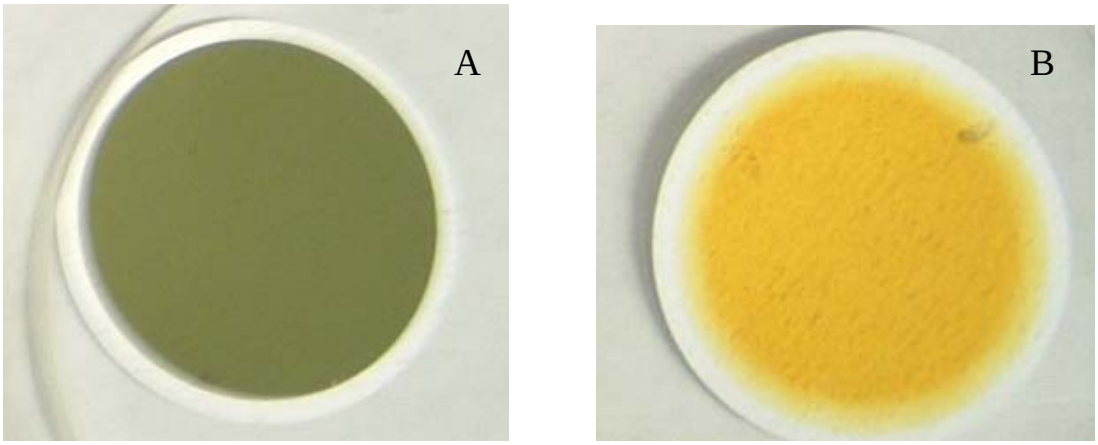

Figure 4-9. Collected vanadium particles on filter A) with water vapor B) without water vapor at 740 ^{o}C

Sorbent injection. Since vapor diffusivity is relatively large, the rate limiting step for effective capture of vanadium vapor for the condensation case will be the surface interaction. Two sets of experiments were conducted to determine the effective surface interaction in the system. In the first set Ca-based sorbent, which showed strong chemical affinity with vanadium in the equilibrium analysis, was used. In the second set Si- based sorbent which has high surface area but no chemical affinity with vanadium, was studied. Comparing results of these two experimental conditions helps reveal the preferable mechanism for surface interaction: chemisorption or physisorption.

Case 1. Ca-based sorbent. Figure 4-10 displays the element PSD of vanadium and calcium. When only VTIPO was introduced, most vanadium was concentrated in the filter stage. After $CaCO_3$ sorbent was injected, vanadium PSD was shifted to around 1 μm size range. Since condensation depends on the surface area of sorbent, the surface area fraction distribution of the sorbent was also plotted in Figure 4-11. As shown, PSD of vanadium when sorbent was injected is very similar to the sorbent surface area fraction distribution, verifying condensation to be the key mechanism in the system.

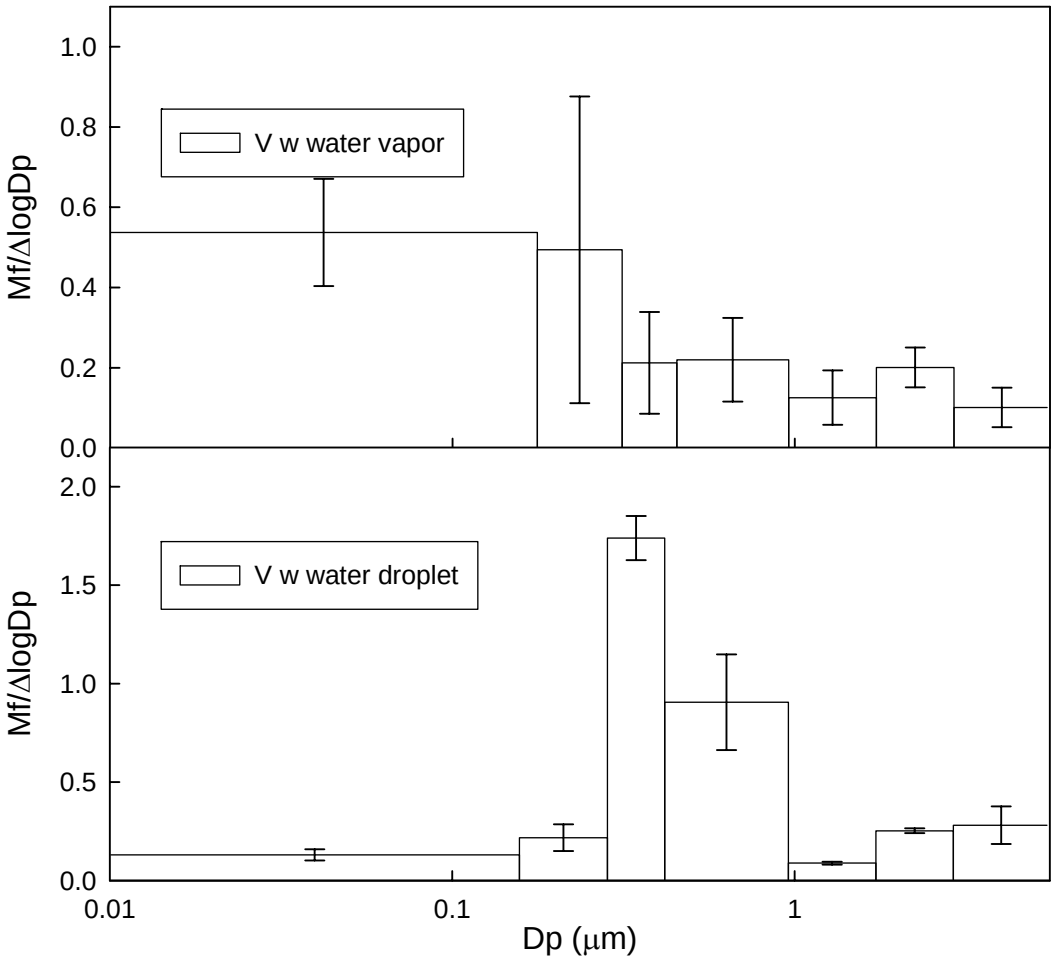

Figure 4-10. Element PSD of vanadium when water droplet injected at 740 oC

Figure 4-12A shows the morphology of $CaCO_3$ sorbent particles in the range of 1.73-0.96 μm. Instead of being present as individual particles in that size range, the collected material appeared to be a big chunk that resulted from merging. It should be noted that all collected materials were placed in a desiccator before characterization. However, the strong hygroscopic property of $CaCO_3$ still yielded merging of the material. Figure 4-12B shows the morphology of particles collected on the same size range when both vanadium and the sorbent were present. It is interesting to observe individual spherical particles in this case, totally different morphology from the sorbent only case. The comparison of these morphologies indicate that when vanadium oxide compounds

were well coated on the surface of sorbent particles, those particles became insensitive to moisture.

In the latter case, vanadium oxide compound formed by surface hydrolysis will deposit on the surface of sorbent. Figure 4-13A shows SEM/EDX for the particles when both $CaCO_3$ and vanadium were present while Figure 4-13B is the Ca mapping and Figure 4-13C is the V- mapping. As shown in Figures 4-13B and 13C, vanadium was much widely distributed than calcium was. If surface chemical reaction forming calcium-vanadium compounds was the main mechanism, these two mapping should show a similar distribution pattern. Figure 4-14 is a SEM picture of one single particle and its corresponding EDX spectrum. As shown, the intensity of vanadium is much stronger than that of calcium. Since calcium and vanadium has similar atomic number, its corresponding concentration based on intensity for vanadium was higher than calcium. However, this is relative value. For the precise quantification of measured particles the calibration of EDX with standard sample are needed. EDX measurement could show that calcium and vanadium were on the one single particle. However, it could not determine the surface interaction.

Case 2. Si- based sorbent. Since chemical affinity between vanadium and the sorbent is not necessary, experiments were carried out using silica to verify if physical adsorption alone can be a possible mechanism for the surface interaction. Silica is hydrophilic but it does not dissolve in water. Thus, silica was selected to investigate the hypothesis. It was well mixed and suspended in 2% nitric acid, then sonicated. Silica sorbent aerosol was generated using the same ultrasonic nebulizer. As baseline, silica sorbent PSD was

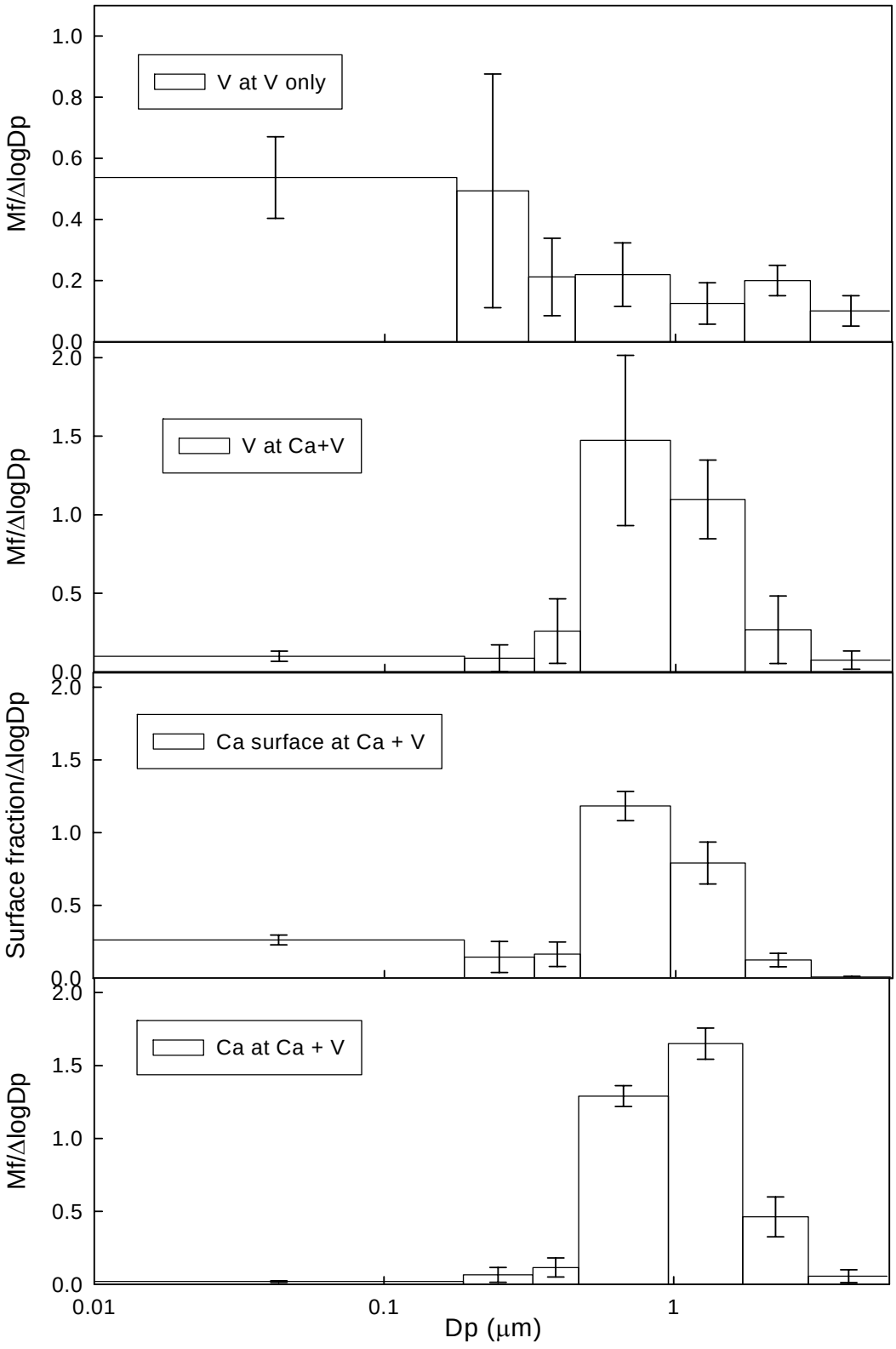

Figure 4-11. Element PSD of vanadium and calcium at 740°C by mass fraction and surface area fraction

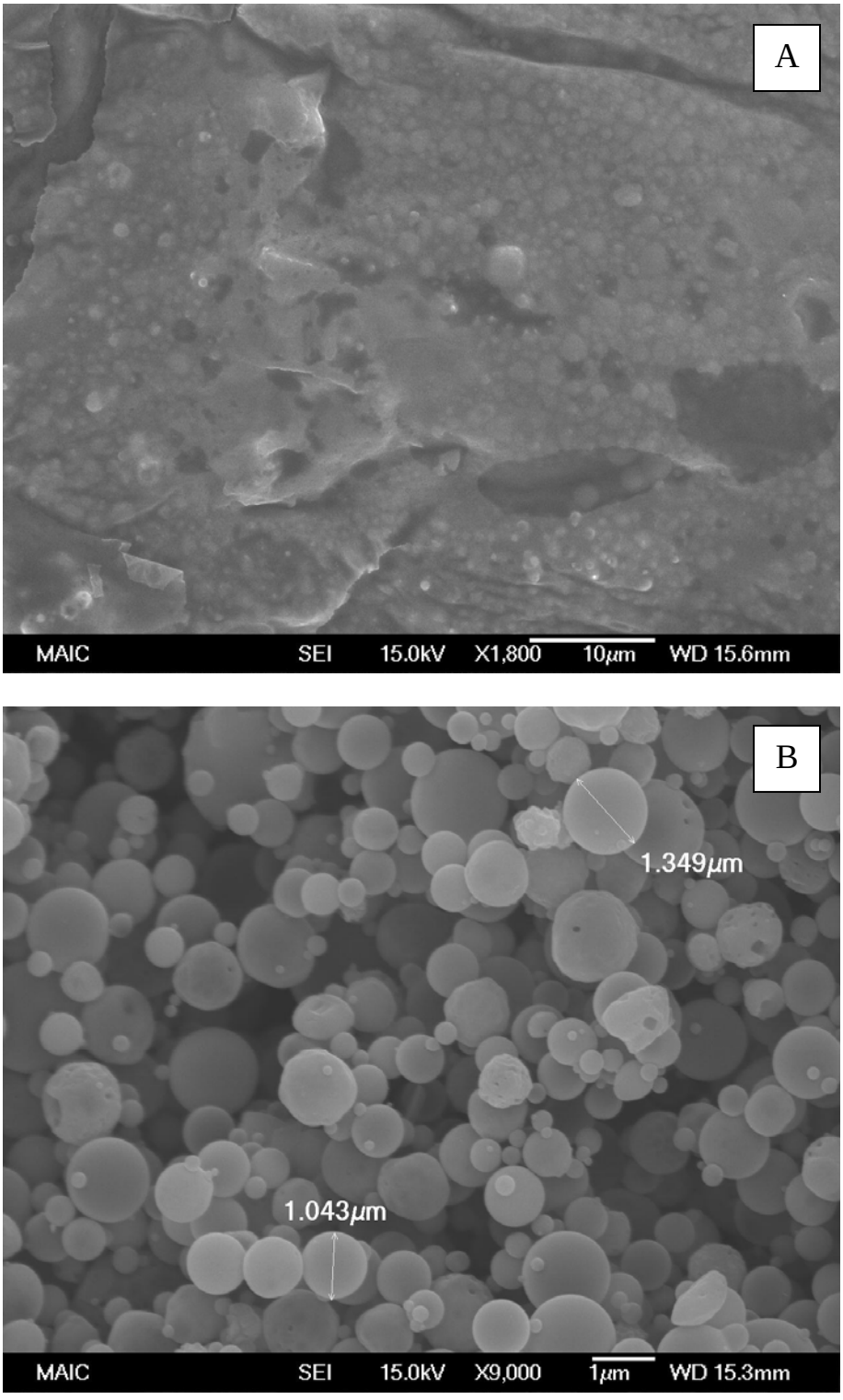

Figure 4-12. Morphology of collected particles when A) Ca-based sorbent was injected and B) Ca-based sorbent with VTIPO were injected

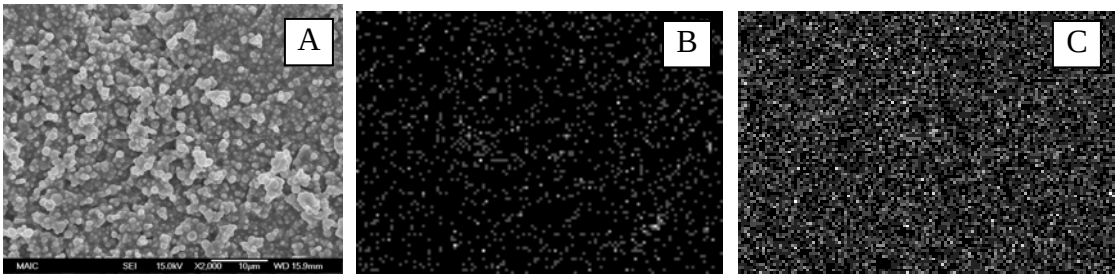

Figure 4-13. SEM picture of A) whole product and EDX mapping B) of Ca and C) of V

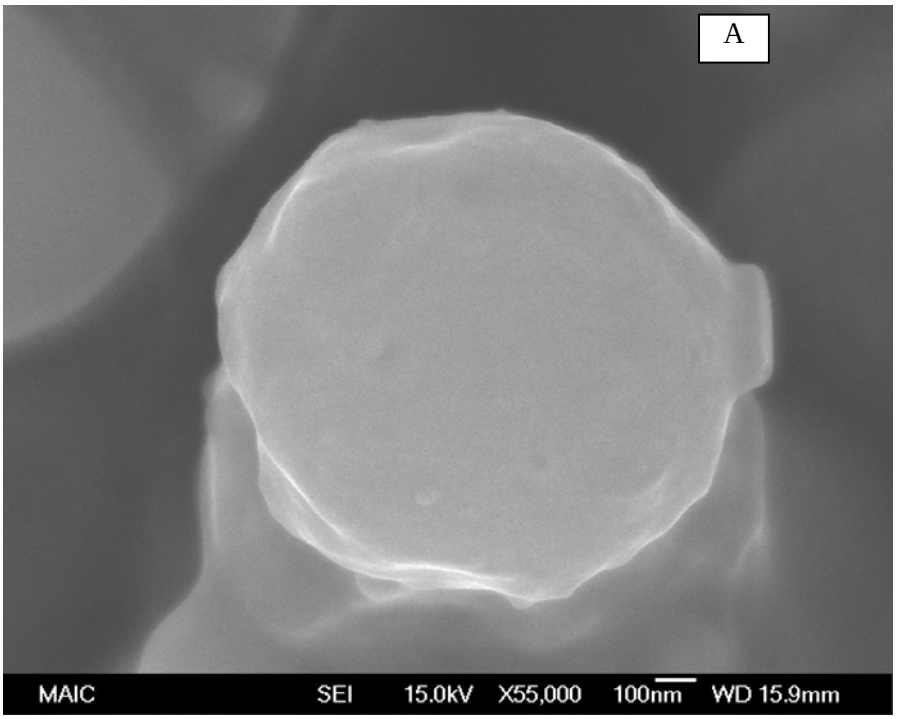

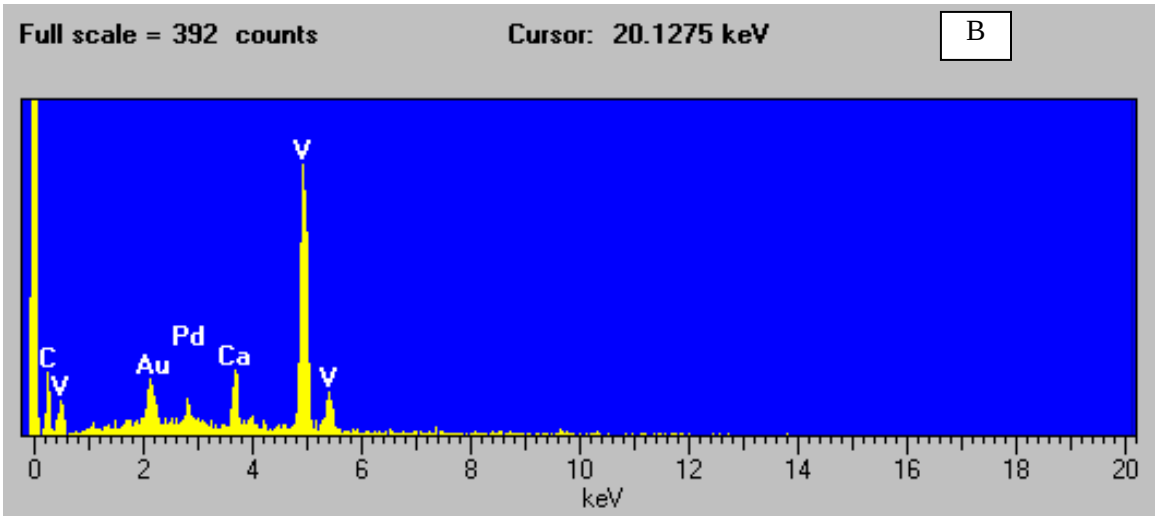

Figure 4-14. SEM picture of A) single particle and B) corresponding EDX spectrum

measured. Experiments were then carried out by injecting sorbent with VTIPO to the reactor.

Figure 4-15 shows element PSD of silica and vanadium. Silica sorbent was mostly concentrated on the 1st and 2nd stages (> 5 μm). When silica sorbent was injected, interestingly vanadium PSD shifted to the 1st and 2nd stages as well. Since silica has high inner pore surface area, its fractional surface area PSD is the same as its fractional mass PSD. Consequently, more vanadium was captured in the 1st and 2nd stages. Although gas phase hydrolysis with water vapor was still present in this system, the results clearly indicated hydrolysis at the pores was the dominating process.

Figure 4-16A shows the SEM image of silica only and Figure 4-16B shows the SEM image of silica with vanadium. As shown, no discernible difference in morphology can be observed indicating that vanadium was captured inside the pores of silica.
As discussed above, both $CaCO_3$ and SiO_2 have been tested for their sorption capability. If the metal capture is limited to chemical adsorption, silica sorbent would not capture any vanadium. The fact that silica sorbent collected the same amount (2.5 mg for 20 minute) of vanadium as $CaCO_3$ sorbent demonstrates that chemical adsorption to form metal-sorbent product is not a necessary step for capturing the metal. In this system studied, surface hydrolysis is the critical mechanism. In a study using silica spheres (Iida et al., 2004) also reported physical condensation to be responsible for manganese vapor removal. Because of the humid condition in the ultrasonic nebulizer, the carrier air was saturated. Hence gas phase hydrolysis was inevitable when sorbent particles were generated by the ultrasonic nebulizer. Once small particles are formed by gas phase hydrolysis, they can not be adsorbed by surface hydrolysis. Consequently, increasing

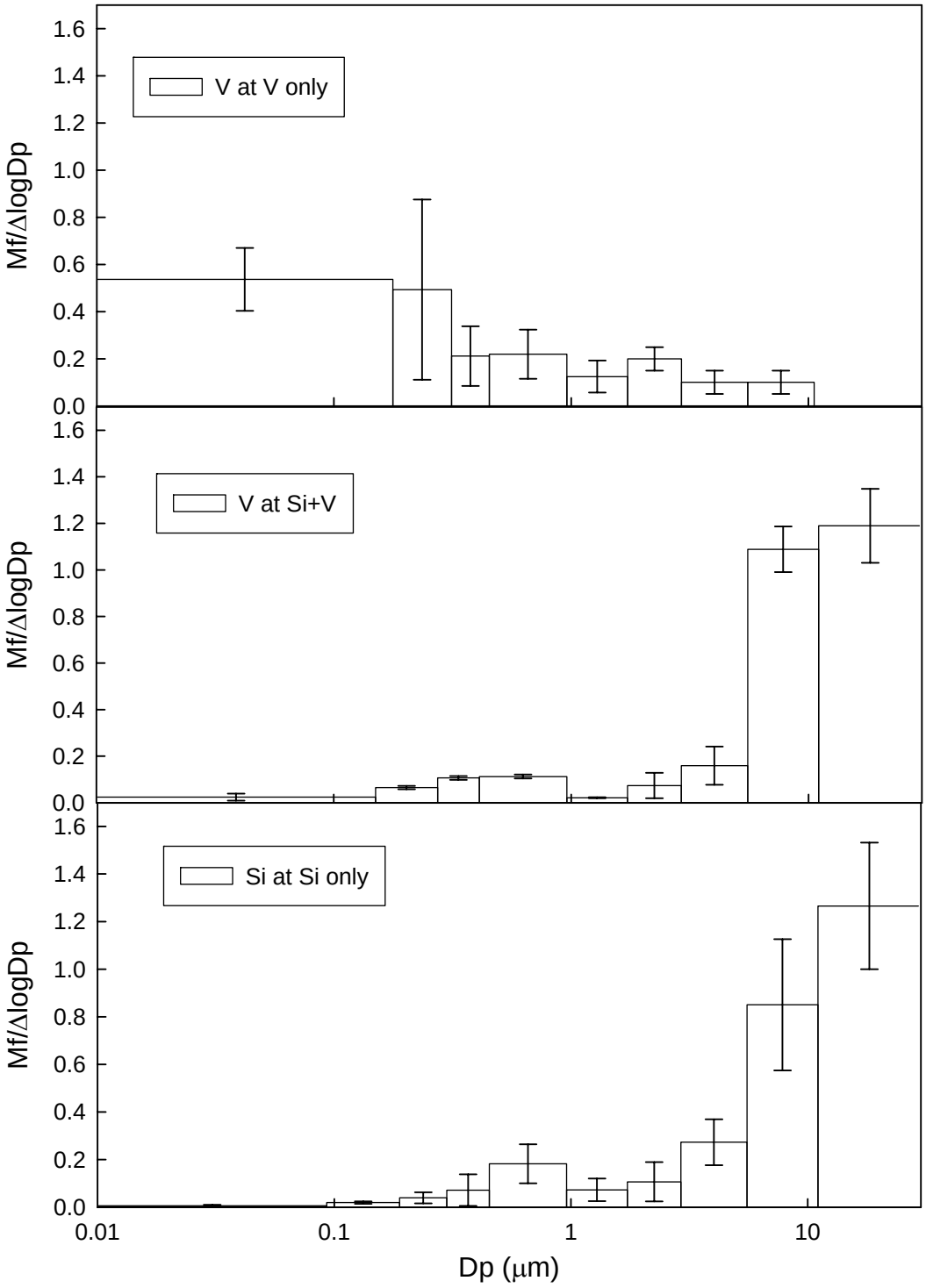

Figure 4-15. Element PSD of vanadium and silica at 740°C

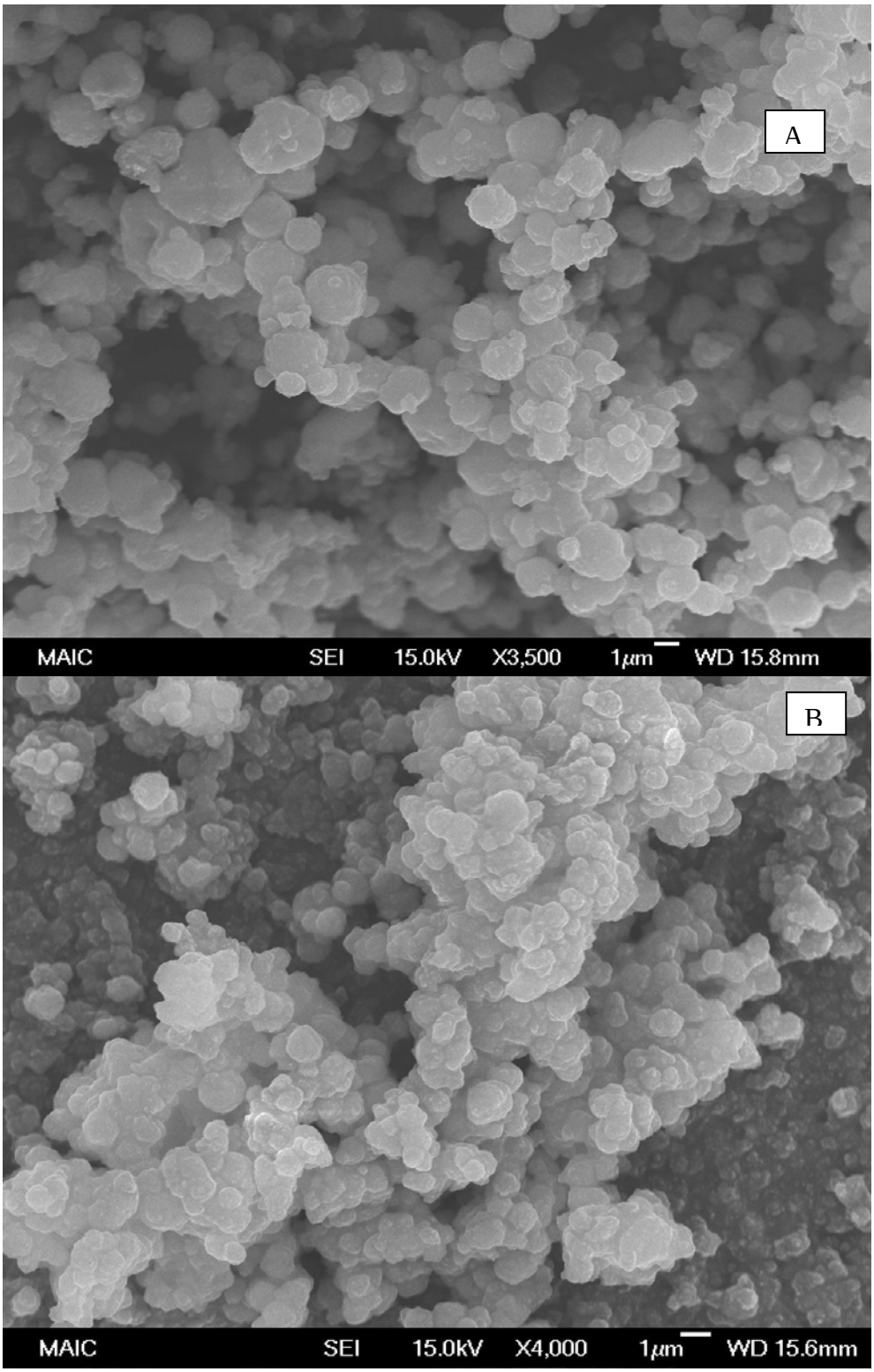

Figure 4-16. Morphology of product A) when silica only are injected and B) when silica with VTIPO was injected 740^{o}C

surface hydrolysis and reducing gas phase hydrolysis are the key factor to enhance the effectiveness of sorbent injection technique in this system.

Bimodal Lognormal Model Study

To gain insight into the effective mechanisms of sorbent injection technique, a bimodal lognormal model study was conducted. In this model, both coagulation and condensation were the key mechanisms considered. The reduction of the fine mode volume and the increase of MMD of the fine mode (more than 1 μm) are the key parameters showing the effectiveness of sorbent injection technique.

Case 1: Bimodal coagulation only and unimodal coagulation only

When sorbent particles were injected where vapor had nucleated instantly, the system undergoes bimodal coagulation. The MMD of the fine mode grows by bimodal coagulation (inter-coagulation and intra-coagulation), however the volume of the fine mode can be removed by only inter-coagulation. To evaluate the effects of inter-coagulation in bimodal coagulation, simulation was also conducted for unimodal coagulation (i.e. no coarse mode sorbent particles). As shown in Figure 4-17A, the initial total number concentration was the same for both cases (bimodal coagulation, dot line, and unimodal coagulation, solid line) and they rapidly decreased from 10^{13} to 10^{10} in 0.05 seconds. However, the final number concentration of bimodal coagulation was less than that of unimodal coagulation indicating the effect of inter-coagulation. The fine mode total volume concentration for bimodal coagulation decreased very slowly (Figure 4-17B, dotted line) and 6% of the initial volume was removed. Since the total volume is conserved in intra-coagulation, this reduction was due to inter-coagulation. The geometric standard deviation of the fine mode for unimodal coagulation approached 1.326 (Figure 4-17C, solid line) which is the asymptotic value for coagulating aerosols in

the transition regime, while for bimodal coagulation it reached 1.172 indicating the effect of inter-coagulation (Figure 4-17C, dotted line). The MMD of fine mode reached 0.0178 μm for unimodal coagulation and 0.0203 μm for bimodal coagulation (Figure 4-17D). As explained in Chapter 3, the inter-coagulation rate of the small particles in the fine mode was faster than that of the large particles in the fine mode. Hence the smaller particles of the fine mode were removed more by inter-coagulation resulting in 20% number concentration reduction with 6% volume reduction. The larger particles in the fine mode, however, were not affected much by inter-coagulation. The MMD of the fine mode for bimodal coagulation increased slightly faster than that of unimodal coagulation (Figure 4-17D); however, the MMD was still much less than 1 μm within the given residence time. The above results demonstrate that coagulation only could not be an effective mechanism for removing fine mode particles.

Case 2: Condensation only

When condensation was the only mechanism, its vapor consumption rate was very fast. As shown in Figure 4-17E (dash-dotted line), the vapor was depleted in 0.036 seconds (i.e., its saturation ratio reached 0). Figure 4-17F shows the change of MMD of the coarse mode as a function of time. MMD of the coarse mode increased rapidly until 0.036 seconds. It then did not change after vapor was depleted. This clearly showed that condensation was a faster process for mass transfer of the metal to coarse particles compared to inter-coagulation. It can also be concluded that the preferable condition for sorbent injection technique is condensation.

Case 3: 50% instant nucleation

Since the nucleation rate of vanadium particles is unknown, simulation was conducted for a scenario where 50% of the vapor has instantly nucleated. This allowed for evaluation of the competition of these two mechanisms (bimodal coagulation and condensation) on the evolution of the fine mode aerosol. Interestingly, as shown in Figure 4.17E, the saturation ratio (dash line) went down to 0 rapidly ($4.3x10^{-3}$ seconds) which was faster than the condensation only case (dash-dotted line). The high number concentration of instantly nucleated fine mode particles had a high surface area that was responsible for the rapid scavenge of the metal vapor in the system. The total volume of the fine mode particles was increased by condensation in a short period of time ($4.3x10^{-3}$ seconds) showing that metal vapor condensed on the fine mode particles (Figure 4-17B, dash line). The increase of the fine mode volume due to condensation was greater than the reduction due to inter-coagulation. Nonetheless MMD of the fine mode reached only 0.019 μm (Figure 4-17D) which was much less than the desired MMD (> 1 μm). The initial number concentration of the fine mode was half of the bimodal coagulation case. As shown in Figure 4.17A, nevertheless its number concentration quickly approached that of the bimodal coagulation case (dash line and dotted line were overlapped).

Although fast condensation on coarse mode particles was desired, metal vapor condensation on fine mode aerosol had an adverse effect. As shown in Figure 4-17A, the number concentration of the fine mode was high and intra-coagulation was still the dominant for the fine mode particles. Consequently, the removal of the fine mode volume concentration by inter-coagulation in this case was still negligible as shown in Figure 4-17B. Figure 4-17E shows MMD of the coarse mode as a function of time. In the 50%

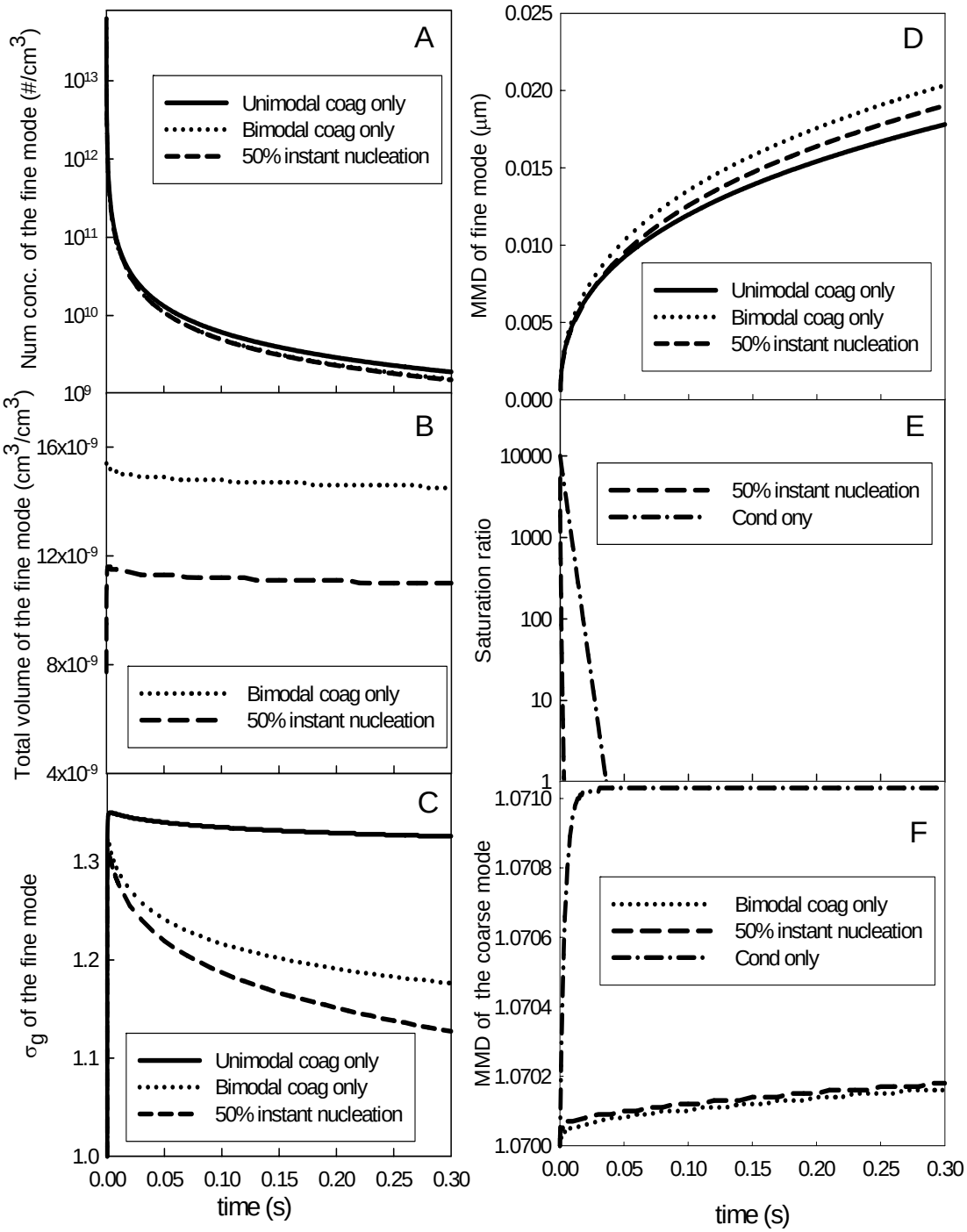

Figure 4-17. The change of A) total number concentration of the fine mode, B) total volume concentration of the fine mode, C) geometric standard deviation (σ_g) of the fine mode, D) MMD of the fine mode, E) Saturation ratio of V vapor, and F) MMD of the coarse mode as function of time.

instant nucleation case, some vapor also condensed on the coarse mode particles that grow slightly larger than the bimodal coagulation case. However, the condensation on the coarse mode was relatively insignificant once a high number of fine mode aerosol was present. As discussed earlier, the vapor dominantly condensed on the fine mode particles. Since the removal of the fine mode by inter-coagulation was slow, the contribution to the coarse mode growth through inter-coagulation was insignificant. These observations clearly demonstrate that nucleation is not desired for the sorbent injection technique. If gas phase hydrolysis or thermal decomposition occurs, it forms a high number concentration of fine mode particles that can not be effectively removed by coarse mode particles due to slow inter-coagulation. In addition, the fine mode is competing with the coarse mode for the metal vapor and is actually more effective. Such a competition renders the sorbent technique less effective.

Conclusions

A mechanistic study for sorbent injection technique was conducted theoretically and experimentally. The feasibility study verified the results of the thermodynamic equilibrium analysis and assisted in selecting the sorbent candidate for chemical adsorption (Ca-based sorbent). Experiments were divided into coagulation dominant and condensation dominant cases. The results of experiments clearly showed that condensation was the preferred mechanism for mass transfer process.

In the coagulation only case, element vanadium PSD showed only a slight shift to larger particles. At least $10^7/cm^3$ number concentration of sorbent particles was needed to improve the efficiency of sorbent injection technique by coagulation in the system studied that had a residence time of a few seconds. In the condensation case, the experimental results clearly showed that elemental vanadium PSD was shifted to the

larger sizes of sorbent particles. $CaCO_3$ sorbent which has high affinity with vanadium and silica sorbent which has no affinity but high surface area both exhibited the similar capture efficiency. Gas phase hydrolysis resulted in the formation of fine particles while the surface hydrolysis enhanced physical adsorption. Thus, surface hydrolysis was the key mechanism to effectively capture the metal.

The bimodal lognormal model study showed that complete vapor consumption was achieved within 0.03 seconds, proving surface interaction was the rate limiting process. The reduction of the fine mode volume concentration and number concentration for coagulation only case were 6% and 20% in 0.3 second residence time. Smaller particles in the fine mode were removed more than bigger particles in fine mode. However, slow inter-coagulation rate by high number concentration of fine mode particles supported that condensation was the preferable mechanism for sorbent technique. Instant nucleation formed high surface area of fine particles resulting in fast metal vapor condensation on fine mode particles. Its condensed volume was more than reduced volume by inter-coagulation. These results clearly demonstrated that nucleation was not desired for the sorbent injection technique.

In conclusion, the preferable mechanism for mass transfer is condensation with fast surface interaction such as surface hydrolysis. Alternatively, other scenarios that can result in fast surface interaction are also desired, e.g. maintaining metals in the vapor state at high temperature so that nucleation can be avoided. If in a system where it is impossible to suppress nucleation, a sufficiently high number concentration of sorbent particles must be provided to achieve a good collection efficiency by inter-coagulation.

CHAPTER 5
CONCLUSION AND RECOMMENDATIONS

Vanadium is one of the potential hazardous metal compounds from combustion sources. It is concentrated in the submicron regime and sorbent injection is one promising measure to control submicron vanadium particles. This study was carried out theoretically and experimentally to evaluate sorbent injection technique for the control of vanadium emission from combustion sources.

Theoretical study includes thermodynamic equilibrium analysis and bimodal lognormal model study. Potential material for sorbent injection technique was determined by thermodynamic equilibrium analysis, and bimodal lognormal model study used to gain the insight of aerosol dynamic as the mechanisms of sorbent injection technique. Experimental study includes pot experiment and aerosol reactor experiments. Pot experiment verified the results of thermodynamic analysis. Aerosol reactor experiment determined preferable mechanism and investigated the surface interaction for sorbent injection technique.

By thermodynamic equilibrium analysis, Na-, Ca-, and Mg-based sorbents were found to be effective in a wide range of temperatures. However, sulfur and sorbents were shown to have high affinity (forming sulfates) at temperatures lower than 1000 K. The strong affinity resulted in the depletion of available sorbents in the system. Sufficient sorbent in excess of sulfur should be provided in this temperature range to effectively capture vanadium compounds. At high temperatures (> 1000 K), the effectiveness of Na-

and Ca-based sorbents to capture vanadium revived as sorbent sulfates became less stable, releasing available sorbents to react with vanadium.

When vanadium formed submicron particles by nucleation, inter-coagulation was the only mechanism to remove these particles by sorbent particles. Hence, the effects of inter-coagulation on removing fine mode aerosol were studied using a bimodal lognormal model. Number concentration of coarse mode, geometric standard deviation of fine mode, and MMD of fine mode were found to be important parameters for inter-coagulation rate. Interestingly when inter-coagulation was the dominant mechanism for removing fine mode particles, its geometric standard deviation approached monodisperse. For coarse mode particles, the geometric standard deviation approached the asymptotic value because intra-coagulation was still the dominant mechanism. The removal time could also be expressed in the dimensionless form and two formulas were developed for inter-coagulation dominant and intra-coagulation dominant respectively. The developed formula could be used as a convenient tool to estimate the removal time once the particle scavenge characteristic time was determined.

Ca-based sorbent and Na-based sorbent showed their chemical affinity with vanadium in the pot experiments. Aerosol reactor experiments were divided into coagulation dominant and condensation dominant cases. The results of experiments clearly showed that condensation is the preferred mechanism for mass transfer process. In the coagulation only case, element vanadium PSD showed only a slight shift to supermicron. Formulas developed by inter-coagulation study showed that at least $10^7/cm^3$ number concentration of sorbent particles were needed to improve the efficiency of sorbent injection technique by coagulation for a typical combustion system with a

residence time of a few seconds. In the condensation case, the experimental results clearly showed that element vanadium PSD was shifted to the larger sizes of sorbent particles. $CaCO_3$ sorbent which had high affinity with vanadium and silica sorbent which had no affinity but high surface area both exhibited the similar capture efficiency. Gas phase hydrolysis resulted in the formation of fine particles while the surface hydrolysis enhanced physical adsorption. Silica sorbent which had no chemical affinity with vanadium also successfully captured vanadium vapor. Vanadium PSD shifted to the size where the surface area of sorbent was high. This was the strong evidence for physical adsorption. In real system, atomic vanadium vapor can be possibly condensed on sorbent particles. Condensation rate is not limiting process, however its fast nucleation rate may affect on the efficiency of sorbent injection.

A bimodal lognormal modeling study based on the initial condition of experiments showed that condensation was the preferable mechanism. When condensation (based on vanadium pentaoxide vapor) was the only mechanism, it showed the fastest and complete collection of vanadium vapor. If nucleation occurred, condensation on the instantly nucleated fine particles could yield undesired results because of the slow inter-coagulation rate that would not be effective in removing them. Meanwhile, the amount condensed on the fine mode was insufficient to increase MMD of fine mode to greater than 1 μm.

In conclusion, the preferable mechanism for mass transfer was condensation with the fast surface interaction such as surface hydrolysis. Alternatively, other scenarios that could result in fast surface interaction were also desired, e.g. maintaining metals in the vapor state at high temperature so that nucleation could be avoided. If in a system where

it is impossible to suppress nucleation, a sufficiently high number concentration of sorbent particles must be provided to achieve a good collection efficiency.

Based on the conclusions presented above and the experience gained in performing this research, recommendations can be made that should further the understanding and application of sorbent technique to the control of vanadium.

1. According to thermodynamic equilibrium analysis, most stable compound in combustion temperature was vanadium pentaoxide. However, if atomic vanadium vapor is formed, its nucleation rate is faster than vanadium pentaoxide at same temperature because of its higher saturation ratio. It consequently results adverse effect on sorbent injection. Hence, formed chemical species analysis and nucleation rate study need to be performed.

2. There will be the relationship among number concentration of nucleated particles, condensable vapor and PSD of sorbent particles to suppress nucleation. The bimodal lognormal model which is used in this study could be an excellent tool for this study.

3. Collison nebulizer and ultrasonic nebulizer used in this study generated polydisperse particles. They also generated undesired submicron particles. Theoretical study performed by this work showed that monodisperse articles around 1 μm particles was the most effective PSD of sorbent. Experimental studies are needed to verify the theoretical finding.

4. Surface hydrolysis enhanced sorbent injection technique. However, its final product on the surface of sorbent was unknown in this study. Based on the thermodynamic equilibrium study and the study of TTIP hydrolysis which has similar structure, the final product might be vanadium pentaoxide which is an excellent catalyst for NOx removal. Hence, performing further study of the surface hydrolysis can determine the surface interaction. This process can also be used to make micron particles coated by nanosize vanadium pentaoxides.

5. Physical adsorption should be further studied. In this study, silica particles captured vanadium vapor successfully which is the evidence of the importance of physical adsorption. However, there was the surface hydrolysis supporting physical adsorption. Studies should be carried out to examine if other surface interaction in addition to hydrolysis can also help physical condensation. Dry silica particles with different particle generation methods such as dust feeder and screw feeder can be used for this type of study.

APPENDIX A
FORTRAN CODE FOR BIMODAL LOGNORMAL MODEL

```
!     Bimodal lognormal aerosol model
!     Written by Sang-Rin Lee
!          4/28/2003
      IMPLICIT DOUBLE PRECISION (A-H,K-Z)
      Dimension M1coag(3),M1cond(3),M1nu(3),M2coag(3),M2cond(3),M2nu(3)
      Dimension M1(3),M2(3),dM1(3),dM2(3)
      COMMON/INDEX1/idym,idym1,idym2
      COMMON/moment/sg1,sg2,M1,M2,Dgn1,Dgn2
      COMMON/gas2/Sv,Ps,vm,sig,mm,mg,Dmg,cm
      COMMON/gas3/sl,ns,ks,vs
      COMMON/Index2/icog,icodd1,icodd2
      COMMON/EFF/ROV1
      COMMON/kelvin/idps
      COMMON/part/dps,dpmol
      OPEN(11,FILE='OUTPUT1.txt',STATUS='old')
      OPEN(12,FILE='OUTPUT2.txt',STATUS='old')
      OPEN(13,FILE='input.txt',STATUS='old')
      OPEN(2,FILE='dp_limit_input.txt',status='old')
      OPEN(19,FILE='debug.txt',STATUS='old')
      OPEN(20,FILE='critica.txt',STATUS='old')
      Call read1(iter,dt,idex,cont,M1org,out1)  ! select simulation condition
!     initialize value of moments
      do 10 i=1,3
      M1coag(i)=0.D0
      M1cond(i)=0.D0
      M1nu(i)=0.D0
      M2coag(i)=0.D0
      M2cond(i)=0.D0
      M2nu(i)=0.D0
10     continue
      irv=0
```

```
      icod1=0
      icod2=0
      icod3=0
      icod4=0
      icog=0
      icc=0
      icodd1=0
      icodd2=0
      iter=100000000000
      WRITE(*,*) "Write starting time "
      READ(*,*) cont
      DO 20 i=1,iter
      if (idym.ne.1) GOTO 100
      call coagulation(idex,M1coag,M2coag,i)
100    if (idym1.ne.1) GOTO 110
      call condensation(idex,M1cond,M2cond)
110    if (idym2.ne.1) GOTO 120
      call nucleation(idex,M1nu)
120    do 12 i1=1,3
      dM1(i1)=M1coag(i1)+M1nu(i1)+M1cond(i1)
      dM2(i1)=M2coag(i1)+M2cond(i1)
!      WRITE(*,*) "coag, cond, nu ",M1coag(i1)," ",M1cond(i1)
12     continue
123    dS1=ns*vm
!      WRITE(*,*)"ds1 dps= ",dps
      dS=-1.*(M1nu(1)*ks/ns)-1.*((M1cond(2)+M2cond(2))/ds1)
!      dM1nu=M1nu(1)*ks/ns
!      WRITE(*,*)"dM1nu= ",dM1nu
!      ds2=-1*(M1nu(1)*ks/ns)
!      ds3=-1.*((M1cond(2)+M2cond(2))/ds1)
      IF (i.NE.1) GOTO 19
      CoagI=M1(1)/(M1coag(1)+M1nu(1))
      WRITE(*,*)"Time for CoagI= ",CoagI
      Tcond1=((Sv-1)*dS1)/M1(2)
!      WRITE(*,*) "M1(2)= ",M1(2)
      WRITE(*,*)"S effect on volume I= ",Tcond1
!      WRITE(20,*)"S effect on volume I= ",Tcond1
```

```
!       WRITE(20,*)"M1(1)= ",M1(1)
!       WRITE(20,*)"Time for CoagI= ",CoagI
!       WRITE(20,*)"M1(2)    = ",M1(2)
!       WRITE(20,*)"M1cond(2)= ",M1cond(2)," M1nu(2)= ",M1nu(2)
        TS=Sv/dS
        WRITE(*,*)"Time for S= ",TS
        IF(idex.eq.1) goto 28
        CoagII=M2(1)/(M2coag(1)+M2nu(1))
        WRITE(*,*)" Time for CoagII= ",CoagII
!       WRITE(20,*)" Time for CoagII= ",CoagII
!       WRITE(20,*)"M2(1)    = ",M2(1),"   M2(2) = ",M2(2)
!       WRITE(20,*)"M2coag(1)= ",M2coag(1)," M2cond(2)= ",M2cond(2)
        Tcond2=((Sv-1)*dS1)/(M2(2))
        WRITE(*,*)"S effect on volume II= ",Tcond2
!       WRITE(20,*)"S effect on volume II= ",Tcond2
28      WRITE(*,*) "Time step(dt)?"
        READ (*,*) dt
        WRITE(*,*) "Iteration times ?"
        Read (*,*) iter1
        time1=iter1*dt
        WRITE(*,89) time1,dt
89          FORMAT(" Runtime = ",e12.5," dt= ",e10.2)
        WRITE(11,89) time1,dt
19      DO 30 i2=1,3
        M11=M1(i2)
        M21=M2(i2)
        dm11=dM1(i2)
        dm21=dM2(i2)
        cont1=cont
        cont2=cont
!       WRITE(*,*) "M1 bf ",M11,"m1(i)= ",M1(i2)
        CALL RKF5(cont1,M11,dt,dm11,M12)
        CALL RKF5(cont2,M21,dt,dm21,M22)
        M1(i2)=M12
        M2(i2)=M22
!       WRITE(*,*) "M1 af ",M12,"m1(i)= ",M1(i2)
30      continue
```

```
      IF(idym1.ne.1.and.idym2.ne.1) GOTO 189
      MS1=Sv
      dms=dS
      cont3=cont
!      WRITE(*,*) "3"
      Call RKF5(cont3,MS1,dt,dms,MS2)
      Sv=MS2
189    i2=iter-i
!      M1org=0.784E-07
      ROV=(1-M1(2)/M1org)*100.
      IF (ROV.GE.ROV1) THEN
        IF(irv.eq.0) then
        WRITE(11,*) "time= ",cont," Mode 1 removed"
        WRITE(*,*) "time= ",cont," Mode 1 removed"
        irv=1
        else
          GO TO 50
        endif
      END IF
50     IF (M1cond(2).lt.0) Then
        IF(icod1.eq.0) then
        WRITE(11,*) "time= ",cont," Mode 1 evaporation"
        WRITE(*,*) "time= ",cont," Mode 1 evaporation"
        icod1=1
        Else
        GO TO 31
        endif
      Endif
31     IF (M2cond(2).lt.0) Then
        IF(icod2.eq.0) then
        WRITE(11,*) "time= ",cont," Mode 2 evaporation"
        WRITE(*,*) "time= ",cont," Mode 2 evaporation"
        icod2=1
        else
          GO TO 32
        endif
      endif
```

```
32     IF(M1(1).le.1) THEN
        icog=1.
        IF(icc.eq.0) then
         WRITE(*,*) " Time= ",cont," Small particles are scavenged !"
         WRITE(11,*) " Time= ",cont," Small particles are scavenged !"
         icc=1
        ELSE
         GOTO 33
        END if
       END if
33     IF (M1(2).lt.0.D0) THEN
        icodd1=1
        if (icod3.eq.0) then
        WRITE (*,*) " Time= ",cont," No more condensation for mode 1!"
        WRITE (11,*) " Time= ",cont," No more condensation for mode 1!"
        icod3=1.
        M1(2)=ABS(M1(2))
        ELSE
           GOTO 34
        END if
       END IF
34     IF (M2(2).lt.0.D0) THEN
        icodd2=0
        if (icod4.eq.0) then
        WRITE (*,*) " Time= ",cont," No more condensation for mode 2!"
        WRITE (11,*) " Time= ",cont," No more condensation for mode 2!"
        icod4=1.
        M2(2)=ABS(M2(2))
        else
          GOTO 35
        ENDIF
       END IF
35     CALL Newmoment(idex)
       cont=cont+dt
       IF (MOD(i,out1).NE.0) goto 21
       Ileft=iter1-i
       WRITE(*,*) Ileft," step left"
```

```
      CALL Output(idex,i,cont) ! write results in formated way.
!      WRITE(*,245)cont,i,i2
245    FORMAT(" Time= ",E10.3," It= ",i7," left= ",i7)
21     IF(i.eq.iter1) goto 23
      IF(Sv.lt.0.1) then
      idym1=2.
      idym2=2.
      else
      ENDif
20     continue
23     STOP
      END
!
      SUBROUTINE Read1(iter,dt,idex,cont,M1org,out1)
      IMPLICIT DOUBLE PRECISION (A-H,K-Z)
      Dimension M1(3),M2(3),k1ml(26),k1mu(26),k2ml(26),K2mu(26)
      INTEGER n
      COMMON/kelvin/idps
      COMMON/INDEX1/idym,idym1,idym2
      COMMON/moment/sg1,sg2,M1,M2,Dgn1,Dgn2
      COMMON/klimit/k1ml,k1mu,k2ml,k2mu
      COMMON/gas/kb,T,lob,mu,lamda
      COMMON/gas2/Sv,Ps,vm,sig,mm,mg,Dmg,cm
      COMMON/gas3/sl,ns,ks,vs
      COMMON/EFF/ROV1
      COMMON/part/dps,dpmol
      COMMON/nod/n
!     Initial display
5      WRITE (*,*) "Choose following option"
      WRITE (*,*) "Unimodal: 1, bimodal: press any number key"
      READ (*,*) idex
      if (idex.eq.1) then
        WRITE(*,*) "Your chioce is UNIMODAL model simulation"
        WRITE(11,*) "Your chioce is UNIMODAL model simulation"
        else
        WRITE(*,*) "Your chioce is BIMODAL model simulation"
        WRITE(11,*) "Your chioce is BIMODAL model simulation"
```

```
end if
WRITE (*,*) "Include coagulation ?"
WRITE (*,*) "Yes: 1, No: any number key"
READ (*,*) idym
WRITE (*,*) "Include condensation ?"
WRITE (*,*) "Yes: 1, No: any number key"
READ (*,*) idym1
WRITE (*,*) "Include nucleation ?"
WRITE (*,*) "Yes: 1, No: any number key"
READ (*,*) idym2
WRITE (*,*) "Your final choices are "
WRITE (11,*) "Your final choices are "
if (idym.eq.1) then
  if (idym1.eq.1) then
    if (idym2.eq.1) then
    WRITE(*,*) "coagulation, condensation, and nucleation"
    WRITE(11,*) "coagulation, condensation, and nucleation"
      else
    WRITE(*,*) "coagulation, and condensation"
    WRITE(11,*) "coagulation, and condensation"
      endif
  else
    if (idym2.eq.1) then
    WRITE(*,*) "coagulation, and nucleation"
    WRITE(11,*) "coagulation, and nucleation"
      else
    WRITE(*,*) "coagulation only"
    WRITE(11,*) "coagulation only"
      endif
  endif
else
  if (idym1.eq.1) then
    if (idym2.eq.1) then
    WRITE(*,*) "condensation, and nucleation"
    WRITE(11,*) "condensation, and nucleation"
      else
    WRITE(*,*) "condensation only"
```

```
          WRITE(11,*) "condensation only"
            endif
        else
          if (idym2.eq.1) then
          WRITE(*,*) "nucleation only"
          WRITE(11,*) "nucleation only"
            else
          WRITE(*,*) "No choice of dynamic !!"
          WRITE(11,*) "No choice of dynamic !!"
            end if
        end if
      endif
      WRITE(*,*) "Do you want to change option? "
      WRITE(*,*) "Yes: 1, No: any number key"
      READ (*,*) icho
      If (icho.eq.1) GO TO 5
      READ(13,*) sg1
      READ(13,*) M1(1)
      READ(13,*) Dgn1
      READ(13,*) sg2
      READ(13,*) M2(1)
      READ(13,*) Dgn2
      READ(13,*) kb
      READ(13,*) T
      READ(13,*) lamda
      READ(13,*) mm
      READ(13,*) mg
      READ(13,*) Dmg
      READ(13,*) cm
      READ(13,*) n
      READ(13,*) Pin
      READ(13,*) Ps
      READ(13,*) out1
      READ(13,*) ROV1
      READ(13,*) idps
401   FORMAT(F10.2)
      pi=3.14159
```

```
      lobV=2.36-(3.38e-5)*T  ! densitiy of vanadium pentaoxide
      lob=1.
!     Ps=-3031.5*(1/T)+6.8473
!     Ps=10**(Ps)
      Ps=Ps/760*1.01e6
      Pin=Pin/760*1.01e6
      Sv=Pin/Ps
      Nav=6.02e23 !#/mole
      Vr=97.88  ! cm3
      R=8.37e7  ! dyne cm/K/mole
      ns=ps/(R*T)*Nav
!     WRITE(*,*)"ns= ",ns
      vm=181.88/lobV/Nav
      dpmol=(6.*vm/pi)**(1./3.)
!     WRITE(*,*) "dpmol= ",dpmol
      sl=(((6./pi)*vm)**(2./3.))*(pi)
      tau=1./(ns*sl*((kb*T)/(2.*pi*mm))**0.5)
      sig=69.1+0.111*T  ! vanadium pentaoxide surface tension
      dps=4.*sig*vm/(kb*T*LOG(Sv))
      mu=1.81e-4*(T/293)**0.74
      WRITE(11,*) "Input data set "
      Write(11,201) sg1
      Write(11,202) M1(1)
      Write(11,203) Dgn1
      Write(11,204) sg2
      Write(11,205) M2(1)
      Write(11,206) Dgn2
      Write(11,207) kb
      Write(11,208) T
      Write(11,209) lob
      WRITE(11,210) mu
      Write(11,211) lamda
      Write(11,212) Sv
      Write(11,213) vm
      WRITE(11,224) sl
      Write(11,214) sig
      Write(11,215) mm
```

```
      Write(11,216) mg
      Write(11,217) Dmg
      Write(11,218) cm
      WRITE(11,219) ns
      WRITE(11,234) n
      WRITE(11,221) Pin
      WRITE(11,222) Ps
      WRITE(11,223) tau
      WRITE(11,225) ROV1
      WRITE(*,*) "dps= ",dps
      WRITE(*,*) "Tau= ",tau
!     CondI=Dgn1/dps
!     CondII=Dgn2/dps
!     WRITE(20,*) "CondI= ",CondI," CondII= ",COndII
!     IF(condI.lt.1) THEN
!     WRITE(*,*) " mode I --> Evaporation"
!     Endif
!     IF(CondII.lt.1) Then
!     WRITE(*,*) " mode II --> Evaporation"
!     Endif
201   FORMAT(" Sg1   =    ",F10.2)
202   FORMAT(" M1(1) =    ",E10.2," #/cc")
203   FORMAT(" Dgn1  =    ",E10.2," cm")
204   FORMAT(" Sg2   =    ",F10.2)
205   FORMAT(" M2(1) =    ",E10.2," #/cc")
206   FORMAT(" Dgn2  =    ",E10.2," cm")
207   FORMAT(" kb    =    ",E10.2," dyne cm/K")
208   FORMAT(" T     =    ",F10.1," K")
209   FORMAT(" lob   =    ",F10.1," g/cm3")
210   FORMAT(" mu    =    ",E10.2," g/s/cm")
211   FORMAT(" lamda =    ",E10.2," cm")
212   FORMAT(" Sv    =    ",F10.2)
213   FORMAT(" vm    =    ",E10.2," cm3")
224   FORMAT(" sl    =    ",E10.2," cm2")
214   FORMAT(" sig   =    ",E10.2," dyne/cm")
215   FORMAT(" mm    =    ",E10.2," g")
216   FORMAT(" mg    =    ",E10.2," g")
```

```
217    FORMAT(" Dmg   =    ",E10.2," cm2/s")
218    FORMAT(" cm    =    ",E10.2," cm/s")
219    FORMAT(" ns    =    ",E10.2," #/cm3")
234    FORMAT(" n     =    ",I10)
221    FORMAT(" Pin   =    ",E10.2," dyne/cm2")
222    FORMAT(" Ps    =    ",E10.2," dyne/cm2")
223    FORMAT(" tau   =    ",E10.2," s")
225    FORMAT(" R.Eff =    ",F10.2," %")
!      Read k factor limit
       do 10 i=1,26
       read (2,*) k1ml(i),k1mu(i),k2ml(i),K2mu(i)
10     continue
       M1(2)=M1(1)*(Dgn1**3.)*EXP((9./2.)*(LOG(sg1))**2.)
       M1(3)=M1(1)*(Dgn1**6.)*EXP((36./2.)*(LOG(sg1))**2.)
       M2(2)=M2(1)*(Dgn2**3.)*EXP((9./2.)*(LOG(sg2))**2.)
       M2(3)=M2(1)*(Dgn2**6.)*EXP((36./2.)*(LOG(sg2))**2.)
       M1org=M1(2)
!      WRITE(*,*) "M1(2)= ",M1(2)," ",M1(1)," ",Dgn1
!      WRITE(*,*) "M2(2)= ",M2(2)," ",M2(1)," ",Dgn2
       call intio()
       IF (idex.eq.1) THEN
       WRITE(11,101)
101      FORMAT('    time     M10       M11       M12       Sv')
       WRITE(12,112)
112      FORMAT('    time       sg1      Dgn1      dps')
       WRITE(11,113) cont,M1(1),M1(2),M1(3),Sv
113    FORMAT(E10.3,1x,E10.3,1x,E10.3,1x,E10.3,1x,E10.3)
       Dgnw1=Dgn1*10000.
       dpsn=dps*10000.
       WRITE(12,123) cont,sg1,Dgnw1,dpsn
123    FORMAT(E10.3,1x,F10.3,1x,F10.5,1x,F10.5)
       ELSE
       WRITE(11,100)
100      FORMAT('    time     M10       M11       M12       Sv       M20       M21       M22')
       WRITE(12,111)
111      FORMAT('    time       sg1       sg2      Dgn1      Dgn2      dps')
       WRITE(11,110) cont,M1(1),M1(2),M1(3),Sv,M2(1),M2(2),M2(3)
```

```
110
FORMAT(E10.3,1x,E10.3,1x,E10.3,1x,E10.3,1x,E10.3,1x,E10.3,1x,E10.3,1x,E10.3,1x,E10.3)
      Dgnw1=Dgn1*1e4
      Dgnw2=Dgn2*1e4
      dpsn=dps*10000.
      WRITE(12,120) cont,sg1,sg2,Dgnw1,Dgnw2,dpsn
120    FORMAT(E10.3,1x,F10.3,1x,F10.3,1x,F10.5,1x,F10.5,1x,F10.5)
      ENDIF
      Return
      End
!
      SUBROUTINE Output(idex,i,cont)
      IMPLICIT DOUBLE PRECISION (A-H,K-Z)
      DIMENSION M1(3),M2(3)
      COMMON/moment/sg1,sg2,M1,M2,Dgn1,Dgn2
      COMMON/gas2/Sv,Ps,vm,sig,mm,mg,Dmg,cm
      COMMON/part/dps,dpmol
      if (idex.eq.1) then
      WRITE(11,111)cont,M1(1),M1(2),M1(3),Sv
111    FORMAT(E10.3,1x,E10.3,1x,E10.3,1x,E10.3,1x,E10.3)
      Dgnw1=Dgn1*1e4
      dps1=dps*1e4
      WRITE(12,121) cont,sg1,Dgnw1,dps1
121    FORMAT(E10.3,1x,F10.3,1x,F10.5,1x,F10.5)
      Else
      WRITE(11,110)cont,M1(1),M1(2),M1(3),Sv,M2(1),M2(2),M2(3)
110    FORMAT(E10.3,1x,E10.3,1x,E10.3,1x,E10.3,1x,E10.3,1x,E10.3,1x,E10.3,1x,E10.3)
      Dgnw1=Dgn1*1e4
      Dgnw2=Dgn2*1e4
      dps1=dps*1e4
      WRITE(12,120) cont,sg1,sg2,Dgnw1,Dgnw2,dps1
120    FORMAT(E10.3,1x,F10.3,1x,F10.3,1x,F10.5,1x,F10.5,1x,F10.5)
      ENDIF
200    Return
      ENd
!
!
```

```
      SUBROUTINE Newmoment(idex)    ! Calculat new moment after dt passed.
      IMPLICIT DOUBLE PRECISION (A-H,K-Z)
      Dimension M1(3),M2(3)
      COMMON/moment/sg1,sg2,M1,M2,Dgn1,Dgn2
      pi=3.141593
      AM1k1=M1(2)/M1(1)
      AM1k2=M1(3)/M1(1)
!      WRITE(*,*) "m1,m2,m3 ",M1(1)," ",M1(2)," ",M1(3)
!      WRITE(*,*) "Am1k1= ",Am1k1," Am1k2= ",Am1k2
      Dgn1=(AM1k1**(2./3.))*(AM1k2**(-1./6.))
!      WRITE(*,*) "Dgn1 ",Dgn1
      klogin=am1k1/(am1k2**0.5)
!      WRITE(*,*) "inside log= ",klogin
      IF(sg1.lt.1.001.and.sg1.ge.1.000)then
        IF(klogin.gt.1.000.and.klogin.lt.1.001) klogin=0.999999
      else
        GOTO 311
      endif
311    sg11=((-2./9.*LOG(klogin)))**0.5
      sg1=EXP(sg11)
!      WRITE(*,*)"sg1= ",sg1
      IF(idex.eq.1) GOTO 20
      AM2k1=M2(2)/M2(1)
      AM2k2=M2(3)/M2(1)
!      WRITE(*,*) "M1(1),2,3= ",M1(1),M1(2),M1(3)
!      WRITE(19,*) "M2(1),2,3= ",M2(1),M2(2),M2(3)
!      WRITE(19,*) "Am2k1= ",Am2k1," Am2k2= ",Am2k2
      sg21=(-2./9.*LOG(AM2k1/(AM2k2**0.5)))**0.5
      sg2=EXP(sg21)
      Dgn2=(AM2k1**(2./3.))*(AM2k2**(-1./6.))
!     WRITE(19,210) sg1,Dgn1,sg2,Dgn2
210    FORMAT("sg1,Dgn1,sg2,Dgn2",e10.2,1x,e10.2,1x,e10.2,1x,e10.2)
20     Return
      end
!
!
      SUBROUTINE RKF5(x1,y1,h,dm,y12)
```

```
!     Runge-Kutta-Fehlberg 5th order method
!     Written by Sang-Rin Lee
!     05/12/2003
!     V is differential equation
!     V should be recalculated by x2 and y2 ...
!     In this case I assume V is same in dt
!     If differential equation is function of x and y, you must use dm subroutine to get new V.
      Implicit DOUBLE PRECISION (A-H,K-Z)
      Dimension al(6),B(6,6),Gam(6),V(6),x(6),y(6)
      COMMON /RKF/al,B,Gam
!     WRITE(19,*) "RKF"
!     WRITE(19,*) "x1,y1= ",x1," ",y1
      V(1)=dm
      x(1)=x1
      y(1)=y1
      DO 10 i=2,6
      x(i)=x(1)+al(i)*h
!     WRITE(*,*) "x(i)= ",i," ",x(i)
      sumv=0.D0
      j2=i-1
      do 20 j=1,j2
      sumv=sumv+h*B(i,j)*V(j)
!     WRITE(19,*) "B(i,j)= ",i," ",j," ",B(i,j)
20     continue
      y(i)=y(1)+sumv
      x1=x(i)
      y1=y(i)
!     call dm(x1,y1,fxy)
      v(i)=dm
!     WRITE(*,*) "V(i)= ",V(i)
10     continue
      sumy=0.d0
      do 30 i=1,6
      sumy=sumy+h*gam(i)*v(i)
30     continue
      y12=y(1)+sumy
      x1=x(5)
```

```
!       WRITE(*,*) "ynew= ",y1
!       WRITE(*,*) "Xnew= ",X1
        Return
        End
!
!
        SUBROUTINE coagulation(idex,M1coag,M2coag,it1)
        IMPLICIT DOUBLE PRECISION (A-H,K-Z)
        DIMENSION M1coag(3),M2coag(3),M1fm(3),M2fm(3),M1cm(3),M2cm(3),M1(3),M2(3)
        COMMON/INDEX1/idym,idym1,idym2
        COMMON/moment/sg1,sg2,M1,M2,Dgn1,Dgn2
        COMMON/gas/kb,T,lob,mu,lamda
!       Calculate Kng to determine FM or CM
        kng1=2*lamda/Dgn1
        kng2=2*lamda/Dgn2
!        WRITE(19,*) "kngi= ",kng1,"  kngj= ",kng2  !When kng is too big, then I can skip cm later
!        if (kng.gt.1) then
!        end if
        do 10 i1=1,3
        M1fm(i1)=1e30
        M1cm(i1)=1e30
        M2cm(i1)=1e30
        M2fm(i1)=1e30
10       continue
!        IF(kng1.gt.20) GO TO
        call fmcoagulation(idex,M1fm,M2fm,it1)
        call cmcoagulation(idex,M1cm,M2cm,it1)
        DO 20 I=1,3
        M1coag(i)=1./(1./M1fm(i)+1./M1cm(i))
        M2coag(i)=1./(1./M2fm(i)+1./M2cm(i))
20       CONTINUE
        if (it1.GT.1) GOTO 45
!        WRITE(19,222) M1fm(1),M1fm(2),M1fm(3),M2fm(1),M2fm(2),M2fm(3)
222      FORMAT(" M1fm= ",e10.4,1x,e10.4,1x,e10.4," M2fm= ",e10.4,1x,e10.4,1x,e10.4)
!        WRITE(19,223) M1cm(1),M1Cm(2),M1cm(3),M2cm(1),M2cm(2),M2cm(3)
223      FORMAT(" M1cm= ",e10.4,1x,e10.4,1x,e10.4," M2cm= ",e10.4,1x,e10.4,1x,e10.4)
!        WRITE(19,120) M1coag(1),M1coag(2),M2coag(1),M2coag(2)
```

```
120    FORMAT("M1coag(0),M1coag(1)= ",e10.4,1x,e10.4,1x,"M2coag(0),M2coag(1)=
",e10.4,1x,e10.4)
45     return
       END
!
!
       subroutine fmcoagulation(idex,M1fm,M2fm,it1)
       IMPLICIT DOUBLE PRECISION (A-H,K-Z)
       DIMENSION M1fm(3),M2fm(3),Mtra(26)
       INTEGER n
       COMMON/coag1/Mtra
       COMMON/nod/n
!       WRITE(*,*) "fmcoag"
       do 10 i=1,13
       Mtra(i)=0.
10     continue
       if (idex.eq.1) GOTO 30
       call intercoagulation1(idex,it1)
30     continue
       call intracoagulation1(idex)
       do 20 i=1,3
       M1fm(i)=Mtra(i)+Mtra(i+6)
       M2fm(i)=Mtra(i+3)+Mtra(i+9)
20     continue
       iout1=100
      IF (MOD(it1,iout1).NE.0) goto 21
!       WRITE(19,120) Mtra(1),Mtra(7),Mtra(2),Mtra(8),Mtra(3),Mtra(9)
120    FORMAT("M1= ",e10.3," ",e10.3," ",e10.3," ",e10.3," ",e10.3," ",e10.3)
!       WRITE(20,121) Mtra(4),Mtra(10),Mtra(5),Mtra(11),Mtra(6),Mtra(12)
121    FORMAT("M2= ",e10.3," ",e10.3," ",e10.3," ",e10.3," ",e10.3," ",e10.3)
21     return
       end
!
!
       subroutine cmcoagulation(idex,M1cm,M2cm,it1)
       IMPLICIT DOUBLE PRECISION (A-H,K-Z)
       DIMENSION M1cm(3),M2cm(3),Mtra(26)
```

```
      INTEGER n
      COMMON/coag1/Mtra
      COMMON/nod/n
!       WRITE(*,*) "cmcoag"
      do 10 i=14,26
      Mtra(i)=0.
10     continue
      if (idex.eq.1) GOTO 30
      call intercoagulation2(idex)
30     continue
      call intracoagulation2(idex,it1)
      DO 20 i=1,3
      i1=i+13
      i2=i+19
      i3=i+16
      i4=i+22
      M1cm(i)=Mtra(i1)+Mtra(i2)
      M2cm(i)=Mtra(i3)+Mtra(i4)
20     continue
      iout1=1
      IF (MOD(it1,iout1).NE.0) goto 21
!      WRITE(19,120) Mtra(14),Mtra(20),Mtra(15),Mtra(21),Mtra(16),Mtra(22)
120     FORMAT("M1= ",e10.4," ",e10.4," ",e10.4," ",e10.4," ",e10.4," ",e10.4)
!      WRITE(20,121) Mtra(17),Mtra(23),Mtra(18),Mtra(24),Mtra(19),Mtra(25)
121     FORMAT("M2= ",e10.4," ",e10.4," ",e10.4," ",e10.4," ",e10.4," ",e10.4)
21     return
      end
!
!
!
      SUBROUTINE intracoagulation1(idex)
      IMPLICIT DOUBLE PRECISION (A-H,K-Z)
      INTEGER n,n1,n2  !This statement is very important for gauleg.
      Dimension Mtra(26),k1ml(26),k1mu(26),k2ml(26),K2mu(26)
      DIMENSION w1(100),w2(100),x1(100),x2(100),Fx(100),Fxx(100)
      Dimension Gxx(100),Gx(100),M1(3),M2(3)
      COMMON/moment/sg1,sg2,M1,M2,Dgn1,Dgn2
```

```
      COMMON/gas/kb,T,lop,mu,lamda
      COMMON/klimit/k1ml,k1mu,k2ml,k2mu
      COMMON/coag1/Mtra
      COMMON/nod/n
      COMMON/idex2/icog,icodd1,icodd2
!      WRITE(19,*) "intra1coag"
      if (icog.eq.1.) goto 212
      c1=(3.*kb*T/lop)**0.5
      pi=3.141593
!      WRITE(19,*) "c1= ",c1
!     When mono disperse
      n1=n
          n2=n
      do 10 i=1,3
            if (sg1.lt.1.0001) then
                  n1=1.
                  n2=1.
                  w1(1)=1.
                  w2(1)=1.
                  x1(1)=LOG(Dgn1)
                  x2(1)=LOG(Dgn1)
                  goto 29
                else
                endif
      if (i.eq.2) GOTO 25
      k1l1=k1ml(i)
      k1u1=k1mu(i)
      k2l1=k2ml(i)
      k2u1=k2mu(i)
      call limit(k1l1,k1u1,k1l,k1u,Dgn1,sg1)
      call limit(k2l1,k2u1,k2l,k2u,Dgn1,sg1)
      k1l=LOG(k1l)
      k1u=LOG(k1u)
      k2l=LOG(k2l)
      k2u=LOG(k2u)
!      WRITE(19,*) "k1u= ",k1u,"k1l= ",k1l
!      WRITE(19,*) "k2u= ",k2u,"k2l= ",k2l
```

```
      call gauleg(k1l,k1u,x1,w1,n)
      call gauleg(k2l,k2u,x2,w2,n)
!      do 2 i1=1,n
!      WRITE(19,*) "i,x1,x2",i1," ",x1(i1)," ",x2(i1)
!2     continue
29     Mtra(i)=0.
      if (i.eq.1) dp0=-0.5
      if (i.eq.3) dp0=1.
          do 20 ii = 1,n1
      do 20 j = 1,n2
      fx1=((1./EXP(x1(ii)*3.))+(1./EXP(x2(j)*3.)))**0.5
      fx2=(EXP(x1(ii))+EXP(x2(j)))**2.
      fx3=fx1*fx2
      if (i.eq.1) ip=0.
      if (i.eq.3) ip=3.
      dp1=(EXP(x1(ii)))**(ip)
      dp2=(EXP(x2(j)))**(ip)
          if (sg1.lt.1.0001) then
                    Fx(ii)=M1(1)
                    Fxx(j)=M1(1)
                    else
      Fx(ii)=M1(1)/((2*pi)**0.5*LOG(sg1))*EXP(-0.5*(x1(ii)-LOG(Dgn1))**2./(LOG(sg1))**2.)
      Fxx(j)=M1(1)/((2*pi)**0.5*LOG(sg1))*EXP(-0.5*(x2(j)-LOG(Dgn1))**2./(LOG(sg1))**2.)
          endif
      Fxxx=dp0*dp1*dp2*c1*fx1*fx2*Fx(ii)*w1(ii)*w2(j)*Fxx(j)
      Mtra(i)=Mtra(i)+fxxx
!      WRITE(19,101) ii,j,fx1,fx2,Fx(ii),Fxx(j),fxxx,Mtra(i)
101    FORMAT("ii=",i2," j=",i2,1x,e10.3,1x,e10.3,1x,e10.3,1x,e10.3,1x,e10.3,e10.3)
20     continue
25     Mtra(2)=0.
10     continue
!      WRITE(19,*) "Mtra(1),Mtra(3)",Mtra(1)," ",Mtra(3)
212    IF (idex.eq.1) GO TO 100
!      For mode j intra coagulation
      do 30 i=4,6
      if (i.eq.5) GO TO 35
            if (sg2.lt.1.0001) then
```

```
                n1=1.
                n2=1.
                w1(1)=1.
                w2(1)=1.
                x1(1)=LOG(Dgn2)
                x2(1)=LOG(Dgn2)
                goto 49
        else
        endif
    k1l1=k1ml(i)
    k1u1=k1mu(i)
    k2l1=k2ml(i)
    k2u1=k2mu(i)
    call limit(k1l1,k1u1,k1l,k1u,Dgn2,sg2)
    call limit(k2l1,k2u1,k2l,k2u,Dgn2,sg2)
    k1l=LOG(k1l)
    k1u=LOG(k1u)
    k2l=LOG(k2l)
    k2u=LOG(k2u)
    call gauleg(k1l,k1u,x1,w1,n)
    call gauleg(k2l,k2u,x2,w2,n)
49   Mtra(i)=0.
    if (i.eq.4) dp0=-0.5
    if (i.eq.6) dp0=1.
    do 40 ii = 1,n1
    do 40 j = 1,n2
    fx1=((1./EXP(x1(ii)*3.))+(1./EXP(x2(j)*3.)))**0.5
    fx2=(EXP(x1(ii))+EXP(x2(j)))**2.
    if (i.eq.4) ip=0.
    if (i.eq.6) ip=3.
    dp1=(EXP(x1(ii)))**(ip)
    dp2=(EXP(x2(j)))**(ip)
      if (sg2.lt.1.0001) then
            Gx(ii)=M2(1)
            Gxx(j)=M2(1)
      else
    Gx(ii)=M2(1)/((2*pi)**0.5*LOG(sg2))*EXP(-0.5*(x1(ii)-LOG(Dgn2))**2./(LOG(sg2))**2.)
```

```
      Gxx(j)=M2(1)/((2*pi)**0.5*LOG(sg2))*EXP(-0.5*(x2(j)-LOG(Dgn2))**2./(LOG(sg2))**2.)
      endif
          Mtra(i)=Mtra(i)+dp0*dp1*dp2*c1*fx1*fx2*Gx(ii)*w1(ii)*w2(j)*Gxx(j)
!      WRITE(19,102) ii,j,fx1,fx2,Gx(ii),Gxx(j),Mtra(i)
102    FORMAT("ii=",i2," j=",i2,1x,e10.3,1x,e10.3,1x,e10.3,1x,e10.3,1x,e10.3)
40     continue
35     Mtra(5)=0.
30       continue
100    continue
!      WRITE(19,*) "Mtra(4),Mtra(6)",Mtra(4)," ",Mtra(6)
      return
      end
!
!
      SUBROUTINE intercoagulation1(idex,iout)
      IMPLICIT DOUBLE PRECISION (A-H,K-Z)
      INTEGER n,n1,n2
      Dimension Mtra(26),k1ml(26),k1mu(26),k2ml(26),K2mu(26)
      DIMENSION w1(100),w2(100),x1(100),x2(100),Fxx(100),Fx(100)
      Dimension Gxx(100),Gx(100),M1(3),M2(3)
      COMMON/moment/sg1,sg2,M1,M2,Dgn1,Dgn2
      COMMON/gas/kb,T,lop,mu,lamda
      COMMON/klimit/k1ml,k1mu,k2ml,k2mu
      COMMON/coag1/Mtra
      COMMON/nod/n
      COMMON/idex2/icog,icodd1,icodd2
!     WRITE(19,*) "inter1coag"
      n1=n
          n2=n
      c1=(3*kb*T/lop)**0.5
      pi=3.141593
      IF (icog.eq.1) GOTO 212
      do 10 i=7,9
            if (sg1.lt.1.0001) then
                  if (sg2.lt.1.0001) then
                  n1=1.
                  n2=1.
```

```
                w1(1)=1.
                w2(1)=1.
                x1(1)=LOG(Dgn1)
                x2(1)=LOG(Dgn2)
      goto 31
                else
                n1=1.
                w1(1)=1.
                x1(1)=log(Dgn1)
                goto 29
                endif
      else
                if (sg2.lt.1.0001) then
                n2=1.
                w2(1)=1.
                x2(1)=LOG(Dgn2)
      goto 28
                else
                endif
      endif
28    k1l1=k1ml(i)
      k1u1=k1mu(i)
      call limit(k1l1,k1u1,k1l,k1u,Dgn1,sg1)
      k1l=LOG(k1l)
      k1u=LOG(k1u)
      call gauleg(k1l,k1u,x1,w1,n)
      if(sg2.lt.1.0001) goto 31
29    k2l1=k2ml(i)
      k2u1=k2mu(i)
      call limit(k2l1,k2u1,k2l,k2u,Dgn2,sg2)
      k2l=LOG(k2l)
      k2u=LOG(k2u)
      call gauleg(k2l,k2u,x2,w2,n)
31    Mtra(i)=0.
      do 20 ii = 1,n1
      do 20 j = 1,n2
      fx1=((1./EXP(x1(ii)*3.))+(1./EXP(x2(j)*3.)))**0.5
```

```
      fx2=(EXP(x1(ii))+EXP(x2(j)))**2.
      ip=(i-7)*3.
      dp1=(EXP(x1(ii)))**(ip)
          if (sg1.lt.1.0001) then
          Fx(ii)=M1(1)
          else
      Fx(ii)=M1(1)/((2*pi)**0.5*LOG(sg1))*EXP(-0.5*(x1(ii)-LOG(Dgn1))**2./(LOG(sg1))**2.)
      endif
          if (sg2.lt.1.0001) then
          gx(j)=M2(1)
          else
          Gx(j)=M2(1)/((2*pi)**0.5*LOG(sg2))*EXP(-0.5*(x2(j)-LOG(Dgn2))**2./(LOG(sg2))**2.)
      endif
                    Mtra(i)=Mtra(i)-1.*dp1*c1*fx1*fx2*Fx(ii)*w1(ii)*w2(j)*Gx(j)
      IF(MOD(iout,50000).ne.0)GO TO 20
      beta1=1.*dp1*c1*fx1*fx2
      mta=1.*dp1*c1*fx1*fx2*Fx(ii)*w1(ii)*w2(j)*Gx(j)
!      WRITE(19,324) ii,j,beta1,mta
324    FORMAT(1x,i2,1x,i2,1x,e10.4,1x,e10.4)
!      Write(19,*)"x1 ",ex1,"x2 ",ex2,"fx3 ",fx3,"n1 ",fx(ii),"n2 ",gx(j),Mtra(i)
20     continue
10     continue
!      WRITE(19,*) "Mtra(7),(8),(9)=",mtra(7)," ",Mtra(8)," ",Mtra(9)
212    IF (idex.eq.1) GO TO 100
!      For mode j inter coagulation
      i=13
                    if (sg1.lt.1.0001) then
                      if (sg2.lt.1.0001) then
                      n1=1.
                      n2=1.
                      w1(1)=1.
                      w2(1)=1.
                      x1(1)=LOG(Dgn1)
                      x2(1)=LOG(Dgn2)
        goto 46
                      else
                      n1=1.
```

```
                    w1(1)=1.
                    x1(1)=log(Dgn1)
                    goto 43
                    endif
      else
                    if (sg2.lt.1.0001) then
                    n2=1.
                    w2(1)=1.
                    x2(1)=LOG(Dgn2)
            goto 45
                    else
                    endif
      endif
45     k1l1=k1ml(i)
      k1u1=k1mu(i)
      call limit(k1l1,k1u1,k1l,k1u,Dgn1,sg1)
      k1l=LOG(k1l)
      k1u=LOG(k1u)
      call gauleg(k1l,k1u,x1,w1,n)
      if(sg2.lt.1.001) goto 46
43                  k2l1=k2ml(i)
      k2u1=k2mu(i)
      call limit(k2l1,k2u1,k2l,k2u,Dgn2,sg2)
      k2l=LOG(k2l)
      k2u=LOG(k2u)
      call gauleg(k2l,k2u,x2,w2,n)
!      do 43 i1=1,n
!      WRITE(19,46) x1(i1),x2(i1)
!46     FORMAT("x1,x2= ",e10.2,1x,e10.2)
!43     continue
46     Mtra(i)=0.
      dp0=2.
      do 40 ii = 1,n1
      do 40 j = 1,n2
      fx1=((1./EXP(x1(ii)*3.))+(1./EXP(x2(j)*3.)))**0.5
      fx2=(EXP(x1(ii))+EXP(x2(j)))**2.
      ip=3.
```

```
      dp1=(EXP(x1(ii)))**(ip)
      dp2=(EXP(x2(j)))**(ip)
          if (sg1.lt.1.0001) then
          Fx(ii)=M1(1)
          else
      Fx(ii)=M1(1)/((2*pi)**0.5*LOG(sg1))*EXP(-0.5*(x1(ii)-LOG(Dgn1))**2./(LOG(sg1))**2.)
      endif
          if (sg2.lt.1.0001) then
          Gx(j)=M2(1)
          else
          Gx(j)=M2(1)/((2*pi)**0.5*LOG(sg2))*EXP(-0.5*(x2(j)-LOG(Dgn2))**2./(LOG(sg2))**2.)
      endif
          Mtra(i)=Mtra(i)+dp0*dp1*dp2*c1*fx1*fx2*Fx(ii)*w1(ii)*w2(j)*Gx(j)
!      IF(MOD(iout,50000).ne.0)GO TO 40
      beta1=dp0*dp1*dp2*c1*fx1*fx2
      mta=dp0*dp1*dp2*c1*fx1*fx2*Fx(ii)*w1(ii)*w2(j)*Gx(j)
!      WRITE(20,325) ii,j,beta1,mta
325    FORMAT(1x,i2,1x,i2,1x,e10.4,1x,e10.4)
40     continue
      Mtra(10)=0.D0
      Mtra(11)=-Mtra(8)
      Mtra(12)=-Mtra(9)+Mtra(13)
100    continue
!      WRITE(19,*) "Mtra(10),Mtra(11),Mtra(12)= ",Mtra(10),Mtra(11),Mtra(12)
      return
      end
!
    SUBROUTINE intracoagulation2(idex)
    IMPLICIT DOUBLE PRECISION (A-H,K-Z)
    INTEGER n,n1,n2
    Dimension Mtra(26),k1ml(26),k1mu(26),k2ml(26),K2mu(26)
    DIMENSION w1(100),w2(100),x1(100),x2(100),Fx(100),Fxx(100)
    Dimension Gxx(100),Gx(100),M1(3),M2(3)
    COMMON/moment/sg1,sg2,M1,M2,Dgn1,Dgn2
    COMMON/gas/kb,T,lop,mu,lamda
    COMMON/klimit/k1ml,k1mu,k2ml,k2mu
    COMMON/coag1/Mtra
```

```
      COMMON/nod/n
      COMMON/idex2/icog,icodd1,icodd2
!     WRITE(*,*) "intra2coag"
      n1=n
      n2=n
      pi=3.141593
      Kng1=2*lamda/Dgn1
      Kng2=2*lamda/Dgn2
      A1=1.392*Kng1**0.0783
      A2=1.392*Kng2**0.0783
      IF (icog.eq.1) GOTO 212
      do 10 i=14,16
      if (i.eq.15) GOTO 25
      if (sg1.lt.1.0001) then
                        n1=1.
                        n2=1.
                        w1(1)=1.
                        w2(1)=1.
                        x1(1)=LOG(Dgn1)
                        x2(1)=LOG(Dgn1)
                        goto 29
      else
      endif
      k1l1=k1ml(i)
      k1u1=k1mu(i)
      call limit(k1l1,k1u1,k1l,k1u,Dgn1,sg1)
      k1l=LOG(k1l)
      k1u=LOG(k1u)
      call gauleg(k1l,k1u,x1,w1,n)
      k2l1=k2ml(i)
      k2u1=k2mu(i)
      call limit(k2l1,k2u1,k2l,k2u,Dgn1,sg1)
      k2l=LOG(k2l)
      k2u=LOG(k2u)
      call gauleg(k2l,k2u,x2,w2,n)
29    Mtra(i)=0.
      if (i.eq.14) dp0=-0.5
```

```
      if (i.eq.16) dp0=1.
      do 20 ii = 1,n1
      do 20 j = 1,n2
      Dp1=kb*T/(3*pi*mu*EXP(x1(ii)))*(1+A1*2*lamda/EXP(x1(ii)))
      Dp2=kb*T/(3*pi*mu*EXP(x2(j)))*(1+A2*2*lamda/EXP(x2(j)))
      fx1=2.*pi*(EXP(x1(ii))+EXP(x2(j)))
      ip=(i-14)*3./2.
      ddp1=(EXP(x1(ii)))**(ip)
      ddp2=(EXP(x2(j)))**(ip)
      if(sg1.lt.1.0001) then
      Fx(ii)=M1(1)
      Fxx(j)=M1(1)
      else
      Fx(ii)=M1(1)/((2*pi)**0.5*LOG(sg1))*EXP(-0.5*(x1(ii)-LOG(Dgn1))**2./(LOG(sg1))**2.)
      Fxx(j)=M1(1)/((2*pi)**0.5*LOG(sg1))*EXP(-0.5*(x2(j)-LOG(Dgn1))**2./(LOG(sg1))**2.)
      endif
      Mtra(i)=Mtra(i)+dp0*ddp1*ddp2*(Dp1+Dp2)*fx1*Fx(ii)*w1(ii)*w2(j)*Fxx(j)
20    continue
25    Mtra(15)=0.
10    continue
212   IF (idex.eq.1) GO TO 100
!     For mode j intra coagulation
      do 30 i=17,19
      if (i.eq.18) GO TO 35
      if (sg2.lt.1.0001) then
                  n1=1.
                  n2=1.
                  w1(1)=1.
                  w2(1)=1.
                  x1(1)=LOG(Dgn2)
                  x2(1)=LOG(Dgn2)
                  goto 49
      else
      endif
      k1l1=k1ml(i)
      k1u1=k1mu(i)
      k2l1=k2ml(i)
```

```
      k2u1=k2mu(i)
      call limit(k1l1,k1u1,k1l,k1u,Dgn2,sg2)
      call limit(k2l1,k2u1,k2l,k2u,Dgn2,sg2)
      k1l=LOG(k1l)
      k1u=LOG(k1u)
      k2l=LOG(k2l)
      k2u=LOG(k2u)
      call gauleg(k1l,k1u,x1,w1,n)
      call gauleg(k2l,k2u,x2,w2,n)
49    Mtra(i)=0.
      if (i.eq.17) dp0=-0.5
      if (i.eq.19) dp0=1.
      do 40 ii = 1,n1
      do 40 j = 1,n2
      Dp1=kb*T/(3*pi*mu*EXP(x1(ii)))*(1+A1*2*lamda/EXP(x1(ii)))
      Dp2=kb*T/(3*pi*mu*EXP(x2(j)))*(1+A2*2*lamda/EXP(x2(j)))
      fx1=2.*pi*(EXP(x1(ii))+EXP(x2(j)))
      ip=(i-17)*3./2.
      ddp1=(EXP(x1(ii)))**(ip)
      ddp2=(EXP(x2(j)))**(ip)
      if(sg2.lt.1.0001) then
      Gx(ii)=M2(1)
      Gxx(j)=M2(1)
      else
      Gx(ii)=M2(1)/((2*pi)**0.5*LOG(sg2))*EXP(-0.5*(x1(ii)-LOG(Dgn2))**2./(LOG(sg2))**2.)
      Gxx(j)=M2(1)/((2*pi)**0.5*LOG(sg2))*EXP(-0.5*(x2(j)-LOG(Dgn2))**2./(LOG(sg2))**2.)
      endif
      Mtra(i)=Mtra(i)+dp0*ddp1*ddp2*(Dp1+Dp2)*fx1*Gx(ii)*w1(ii)*w2(j)*Gxx(j)
40    continue
35    Mtra(18)=0.
30    continue
100   continue
      return
      end
!
!
      SUBROUTINE intercoagulation2(idex,iout)
```

```
IMPLICIT DOUBLE PRECISION (A-H,K-Z)
INTEGER n,n1,n2
DIMENSION Mtra(26),k1ml(26),k1mu(26),k2ml(26),K2mu(26)
DIMENSION w1(100),w2(100),x1(100),x2(100),Fx(100),Fxx(100)
Dimension Gxx(100),Gx(100),M1(3),M2(3)
COMMON/moment/sg1,sg2,M1,M2,Dgn1,Dgn2
COMMON/gas/kb,T,lop,mu,lamda
COMMON/klimit/k1ml,k1mu,k2ml,k2mu
COMMON/coag1/Mtra
COMMON/nod/n
COMMON/idex2/icog,icodd1,icodd2
n1=n
n2=n
Kng1=2*lamda/Dgn1
Kng2=2*lamda/Dgn2
A1=1.392*Kng1**0.0783
A2=1.392*Kng2**0.0783
pi=3.141593
IF (icog.eq.1) GOTO 212
do 10 i=20,22
if (sg1.lt.1.0001) then
        if (sg2.lt.1.0001) then
                n1=1.
                n2=1.
                w1(1)=1.
                w2(1)=1.
                x1(1)=LOG(Dgn1)
                x2(1)=LOG(Dgn2)
          goto 31
        else
                n1=1.
                w1(1)=1.
                x1(1)=log(Dgn1)
                goto 29
        endif
else
        if (sg2.lt.1.0001) then
```

```
                n2=1.
                w2(1)=1.
                x2(1)=LOG(Dgn2)
      goto 28
          else
          endif
    endif
28   k1l1=k1ml(i)
    k1u1=k1mu(i)
    call limit(k1l1,k1u1,k1l,k1u,Dgn1,sg1)
    k1l=LOG(k1l)
    k1u=LOG(k1u)
    call gauleg(k1l,k1u,x1,w1,n)
    if(sg2.lt.1.0001) goto 31
29   k2l1=k2ml(i)
    k2u1=k2mu(i)
    call limit(k2l1,k2u1,k2l,k2u,Dgn2,sg2)
    k2l=LOG(k2l)
    k2u=LOG(k2u)
    call gauleg(k2l,k2u,x2,w2,n)
31   Mtra(i)=0.
    dp0=-1.
    do 20 ii = 1,n1
    do 20 j = 1,n2
    Dp1=kb*T/(3*pi*mu*EXP(x1(ii)))*(1+A1*2*lamda/EXP(x1(ii)))
    Dp2=kb*T/(3*pi*mu*EXP(x2(j)))*(1+A2*2*lamda/EXP(x2(j)))
    fx1=2.*pi*(EXP(x1(ii))+EXP(x2(j)))
    ip=(i-20)*3.
    ddp1=(EXP(x1(ii)))**(ip)
    if(sg1.lt.1.0001) then
    Fx(ii)=M1(1)
    else
    Fx(ii)=M1(1)/((2*pi)**0.5*LOG(sg1))*EXP(-0.5*(x1(ii)-LOG(Dgn1))**2./(LOG(sg1))**2.)
    endif
    if(sg2.lt.1.0001)then
    Gx(j)=M2(1)
    else
```

```
      Gx(j)=M2(1)/((2*pi)**0.5*LOG(sg2))*EXP(-0.5*(x2(j)-LOG(Dgn2))**2./(LOG(sg2))**2.)
      endif
      Mtra(i)=Mtra(i)+dp0*ddp1*(Dp1+Dp2)*fx1*Fx(ii)*w1(ii)*w2(j)*Gx(j)
20    continue
10    continue
212   IF (idex.eq.1) GO TO 100
!     For mode j inter coagulation
      i=26
       if (sg1.lt.1.0001) then
                    if (sg2.lt.1.0001) then
                    n1=1.
                    n2=1.
                    w1(1)=1.
                    w2(1)=1.
                    x1(1)=LOG(Dgn1)
                    x2(1)=LOG(Dgn2)
              goto 46
                    else
                    n1=1.
                    w1(1)=1.
                    x1(1)=log(Dgn1)
                    goto 43
                    endif
        else
                    if (sg2.lt.1.0001) then
                    n2=1.
                    w2(1)=1.
                    x2(1)=LOG(Dgn2)
              goto 45
                    else
                 endif
       endif
45    k1l1=k1ml(i)
      k1u1=k1mu(i)
      call limit(k1l1,k1u1,k1l,k1u,Dgn1,sg1)
      k1l=LOG(k1l)
      k1u=LOG(k1u)
```

```
      call gauleg(k1l,k1u,x1,w1,n)
      if(sg2.lt.1.0001) goto 46
43    k2l1=k2ml(i)
      k2u1=k2mu(i)
      call limit(k2l1,k2u1,k2l,k2u,Dgn2,sg2)
      k2l=LOG(k2l)
      k2u=LOG(k2u)
      call gauleg(k2l,k2u,x2,w2,n)
46    Mtra(i)=0.
      dp0=2.
      do 40 ii = 1,n1
      do 40 j = 1,n2
      Dp1=kb*T/(3*pi*mu*EXP(x1(ii)))*(1+A1*2*lamda/EXP(x1(ii)))
      Dp2=kb*T/(3*pi*mu*EXP(x2(j)))*(1+A2*2*lamda/EXP(x2(j)))
      fx1=2.*pi*(EXP(x1(ii))+EXP(x2(j)))
      ip=3.
      ddp1=(EXP(x1(ii)))**(ip)
      ddp2=(EXP(x1(j)))**(ip)
      if(sg1.lt.1.0001) then
      Fx(ii)=M1(1)
      else
      Fx(ii)=M1(1)/(2*pi)**0.5*LOG(sg1)*EXP(-0.5*(x1(ii)-LOG(Dgn1))**2./(LOG(sg1))**2.)
      endif
      if(sg2.lt.1.0001) then
      Gx(j)=M2(1)
      else
      Gx(j)=M2(1)/(2*pi)**0.5*LOG(sg2)*EXP(-0.5*(x2(j)-LOG(Dgn2))**2./(LOG(sg2))**2.)
      endif
      Mtra(i)=Mtra(i)+dp0*ddp1*ddp2*(Dp1+Dp2)*fx1*Fx(ii)*w1(ii)*w2(j)*Gx(j)
!     beta2=dp0*ddp1*ddp2*(Dp1+Dp2)*fx1
!     mta=dp0*ddp1*ddp2*(Dp1+Dp2)*fx1*Fx(ii)*w1(ii)*w2(j)*Gx(j)
!     IF(MOD(iout,50000).ne.0)GO TO 40
!     WRITE(20,325) ii,j,beta2,mta
!325   FORMAT(1x,i2,1x,i2,1x,e10.4,1x,e10.4)
!     WRITE(19,103) ii,j,Mtra(i)
103   FORMAT("ii=",i2," j=",i2,1x,e10.3,1x,e10.3,1x,e10.3,1x,e10.3,1x,e10.3)
40    continue
```

```
      Mtra(23)=0.D0
      Mtra(24)=-Mtra(21)
      Mtra(25)=-Mtra(22)+Mtra(26)
100   continue
      return
      end
!
      SUBROUTINE limit(k1l,k1u,dpl,dpu,Dgn,sg)
      IMPLICIT DOUBLE PRECISION (A-H,K-Z)
      Dgkl=Dgn*EXP(k1l*(LOG(sg))**2.)
      Dgku=Dgn*EXP(k1u*(LOG(sg))**2.)
      dpl=Dgkl/(sg**4.)
      dpu=Dgku*sg**4.
!     WRITE(*,*) "k1l,k1u= ",k1l," ",k1u
!     WRITE(*,*) "dpl,dpu= ",dpl," ",dpu
      Return
      END SUBROUTINE
!
       subroutine gauleg(x1,x2,x,w,n)
       integer n
       DOUBLE precision x1,x2,x(n),w(n)
       DOUBLE PRECISION EPS
       PARAMETER (EPS=3.d-14)
!            Given the lower and upper limits of integration x1 and x2, and given n, this routine
returns
!            arrays x(1:n) and w(1:n) of length n, containing the abscissas and weights of the
Gauss-
!            Legendre n-point quadrature formula.
       INTEGER i,j,m
             DOUBLE PRECISION p1,p2,p3,pp,xl,xm,z,z1
!            High precision is a good idea for this routine
       m=(n+1)/2
       xm=0.5d0*(x2+x1)
       xl=0.5d0*(x2-x1)
       do 10 i=1,m
        z=COS(3.141592652d0*(i-0.25d0)/(n+0.5d0))
```

```
!             Starting with the above approximation to the ith root, we enter the main loop of
refinement
!             Newton's method.
1       continue
         p1=1.d0
         p2=0.d0
         do 20 j=1,n
           p3=p2
           p2=p1
           p1=((2.d0*j-1.d0)*z*p2-(j-1.d0)*p3)/j
!         WRITE(*,*) "i= ",j," ","p1= ",p1
20        continue
!             p1 is now the desired Legendre polynomial. We next compute pp, its derivative, by
!             a standard relation involving also p2, the polynomial of one lower order.
         pp=n*(z*p1-p2)/(z*z-1.d0)
           z1=z
           z=z1-p1/pp
         IF(ABS(z-z1).gt.EPS) GOTO 1
         x(i)=xm-xl*z
!         WRITE(*,*) "xm= ",xm," xl= ",xl," z= ",z
         x(n+1-i)=xm+xl*z
         w(i)=2.d0*xl/((1.d0-z*z)*pp*pp)
         w(n+1-i)=w(i)
10      continue
       return
       end
!
!
       subroutine intio()
       IMPLICIT DOUBLE PRECISION (A-H,K-Z)
       Dimension al(6),B(6,6),Gam(6)
       COMMON /RKF/al,B,Gam
       al(2)=1./4.
       al(3)=3./8.
       al(4)=12./13.
       al(5)=1.
       al(6)=1./2.
```

```
      B(2,1)=1./4.
      B(3,1)=3./32.
      B(3,2)=9./32.
      B(4,1)=1932./2197.
      B(4,2)=-7200./2197.
      B(4,3)=7296./2197.
      B(5,1)=439./216.
      B(5,2)=-8.
      B(5,3)=3680./513.
      B(5,4)=-845./4104.
      B(6,1)=-8./27.
      B(6,2)=2.
      B(6,3)=-3544./2565.
      B(6,4)=1859./4104.
      B(6,5)=-11./40.
      Gam(1)=16./135.
      Gam(2)=0.
      Gam(3)=6656./12825.
      Gam(4)=28561./56430.
      Gam(5)=-9./50.
      Gam(6)=2./55.
      RETURN
      End
!
      SUBROUTINE condensation(idex,Cond1,Cond2)
      IMPLICIT DOUBLE PRECISION (A-H,K-Z)
      DIMENSION x1(50),w1(50),M1(3),M2(3),cond1(3),cond2(3)
      INTEGER n,n1,n2   ! You must define integer to get x1 and w1.
      COMMON/moment/sg1,sg2,M1,M2,Dgn1,Dgn2
      COMMON/gas/kb,T,lop,mu,lamda
      COMMON/gas2/Sv,Ps,vm,sig,mm,mg,Dmg,cm
      COMMON/nod/n
      COMMON/Index2/icoag,icond1,icond2
      COMMON/part/dps,dpmol
      COMMON/idex2/icog,icodd1,icodd2
      COMMON/kelvin/idps
      pi=3.14159
```

```
      k1l1=-3.
      k1u1=3.
      IF (icodd1.eq.1) GOTO 212
      if (sg1.lt.1.0001) then
            n1=1.
            w1(1)=1.
            x1(1)=LOG(Dgn1)
        GOTO 127
      else
        n1=n
      endif11
      call limit(k1l1,k1u1,k1l,k1u,Dgn1,sg1)
!     WRITE(*,*) "k1l, k1u= ",k1l," ",k1u
      k1l=LOG(k1l)
      k1u=LOG(k1u)
      call gauleg(k1l,k1u,x1,w1,n1)
127   z=mm/mg
      lfs=3*Dmg/cm
      lD=2*Dmg/cm
      ! sig = surface tension
      ! Sv  = Saturation ratio
      ! vm  = molecular volume
!     WRITE(*,*)"vm= ",vm
      dps=4*sig*vm/(kb*T*LOG(Sv))
      IF(dps.lt.dpmol) dps=dpmol
      dps1=dps
      IF(idps.eq.1) dps1=0.   ! No kelvin effect
!     WRITE(*,*) "at cond dps= ",dps
      Cond1(1)=0
      DO 10 i=2,3
      Cond1(i)=0.
      c1=4*(3*(i-1))*Dmg*Ps/(kb*T)*vm
      do 22 ii = 1,n1
      dpx=exp(x1(ii))
      Knfs=2*lfs/dpx
      KnD1=2*ld/dpx
      if (z.lt.1) then
```

```
      cfs=(1+Knfs)/(1+1.71*Knfs+(4./3.)*Knfs**2.)  ! z << 1
      else
      cfs=(1+KnD1)/(1+2*KnD1*(1+KnD1))  ! z = 1
      endif
      dp0=dpx**(3*(i-1)-2)
      IF(sg1.ge.1.0000.and.sg1.lt.1.0001)then
      Fxx=M1(1)
      else
      Fxx=M1(1)/((2*pi)**0.5*LOG(sg1))*EXP(-1*0.5*(x1(ii)-LOG(Dgn1))**2./(LOG(sg1))**2.)
      endif
      fx1=dps1/dpx
      fx=dp0*(Sv-Sv**(fx1))*cfs
      fx=dp0*Sv*cfs
!     fx3=Sv-Sv**fx1
      Cond1(i)=Cond1(i)+c1*fx*Fxx*w1(ii)
!     WRITE(*,*) " c1 ",c1," fx ",fx
22    continue
!     WRITE(*,*) " cond1= ",cond1(i)
10    continue
!     For j mode condensation
212   IF (icodd2.eq.1) GOTO 33
      IF (idex.eq.1) GOTO 33
      if (sg2.lt.1.0001) then
            n2=1.
            w1(1)=1.
            x1(1)=LOG(Dgn2)
        GOTO 128
        else
        n2=n
      endif
      k1l1=-3.
      k1u1=3.
      call limit(k1l1,k1u1,k1l,k1u,Dgn2,sg2)
 !    WRITE(*,*) "mode 2 k1l, k1u= ",k1l," ",k1u
      k1l=LOG(k1l)
      k1u=LOG(k1u)
!     WRITE(*,*)"n2 ",n2
```

```
      call gauleg(k1l,k1u,x1,w1,n2)
      ! sig = surface tension
      ! Sv  = Saturation ratio
      ! vm  = molecular volume
!     WRITE(*,*) "k1l, k1u ",k1l," ",k1u
128   Cond2(1)=0
      DO 13 i=2,3
      Cond2(i)=0.
      c1=4*(3*(i-1))*Dmg*Ps/(kb*T)*vm
!     WRITE(*,*) "c1 ",c1
      do 23 ii = 1,n2
!     WRITE(*,*) "x1= ",x1(ii)," w1 ",w1(ii)
      dpx=exp(x1(ii))
      Knfs=2*lfs/dpx
      KnD1=2*ld/dpx
      if (z.lt.1) then
      cfs=(1+Knfs)/(1+1.71*Knfs+4./3.*Knfs**2.)  ! z << 1
      else
      cfs=(1+KnD1)/(1+2*KnD1*(1+KnD1))  ! z = 1
      endif
      dp0=dpx**(3*(i-1)-2)
      IF(sg2.ge.1.0000.and.sg2.lt.1.0001) then
      Fxx=M2(1)
      else
      Fxx=M2(1)/((2*pi)**0.5*LOG(sg2))*EXP(-0.5*(x1(ii)-LOG(Dgn2))**2./(LOG(sg2))**2.)
      endif
      fx1=dps1/dpx
!     fx=dp0*(Sv-Sv**(fx1))*cfs
      fx=dp0*(Sv)*cfs
!     fx3=Sv-Sv**fx1
      Cond2(i)=Cond2(i)+c1*fx*Fxx*w1(ii)
23    continue
!     WRITE(*,*) " cond2= ",cond2(i)," x1= ",x1(ii)
13    continue
33    Return
      END
      SUBROUTINE nucleation(idex,nu)
```

```
      IMPLICIT DOUBLE PRECISION (A-H,K-Z)
      DIMENSION NU(3)
      COMMON/gas/kb,T,lop,mu,lamda
      COMMON/gas2/Sv,Ps,vm,sig,mm,mg,Dmg,cm
      COMMON/gas3/sl,ns,ks,vs
      COMMON/part/dps,dpmol
      ! Classical Becker-Doring nucleation theory
      ! sl : monomer surface area
      ! ml : monomer mass
      ! vl : monomer volume
      pi=3.14159
      dps=4*sig*vm/(kb*T*LOG(Sv))
      IF(dps.lt.dpmol) dps=dpmol
!     dps=6.29e-8
      Sig1=sig*(vm**(2./3.))/(kb*T)
      ks=pi/6.*(4.*Sig1/LOG(Sv))**3.
      C1=(ns**2.)*sl*((kb*T/(2.*pi*mm))**0.5)*(Sv**2.)
      C2=((2./(9.*pi))**(1./3.))*(Sig1**0.5)*EXP(-1*ks*LOG(Sv)/2.)
      NU1=C1*C2
      vs=(dps**3.)
      NU(1)=NU1
      NU(2)=NU1*vs
      NU(3)=NU1*(vs**2.)
!     WRITE(*,*) "NU1= ",NU(1),"NU2= ",NU(2)
!     WRITE(19,*) "C1= ",C1," C2= ", C2
!     WRITE(19,*) "NU1= ",NU(1)," ",NU(2)," ",NU(3)
      RETURN
      END
```

APPENDIX B

MOMENT RELATIONSHIPS FOR THE LOGNORMAL DISTRIBUTION

The integral moments of a distribution are defined as,

$$M_k = \int_0^\infty d_p^k n(d_p) d(d_p) \tag{b-1}$$

which can also be expressed in terms of $\ln(d_p)$ as

$$M_k = \int_{-\infty}^\infty d_p^k n(\ln d_p) d(\ln d_p) \tag{b-2}$$

The lognormal number distribution function is

$$n(\ln d_p) = \frac{dN}{d(\ln d_p)} = \frac{N}{\sqrt{2\pi}\ln\sigma_g} \exp\left[-0.5\frac{(\ln d_p - \ln D_{gn})}{\ln^2 \sigma_g}\right] \tag{b-3}$$

It is convenient to make a change of variables as

$$x = \frac{(\ln d_p - \ln D_{gn})}{\ln \sigma_g}$$

$$d_p = D_{gn} \exp(x \ln \sigma_g)$$

$$dx = d(\ln d_p) / \ln \sigma_g$$

Using this change of variables and substituting eq. (b-2) into eq. (b-3) yields

$$M_k = \frac{N D_{gn}}{\sqrt{2\pi}} \int \exp(-0.5x^2 + kx \ln \sigma_g) dx \tag{b-4}$$

Expanding the exponential term, completing the square, and substituting

$y = x - (k \ln \sigma_g)$ into eq. (b-4) yields

$$M_k = \frac{N D_{gn}}{\sqrt{2\pi}} \exp(0.5k^2 \ln^2 \sigma_g) \int_{-\infty}^\infty \exp(-0.5y^2) dy \tag{b-5a}$$

$$= ND_{gn}^{k} \exp(k^2 / 2\ln^2 \sigma_g) \qquad \text{(b-5b)}$$

By defining average moments and $\overline{M_{k1}}$ as $\overline{M_{k2}}$ as

$$\overline{M_{k1}} = D_{gn}^{k1} \exp(k_1^2 / 2\ln^2 \sigma_g) \qquad \text{(b-6a)}$$

$$\overline{M_{k2}} = D_{gn}^{k2} \exp(k_2^2 / 2\ln^2 \sigma_g) \qquad \text{(b-6b)}$$

and solving for D_{gn} and σ_g, the conversion equations between D_{gn} and σ_g; M_{k1} and M_{k2} are

$$D_{gn} = \overline{M_{k1}}^{1/[r(k2-k1)]} \overline{M_{k2}}^{r/(k1-k2)} \qquad \text{(b-7a)}$$

$$\ln^2 \sigma_g = \frac{2}{k1(k2-k1)} \ln(\overline{M_{k1}} / \overline{M_{k2}}^{r}) \qquad \text{(b-7b)}$$

where $r = k1/k2$

Substituting eq. (b-7a) and (b-7b) into eq. (b-5b) yields an expression for other moments of the distribution in terms of the moments $\overline{M_{k1}}$ and $\overline{M_{k2}}$

$$M_k = N\overline{M_{k1}}^{\overline{k1}} \overline{M_{k2}}^{\overline{k2}} \qquad \text{(b-8)}$$

where

$$\overline{k1} = [r(k/k1)^2 - (k/k1)]/(r-1)$$
$$\overline{k2} = [r(k/k2) - (k/k2)^2]/(r-1)$$

APPENDIX C
MATERIAL SAFETY DATA SHEET

Section 1. Product Identification

- **Chemical name**: Vanadium (V) tri-i-propoxy oxide, 98+%
- **Product number**: 23-5000
- **CAS resister number**: 5588-84-1
- **Formula**: $VO(OC_3H_7)_3$
- **Einecs number**: 226-997-4
- **Synonym**: Isopropylorthovanadate, Tri-iso-propylvanadate, Vanadyl isopropylate

Section 2. Hazardous Identification

- **Emergency overview**: Flammable liquid and vapor. Inhalation may cause dizziness and headache. Irritating to eyes, skin and mucous membranes. Ingestion may cause nausea and vomiting.
- **Primary routes of exposure**: Eye, skin and inhalation
- **Eye contact**: Cause mild to severe irritation of the eyes
- **Skin contact**: Cause slight to mild irritation of the skin. Prolonged contact may dry the skin and lead to rashes or more severe irritation.
- **Inhalation**: irritating to mouth throat and stomach. May cause dizziness, nausea, vomiting, pain and stomach upset.
- **Acute health effects**: irritating to skin, eyes and mucous membranes. More severe effects (ingestion and inhalation) are dizziness, nausea, vomiting.
- **Chronic health effects**: No information available on long term chromic effects.

Section 3. Handling and Storage

- **Handling and storage**: Store in a cool, dry, well-ventilated area away from heat and direct sunlight. Keep containers tightly sealed. This product will react with

atmospheric moisture and chemically degrade. Transfer material under an inert atmosphere of nitrogen argon or very dry air

Section 4. Exposure Controls and Personal Protection

- **Eye protection**: Always wear safety glasses. If pouring or transferring this substance wear a face shield for additional protection.
- **Skin protection**: Wear protective clothing and groves. Consult with glove manufacturer to determine the proper type of glove.
- **Ventilation**: Work with this product in a well-ventilated area, preferably a fume hood.
- **Respirator**: If ventilation is not available a respirator should be worn. The use of respirators requires a Respirator Protection Program to be in compliance with 29 CFR 1910.134
- **Additional protection**: No additional protection required

Section 5. Physical and Chemical Properties

- **Color and form**: Light yellow to light green liquid.
- **Molecular weight**: 244.20
- **Melting point (^{o}C)**: Not determined
- **Boiling point (^{o}C)**: 60-61^{o}/0.5 mm
- **Vapor pressure**: No data
- **Odor**: none
- **Solubility in water**: reacts with water

LIST OF REFERENCES

Akeredolu, F. A., Barrie, L. A., Olson, M. P., Oikawa, K. K., Pacyna, J. M., and Keeler, G. J., 1994, Flux of anthropogenic trace metals into the Arctic from the mid-latitudes in 1979/80, *Atmospheric Environment,* v 28(8), p 1557-1572.

Alemany, L. J., Larrubia, M. A., and Blasco, J. M., 1998, Catalytic activity in partial oxidation of methane and physico-chemical characterization of a VPO system obtained from boiler ash, *Appl. Catal. B:Environ.,* v 16(2), p 139-147.

Bacci, P., Monte, M. D., Longhetto, A., Piano, A., Prodi, F. and Redaelli, P. (1983). Characterization of the particulate emission by a large oil fuel fired power plant, *J. Aerosol Sci.*, v 14, p 557-572

Barin, I., 3rd Ed., 1995, Thermochemical Data of Pure Substances, VCH, New York

Biswas, P., and Wu, C. Y., 1998, Control of toxic metal emissions from combustors using sorbents: A review, *J. Air & Waste Manage. Assoc.*, v 48, p 113-127.

Boyd, D. W., and Kustin, K., 1984, Vandium: A versatile biochemical effector with an elusive biological function. In C. L. Eichhorn and L. G. Marzilli (Eds.), *Advances in Inorganic Biochemistry*, v 6, p 311-363

Bryers, R. W., 1995, Utilization of petroleum coke and petroleum coke/coal blends as a means of steam raising, *Fuel Processing Technology,* v 44(1-3), p 121-141.

Bylinska, E., 1996., Bioindication of titanium, vanadium and lanthanum coming from long distance emission in Sudety mountain monitoring, In Proceeding of simulation and control international conference on air pollution—computational Mechanics Inc., Billerica, MA, USA. p 753-759.

Campen, M. J., Nolan, J. P., Schladweiler, M. C. J., Kodavanti, U. P., Evansky, P. A., and Costa, D.L., 2001, Cardiovascular and thermoregulatory effects of inhaled PM associated transition metals: a potential interaction between nickel and vanadium sulfate, *Toxicology Sci.*, v 64, p 243-252

Carey, T. R., Richardson, C. F., Chang, R., Meserole, F. B., Rostam-Abadi, M., and Chen, S., 2000, Assessing sorbent injection mercury control effectiveness in flue gas streams, *Environ. Prog.*, v 19(3), p 167-173

Chase, M. W., Davies, C. A., Downey, J. R., Frurip, D. J., McDonald, R. A. and Syverud, A. N., 3rd Edition, 1986, JANAF Thermochemical tables, American Chemical Society and American Institute of Physics for the National Bureau of Standards, Midland, MI.

Chen, J. C., Wey, M. Y., and Liu, Z. S., 2001, Adsorption mechanism of heavy metals on sorbents during incineration, *J. Envron. Env. Eng.*, v 127, p 63-69

Divita, F., Ondov, J.M., and Suarez, A. E., 1996, Size spectra and atmospheric growth of V-containing aerosol in washington DC., *Aerosol Sci. Tech.*, v 25, p 256-273

Energy Information Administration, 1996, Washing D.C., *International Energy Annual Report*

Fan, L. S., Jiang, P., Agnihotri, R., Mahuli, S. K., Zhang, J., Chauk, S., Ghosh-Dastidar, A., 1999, Dispersion and ultra-fast reaction of calcium-based sorbent powders for SO_2 and air toxics removal in coal combustion, *Chemical Engineering Sci.*, v 54, p 5585-5597

Fang, M. X., Luo, Z. Y., Li, X. T., Wang, Q. H., Ni, M. J., and Chen, K. F., 1998**,** Multi-product cogeneration system using combined coal gasification and combustion, *Energy (Oxford)*, v 23(3), p 203-212.

Flagan, R. C. and Seinfeld, J. H., 1988, Fundamentals of Air Pollution Engineering, Prentice Hall, Englewood Cliffs, NJ, p 433-471.

Frenklach, M., and Harris, S.J., 1987, Aerosol dynamics modeling using the method of moments, *J. Colloid Interf. Sci.*, v 118, p 252-261

Friedlander, S. K., Koch, W., and Main, H. H., 1991, Scavenging of a Coagulating fine aerosol by a coarse particle mode, *J. Aerosol Sci.*, v 22, p 1-8.

Gelbard, E., and Seinfeld, J. H., 1980, Simulation of multicomponent aerosol dynamics, *J. Colloid Interface Sci.*, v 78, p 485-501

Harries, R. R., 1993, Process modeling for wet limestone flue gas desulphurization. *ICHEME sym.* Ser. 131, p 167-81

Helble, J. J., and Sarofim, A. F., 1989, Factors determining the primary particle size of flame-generated inorganic aerosols, *J. Coll. Int. Sci.*, v 128 (2), p 348-362.

Hind, W. C., 1999, Aerosol Technology, John Wiley & Sons, Inc., NY, p 428-434

Hogu, C., 2000, Body burdens of pollutants, *Chem. Eng. News*, v 78 (31), p 28 – 29.

Huffman, G. P., Huggins, F. E., Shah, N. R., Huggins, W. P., Linak, C. A., Miller, R. J., Pugmire, H. L. C., Meuzelaar, M., and Seehra, A., 2000, Characterization of Fine Particulate Matter Produced by Combustion of Residual Fuel Oil, *J. Air & Waste Management Assoc.*, v 50, p 1106-1114

Iida, K., Wu, C. Y., and Hahn, D. W., 2004, In situ analysis of the interaction of manganese vapor and silica microspheres in a laboratory-scale combustor, *Combust. Sci. and Technol.*, v 176 (3), p 453-480

Landgrebe, J. D., and Pratsinis, S. E., 1990, A discrete-sectional model for particulate production by gas-phase chemical-reaction and aerosol coagulation in the free-molecular regime, *Colloid Interf. Sci.*, v 139, p 63-86

Lee, C. C., 1988, A model analysis of metal partitioning in a hazardous waste incineration system, *JAPCA*, v 38(7), p 941-945.

Lee, S. R., and Wu, C. Y., 2002, Study of vanadium emission control in combustion systems by thermodynamic equilibrium analyses, *Advances in Environ. Research*, v 7, p 1-10

Lee, S. R., and Wu, C. Y., 2004, Size distribution evolution of fine aerosols due to inter-coagulation with coarse aerosols, submitted to *Aerosol Sci & Tech.* (in process)

Lighty, I. S., Veranth, J. M., and Sarofim, A. F., 2000, 2000 critical review-combustion aerosols: Factors governing their size and composition and implications to human health., *J. Air Wastes Mang. Assoc.*, v 50, p 1565-1618.

Lin, C.Y., and Chiu, C. H., 1995, Emissions of industrial furnaces burning vanadium-contained heavy oils, *Environ. Sci. Health, Part A: Environ. Sci. Eng. Toxic Hazard. Substance*, v 30(1), p 133-142.

Lin, W. Y., and Biwas, P., 1994, Metallic particle formation and growth dynamics during incineration, *Combust. Sci. Technol.*, v 101, p 29-43

Linak, W. P., and Wendt, J. O. L., 1998, Partitioning of the refractory metals, nickel and chromium, in combustion systems, *Combustion Sci. and Tech*, v 134, p. 291-314

Linak, W. P., Miller, C. A., Santoianni, D. A., King, C. J., Shinagawa, T., Wendt, J. O. L., Yoo, J. I., and Seo, Y. C., 2003, Formation of fine particles from residual oil combustion: Reducing nuclei through the addition of inorganic sorbent, *Korean J. Chem. Eng.*, v 20(4), p 664-669

Linak, W. P., Srivastava, R. K., and Wendt, J. O. L., 1995, Sorbent capture of nickel, lead, and cadmium in a laboratory swirl flame incinerator, *Combustion and flame*, v 100, p 241-250

Linak, W. P., and Wendt, J.O.L., 1993, Toxic metal emissions from incineration: Mechanisms and control, *Prog. Energy Combust. Sci.*, v 19, p 145-185

Linak, W. P., and Wendt, J.O.L., 1994, Trace metal transformation mechanisms during coal combustion, *Fuel Process. Technol.*, v 39 (2), p 173-198

Linak, W. P., and Miller, C. A., 2000, Comparison of particle size distributions and elemental partitioning from the combustion of pulverized coal and residual fuel oil, *Air & Waste Mange. Assoc*., v 50, p. 1532-1544.

Lundgren, D. A., and Vanderpool, R. W., 1988, Design and calibration of an in-stack low pressure impactor, US air force, Contract No. F08635-83-C0136

Lyyranen, J., Jokiniemi, J., Kauppinen, E. I., and Joutsensaari, J., 1999, Aerosol characterization in medium-speed diesel engines operating with heavy fuel oils, *J. Aerosol Sci.*, v 30, p 771-784

Mahuli, S., Agnihotri, R., Chauk, S. Ghosh-Dastidar, A., and Fan, L. S., 1997, Mechanism of arsenic sorption by hydrated lime, *Environ. Sci. Technol.*, v 31(11), p 3226-3231.

McMillin, B. K., Biswas, P. and Zachariah, M., 1996, *In Situ* Diagnostics of vapor phase growth of iron oxide-silica nanocomposites Part I: 2-D planar laser-induced fluorescence and mie imaging, *J. Mater. Res.*, v 11(6), p 1552-1561.

Nerin, C., Domeno, C., and Superior, C. P., 1999, Distribution of Pb, V, Cr, Ni, Cd, Cu and Fe in particles formed from the combustion of waste oils, *Chemosphere*,v 38, p 1533-1540

Osan, J., Torok, S., Fekete, J., and Rindby, A., 2000, Case study of the emissions from a heavy-oil-fueled Hungarian power plant, *Energy & Fuels*, v 14, p 986-993

Owens, T. M., and Biswas, P., 1996, Reactions between vapor phase lead compounds and *In Situ* generated silica particles at various lead-silicon feed ratios: applications to toxic metal capture in combustors, *J. Air Waste Manage. Assoc.*, v 46, p 530-538.

Owens, T. M., Wu, C. Y., and Biswas, P., 1995, An equilibrium analysis for reactions of metal compounds with sorbents in high temperature systems, *Chemical Engineering Communications*, v 133, p 31-52.

Pirrone, N., Costa, P., and Pacyna, J. M.; 1999, Past, current and projected atmospheric emissions of trace elements in the Mediterranean region, *Water Sci. Technol.*, v 39(12), p 1-7.

Prastinis, S. E., 1988, Simultaneous nucleation, condensation and coagulation in aerosol reactors, *J. Colloid Interface Sci.*, v 124(2), p 416-427

Punjak, W. A., Uberoi, M., and Shadman F., 1989, High-temperature adsorption of alkali vapors on solid sorbents, *AIChE Journal*, v 35, p 1186-1194

Rahaman, M. N.,1995, Ceramic processing and sintering, Marcl Dekker Inc., Madison Ave., NY, p 201-263.

Reynolds, W. C., 1995, STANJAN-Interactive computer programs for chemical equilibrium analysis, Dept. Mechanical Engineering, Stanford Univ., Standford, CA

Rodriguez, A., and Hall, M. J., 2001, Removal of an airborne low volatility metal under fuel-rich and fuel-lean condition through condensation onto soot and/or sorbent particles. *Waste management*, v 21(7), p 589-607

Rodriguez, A. and Hall, M. J., 2003, The simulation of condensation removal of a heavy metal from exhaust gases onto sorbent particles, *Waste Management*, v 23(6), p 493-502

Scotto, M. V., Uberoi, M., Peterson, T. W., Shadman, F., and Wendt, J. O. L., 1994, Metal capture by sorbents in combustion processes, *Fuel Proc. Technol.*, v 39(1/3), p 357-372.

Swain, E. J., 1991, Power, cement industries shape coke future, *Oil and Gas,* v 89(20), p 49-52.

Tolocka M. P., Lake D. A., Johnston M. V., and Wexler A.S., 2004, Number concentrations of fine and ultrafine particles containing metals, v 38(20), p 3263-3273

Tsang, T. H., and Brock, J. R. (1982). Aerosol coagulation in the plume from a cross-wind line source, *Atmos. Envrion.*, 16: 2229-2235

Tsuboi, I. K, Shigetami, K., Eiichi, K., and Isao, K., 1991, Recovery of gallium and vanadium from coal fly ash, *J. Chem. Eng. Jpn.*, v 24(1), p 15-20.

Uberoi, M., and Shadman, F., 1991, Simultaneous condensation and reaction of metal compound vapors in porous solids, *Ind. Eng. Chem. Res.*, v 30, p 624-631.

Venkatesh, S., Fournier, D. J. Jr., Waterland, L. R. and Carroll, G. J., 1996, Evaluation of Mineral-Based Additives as Sorbents for Hazardous Trace Metal Capture and Immobilization in Incineration Processes, *Haz. Waste. Haz. Mat.*, v 13(1), p 73-94.

Whitby, E. R., McMurry, P. H., Binkowski, F., and Shankar, U., 1991, Modal aerosol dynamics modeling. EPA report for contract No. 68-01-7365.

Whitby, E. R., and McMurry, P. H., 1997, Modal aerosol dynamics modeling, *Aerosol Sci. and Tech.*, v 27(6), p 673-688

Whitby, K. T., 1979, Lumped mode aerosol growth model. Particle Technology Laboratory Publication #395, Mechanical Engineering Department, University of Minnesota, Minneapolis, MN.Wiliams, M. M. R. and Loyalka, S. K., 1991, Aerosol science: Theory and practice, Pergamon Press.

Wu, C. Y., and Barton, T., 2001, A thermodynamic equilibrium analysis to determine the potential sorbent material for the control of arsenic emissions, *Environ. Eng. Sci.*, v 18(3), p 177-190

Wu, C. Y., and Biswas, P., 1993, An equilibrium analysis to determine the speciation of metals in an incinerator, *Combustion and Flame*, v 92, p 31-40.

Wu, C. Y., and Biswas, P., 1998, Study of numerical diffusion in a discrete-sectional model and its application to aerosol dynamics simulation, *Aerosol Sci. and Tech.*, v 29 (5), p 359-378

Wu, C. Y., and Biswas, P., 2000, Lead species aerosol formation and growth in multicomponent high temperature environments, *Env. Eng. Sci.*, v 17(1), p 41-60.

Wu, C. Y., Lee, T. G., Arar, E., Tyree, G., and Biswas, P., 1998, Capture of mercury in combustion environments by *In-Situ* generated titania particles with UV radiation, *Env. Eng. Sci.*, v 15(2), p 137-148.

Yee, B. H., and Rosenquist, W. A., 1996, Petroleum coke as an alternative fuel for new generation and repowering, In Proceedings of the American Power Conference v 2., Illinois Institute of Technology, Chicago, IL, USA. p 838-841.

BIOGRAPHICAL SKETCH

Sang-Rin Lee was born in Pusan, Korea on July 4, 1969. After graduation from Pusan High School, in 1988, he moved to Incheon to attend Inha university. He applied to the Electrical Engineering department but he was admitted to the Environmental Engineering department which became the cornerstone of his life. After receiving Bachelor of Science degree from the Environmental Engineering department in 1993, he continued his graduate study at that same university. His special topic was acid rain modeling. In addition to this model work, he also got involved with lots of projects such as PM10 sampling and air quality consulting. He worked for LG-Product Engineering Research Center for 1 year after receiving his Master of Science degree in 1995. He then moved to Korea Power Engineering Company. He worked as a process engineer for development and construction of the Korean type flue gas desulfurization system at Young-Dong Power Plant (200 MW and 150 MW). He was involved in the design of an Flue Gas Desulfurization system for 2 years and worked at Young-Dong Power Plant for construction and pre-operation for 1 year. With 4 years of valuable experience in the real world he decided to continue his studies in the U.S. He was admitted with a research assistantship from Dr. Chang-Yu Wu in the Environmental Engineering Sciences Department at the University of Florida. He studied aerosol technology and sorbent technology. He was awarded a Ph. D. in May 2005.